

Equation of state and viscosities of the gluon plasma in a holographic approach

Diplomarbeit
zur Erlangung des wissenschaftlichen Grades
Diplom-Physiker

vorgelegt von

Roman Yaresko
geboren am 24.03.1987 in Kiew

Institut für theoretische Physik
der Technischen Universität Dresden
2013

Eingereicht am 08.01.2013

1. Gutachter: Prof. Dr. Burkhard Kämpfer
2. Gutachter: Prof. Dr. Dominik Stöckinger

Kurzdarstellung

Die Zustandsgleichung und die Scher- und Volumenviskositäten des $SU(3)$ Yang-Mills Plasmas werden untersucht im Rahmen der AdS/CFT Korrespondenz. Das holographische Modell besteht aus der Einstein'schen Gravitationstheorie in 5 Dimensionen gekoppelt an ein Skalarfeld mit einem nicht-trivialen Potential. Die neuesten Präzisionsdaten der Gittertheorie für die Zustandsgleichung des $SU(3)$ Yang-Mills Plasmas werden benutzt, um die Parameter des von Gubser benutzten Potentials zu fitten. Verschiedene Parametersätze reproduzieren die Zustandsgleichung des $SU(3)$ Yang-Mills Plasmas in den jeweiligen Temperaturbereichen $1 \leq T/T_c \leq 2$, $2.5 \leq T/T_c \leq 100$, $10 \leq T/T_c \leq 1000$ mit einer sehr guten Genauigkeit. Es wird festgestellt, dass eine Modifikation des Potentials von Gubser nötig ist, um die Zustandsgleichung im gesamten Temperaturbereich $1 \leq T/T_c \leq 1000$ quantitativ genau zu reproduzieren. Die Scher- und Volumenviskositäten werden anschliessend durch eine holographische Auswertung der Kubo-Formeln ermittelt. Das Verhältnis der Scherviskosität η zur Entropiedichte s saturiert die KSS Grenze, $\eta/s = 1/4\pi$. Das Verhältnis der Volumenviskosität ζ zur Entropiedichte zeigt einen starken Anstieg für Temperaturen $T \rightarrow T_c^+$, wobei T_c die Deconfinement Temperatur ist.

Abstract

The equation of state and the shear and bulk viscosities of the $SU(3)$ Yang-Mills plasma are studied within the AdS/CFT correspondence. The holographic model employs five dimensional Einstein gravity coupled to a scalar field with a non-trivial potential. The recent high precision lattice gauge theory data of the $SU(3)$ Yang-Mills theory equation of state is used to optimize the parameters of the potential employed by Gubser. Distinct parameter sets are found to very well reproduce the $SU(3)$ Yang-Mills equation of state in the respective temperature ranges $1 \leq T/T_c \leq 2$, $2.5 \leq T/T_c \leq 100$, $10 \leq T/T_c \leq 1000$. It is found that for the quantitatively accurate reproduction of the whole temperature range $1 \leq T/T_c \leq 1000$ the potential of Gubser has to be modified. Subsequently, the shear and bulk viscosities are computed via a holographic evaluation of the Kubo formulae. The shear viscosity η to entropy density s ratio is found to saturate the KSS bound, $\eta/s = 1/4\pi$. The bulk viscosity ζ to entropy density ratio exhibits a sharp rise for temperatures $T \rightarrow T_c^+$, where T_c stands for the deconfinement temperature.

Contents

1. Introduction	1
2. Quantum Chromodynamics and Yang-Mills theory	3
2.1. Definition and properties	3
2.1.1. The Lagrange densities	3
2.1.2. The β function	4
2.2. Thermodynamics	6
2.2.1. The QCD phase diagram	6
2.2.2. Heavy-Ion Collisions	8
2.2.3. Perturbative methods	9
2.2.4. Lattice Gauge Theory	12
2.3. The AdS/QCD correspondence	12
3. The AdS/CFT correspondence	14
3.1. String theory and branes	14
3.1.1. String theory	14
3.1.2. p -branes and Dp -branes	16
3.2. A sketch of the derivation	16
3.2.1. Supergravity side	17
3.2.2. String theory side	18
3.3. The correspondence	18
3.3.1. Regimes of validity	19
3.3.2. Tests of the correspondence	20
3.3.3. AdS_5/CFT_4 correspondence	21
3.4. Mapping between AdS and CFT	22
3.4.1. Field-Operator Correspondence	22
3.4.2. A massive scalar field Φ on AdS_5	23
3.4.3. Correlators	26
3.5. Application to Yang-Mills theory	28

3.5.1. Limitations	28
3.5.2. Top-down and bottom-up models	29
3.5.3. Yang-Mills plasma thermodynamics and the large-N limit	30
4. Holographic Yang-Mills plasma thermodynamics	33
4.1. The general setup	33
4.2. Approach by Huang et al.	37
4.3. Approach by Gubser et al.	39
5. The equation of state	43
5.1. Approach by Huang et al. - Analysis of the model	43
5.2. Approach by Gubser et al. - Analysis of the model	45
5.3. Reconstruction of the SU(3) Yang-Mills equation of state	54
5.4. Conclusions	67
6. The shear and bulk viscosities	71
6.1. Kubo formulae	71
6.2. The holographic correlator	73
6.2.1. Perturbation of the metric	73
6.2.2. Linearized Einstein equations	74
6.2.3. Construction of the correlator	75
6.2.4. Solution of the linearized equations	79
6.3. Bulk viscosity in the approach by Gubser et al.	83
6.4. Conclusions	87
7. Conclusions	89
A. Einstein equations and Anti-deSitter space	92
A.1. Einstein equations	92
A.2. Anti-deSitter space	93
B. Thermodynamics	96
B.1. Black hole thermodynamics	96
B.2. Standard thermodynamics	97
C. Approximate determination of the parameters	99
D. Reviews of the AdS/CFT correspondence	102

1. Introduction

The fundamental theory of strong interactions is Quantum Chromodynamics (QCD), which describes the interactions among quarks and gluons. As such it also describes composite quark-gluon systems, i.e. hadrons and their interactions. An important aspect of QCD refers to the thermodynamics of strongly interacting matter. There, the phase diagram of QCD and its peculiarities are of utmost importance. Due to the strong coupling at low energies, genuine non-perturbative mechanisms are at work. Lattice QCD became an important numerical tool to cope with such non-perturbative effects. In the last decade, however, the AdS/CFT correspondence has been used to access basic features of QCD in the non-perturbative regime. The advantage of the AdS/CFT method is that it provides a tool to analytically study the strongly coupled regime of QCD. It is the goal of the thesis to employ the duality of a five-dimensional gravity theory and a quantum field theory to understand basic features of the latter one. To be specific, we are going to use the duality to model QCD properties at nonzero temperatures. In particular, we exploit the idea that the breaking of the conformal invariance of the pure gluon plasma due to quantum fluctuations is translated by the gauge/gravity duality into the deformation of the conformally invariant AdS space due to a non-trivial scalar field profile. This correspondence stems from the fact that the gauge theory energy momentum tensor is dual to the gravity theory metric tensor, and the gauge theory operator $\text{Tr}(F_{\mu\nu}F^{\mu\nu})$ is dual to a scalar field ϕ in the gravity theory. This duality allows one to map the potential of the scalar field onto the gauge theory equation of state. We focus on the pure gluon plasma and, after a quantitative reproduction of its equation of state, proceed to compute the shear and bulk viscosities which cannot be directly accessed via lattice calculations.

Outline of the thesis

The thesis is organized as follows. We begin with a few definitions and describe properties of QCD and Yang-Mills theory in chapter 2. We focus in particular on the thermodynamics, mention the relevant experiments and discuss the results and limitations of standard theoretical methods. In chapter 3, we gather the necessary preliminaries and sketch the derivation of the AdS/CFT correspondence. We review its variants and establish the map-

ping between the gauge theory and the gravity theory. We also discuss how the AdS/CFT correspondence can be applied to describe, in particular, the equation of state and the viscosities of the $SU(3)$ Yang-Mills theory, mentioning the limitations and the advantages of the method. In chapter 4, we introduce the holographic model of the Yang-Mills plasma thermodynamics, describe the underlying ideas and discuss its general features. We introduce two approaches to the solution of the model by Huang et al. [1] and by Gubser et al. [2]. In chapter 5, we focus on the equation of state, concentrating on the approach by Gubser et al. After analyzing the specific ansatz made in [2], we proceed to fit the parameters of the model to the equation of state of the $SU(3)$ Yang-Mills theory plasma in various temperature intervals. In chapter 6, we review the calculation of the shear and bulk viscosities via a holographic evaluation of the Kubo formulae and subsequently compute the viscosities for the optimum parameter values found in the preceding chapter. Finally, in chapter 7, we discuss our results, mention the possible improvements to the holographic model and point the directions of future work.

Appendix A is devoted to a brief review of the Einstein field equations of the general theory of relativity and to the AdS space. Appendix B briefly introduces the thermodynamics of black holes and collects standard thermodynamic relations and quantities used throughout the thesis. Appendix C describes how the parameters of the model can be fixed using input from the $SU(3)$ Yang-Mills theory. Appendix D collects some reviews of the AdS/CFT correspondence.

2. Quantum Chromodynamics and Yang-Mills theory

2.1. Definition and properties

We begin with a few definitions and describe some properties of Quantum Chromodynamics and Yang-Mills theory.

2.1.1. The Lagrange densities

Quantum Chromodynamics is a quantum field theory invariant under local gauge transformations of the $SU_c(3)$ gauge group. QCD is based on the lagrangian density

$$\mathcal{L}_{QCD} = \sum_{f=1}^{N_f} \bar{\psi}_f^c (i\gamma^\mu D_\mu - m_f) \psi_f^c - \frac{1}{4} F_a^{\mu\nu} F_{\mu\nu}^a + \mathcal{L}_{fix} + \mathcal{L}_{gh} + \mathcal{L}_{ct}, \quad (2.1)$$

where

$$D_\mu = \partial_\mu + igA_\mu \quad (2.2)$$

is the gauge-covariant derivative with gauge coupling g , and the gauge field strength tensor $F_a^{\mu\nu}$ is defined by

$$F_a^{\mu\nu} = \partial^\mu A_a^\nu - \partial^\nu A_a^\mu - gf_{abc} A_b^\mu A_c^\nu. \quad (2.3)$$

The quark bi-spinors ψ_f^c of color charge c ($c = 1 \dots 3$) and flavor f are in the fundamental representation of $SU_c(3)$, while the gauge fields A_a^μ , representing gluons, of color charge a ($a = 1 \dots 8$) are in the adjoint representation of $SU_c(3)$. The group $SU(3)$ has 8 generators G_a , which can be represented as 3×3 Gell-Mann matrices. The gauge field A^μ is decomposed in the G_a basis by $A^\mu = A_a^\mu G_a$. The quantities f_{abc} , defined by $[G_a, G_b] = if_{abc} G_c$, are the structure constants of $SU(3)$. In general $m_f \rightarrow m_{ff'}$ is a matrix, which may mix quarks of different flavor. Here, we suppose a diagonal form of $m_{ff'}$. Up to now, 6 quark flavors are known, i.e. $N_f = 6$. The terms in (2.1) not stated explicitly are: \mathcal{L}_{fix} , the gauge fixing term; \mathcal{L}_{gh} , the ghost term; \mathcal{L}_{ct} , the counterterms.

The last term in the field strength tensor (2.3), quadratic in the gauge fields, is absent in Quantum Electrodynamics (QED), which is an abelian $U(1)$ gauge theory with $f_{abc} \equiv 0$. In QCD, $f_{abc} \neq 0$, causing self-interactions of gluons. In perturbation theory there are 3-gluon vertices and 4-gluon vertices. This is in contrast to QED, where photons interact with electrons, but not with each other. It is this nonlinear term $\propto A^\mu A^\nu$ that leads to a qualitatively different behavior and a richness of phenomena, but also to computational difficulties, which to this day have not been satisfactorily overcome. In contrast to QED, the QCD coupling g may become large (for energy scales $\mu \lesssim 100$ GeV, $g \gtrsim 1$), rendering the standard method of perturbation theory - a Taylor expansion in the coupling - inefficient or even inapplicable.

In the holographic thermodynamics model, section 4, we will concentrate entirely on the gauge fields, also called pure glue sector or Yang-Mills theory, defined by

$$\mathcal{L}_{YM} = -\frac{1}{4} F_a^{\mu\nu} F_{\mu\nu}^a + \mathcal{L}_{fix} + \mathcal{L}_{gh} + \mathcal{L}_{ct}, \quad (2.4)$$

with $F_a^{\mu\nu}$ given by (2.3). The Yang-Mills theory is classically scale invariant. It can be obtained from (2.1) in the limit of infinite quark masses $m_f \rightarrow \infty$, meaning that the quarks no longer participate in the dynamics. Quantum fluctuations break the scale invariance leading to the trace anomaly, as discussed below.

2.1.2. The β function

Like any other quantum field theory, QCD and Yang-Mills theory have to be regularized and renormalized to obtain finite observables. Regularization introduces an energy scale μ into the theory. Observables should be invariant under a change of the energy scale $\mu \rightarrow \mu'$. The β function describes the dependence of the coupling g on the energy scale μ (often called “running of the coupling”); it is defined by

$$\beta(g) = \mu \frac{dg}{d\mu}. \quad (2.5)$$

For a quantum field theory with a $SU_c(N)$ gauge group and N_f massless quarks the β function to 2-loop order¹ is given by [4]

$$\beta(g) = -(11N - 2N_f) \frac{g^3}{48\pi^2} - \left(34N^2 - 13NN_f + 3\frac{N_f}{N} \right) \frac{g^5}{768\pi^4}. \quad (2.6)$$

¹The β function has been calculated to 4-loop order in [3].

For QCD, $N \equiv N_c = 3$ and assuming $N_f = 3$ active flavors, equation (2.6) gives

$$\beta_{QCD}(g) = -\frac{9}{16\pi^2}g^3 - \frac{67}{256\pi^4}g^5. \quad (2.7)$$

For Yang-Mills theory, i.e. for $N_f = 0$, one obtains from (2.6)

$$\beta_{YM}(g) = -\frac{11}{48\pi^2}Ng^3 - \frac{17}{384\pi^4}N^2g^5, \quad (2.8)$$

and for $N_c = 3$

$$\beta_{YM}(g) = -\frac{11}{16\pi^2}g^3 - \frac{51}{128\pi^4}g^5. \quad (2.9)$$

Note that $\beta_{QCD} < 0$. The coupling g decreases with increasing values of the energy scale μ . This is an important observation. For large energies, the quarks and gluons within QCD are asymptotically free (this fact is usually referred to as ‘‘asymptotic freedom’’), while for low energies the coupling becomes large and the interaction between quarks and gluons is strong (this fact being sometimes called ‘‘infrared slavery’’). As is evident from equation (2.8) the same discussion applies to Yang-Mills theory.

Due to the introduction of the energy scale μ the classical scale invariance of the Yang-Mills theory is broken by quantum fluctuations, as expressed by the following equation:

$$T_\mu^\mu = \frac{\beta(\alpha_S)}{8\pi\alpha_S^2} \text{Tr}(F_{\mu\nu}F^{\mu\nu}), \quad (2.10)$$

where T_μ^μ is the trace of the Yang-Mills theory energy momentum tensor $T^{\mu\nu}$ and $\alpha_S \equiv g^2/(4\pi)$.

Due to renormalization not only the coupling $g(\mu)$ becomes scale dependent. Other parameters of the model, such as the quark masses m_f , but also the classical scaling dimensions Δ_0 of field operators and Green’s functions become functions of the energy scale. Hereby, the scaling dimension Δ of an operator \mathcal{O} is defined as

$$\Delta = -\mathcal{O}^{-1}\mu\frac{d}{d\mu}\mathcal{O}. \quad (2.11)$$

The classical scaling dimension Δ_0 is determined by the dimensional analysis of the unrenormalized lagrangian. After renormalization one has

$$\Delta = \Delta_0 + \gamma, \quad (2.12)$$

where Δ is the actual (renormalized) scaling dimension and the quantity γ , which arises due to renormalization, is called the anomalous dimension. For an operator \mathcal{O} with renormalization constant $Z_{\mathcal{O}}$, γ is defined as

$$\gamma = -Z_{\mathcal{O}}^{-1} \mu \frac{d}{d\mu} Z_{\mathcal{O}}. \quad (2.13)$$

In perturbation theory, γ has the following schematic form:

$$\gamma = \gamma_1 g^2 + \gamma_2 g^4 + \mathcal{O}(g^6), \quad (2.14)$$

where the coefficients γ_i are computed at the respective order.

2.2. Thermodynamics

2.2.1. The QCD phase diagram

The ultimate goal of studying the thermodynamics of QCD is the complete understanding of the QCD phase diagram, figure 2.1.

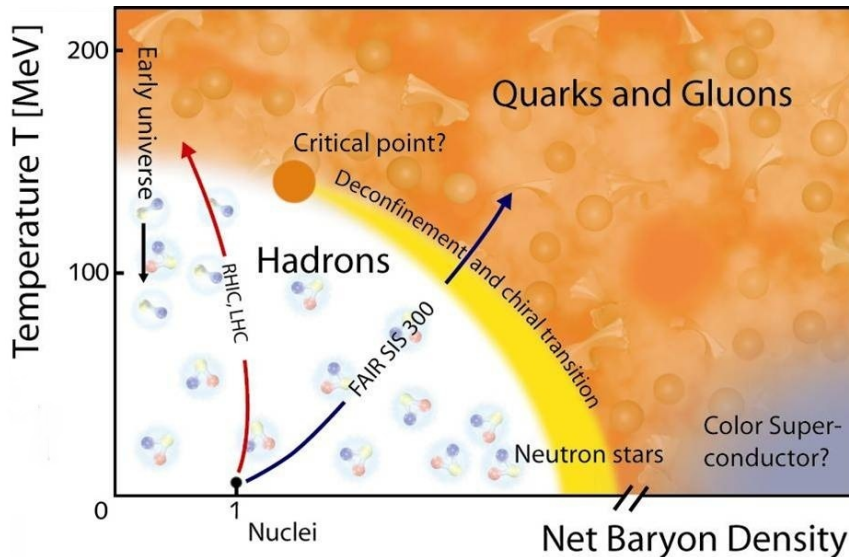


Figure 2.1.: The QCD phase diagram, reproduced from [5], showing different phases of strongly interacting matter in dependence of the temperature T and the baryochemical potential μ_B . See the text for explanations.

Two phases are regarded as established:^{2,3}

- Low T and low μ_B (lower left region of figure 2.1): The confined hadronic phase, in which quarks and gluons exist only as color-neutral bound states. The relevant degrees of freedom are hadrons, i.e. bound states of quarks held together by gluons, and glueballs, i.e. bound states consisting purely of gluons. For increasing T and μ_B , i.e. closer to the (phase) transition, this phase can be modelled by a gas of hadrons, the model being usually referred to as hadron resonance gas.
- High T and/or high μ_B (upper right region of figure 2.1): The deconfined quark-gluon plasma (QGP) phase in which quarks and gluons are the relevant degrees of freedom. They are free, i.e. unconfined, but still interact strongly. Recent experiments suggest that the QGP is a strongly coupled near-ideal liquid.

The deconfinement transition between the hadronic and the QGP phase is thought to be a strong crossover for low μ_B (with $T_c \approx 170$ MeV computed for two light quarks and $T_c \approx 150$ MeV for three light quarks), whereas for higher μ_B a first order phase transition is thought to occur, which presumably starts in a (tri)critical point (see figure 2.1).

The chiral phase transition, during which the chiral symmetry, broken explicitly by the quark masses m_f , and spontaneously by the non-vanishing quark-antiquark vacuum expectation value (the latter is usually referred to as condensate) $\langle \bar{q}q \rangle \neq 0$ is for increasing T restored.⁴ It is thought to occur close to the deconfinement phase transition.

Many questions remain unsettled and are topics of current research. The exact location of the (tri)critical point (if it exists at all) is not known, as well as the exact location of the confinement-deconfinement transition curve for $T > 0$ and $\mu_B > 0$. It is not yet settled how close the chiral symmetry restoration is to the deconfinement transition and whether they are correlated or not. Also, the mechanisms of chiral symmetry breaking and of confinement, although being studied with effective models, are not fully understood as following from the lagrangian (2.1). It is also an open question in which phase the QCD matter exists for low T and high μ_B .

²More exotic phases have been proposed, among them the quarkyonic phase (in the region marked as "Deconfinement and chiral transition" in figure 2.1), the color superconducting phase (CSC) and the color-flavor-locked (CFL) phase (both in the lower right region of figure 2.1), see [5].

³The baryochemical potential μ_B is a measure for the net baryon density defined as $n \equiv n_B - n_{\bar{B}}$, where n_B and $n_{\bar{B}}$ are, respectively, the number of baryons and anti-baryons.

⁴The restoration of the chiral symmetry χ_s is actually not exact: while the quark-antiquark condensate melts, $\langle \bar{q}q \rangle = 0$, the quark masses m_f are still present. However, for light quarks $m_f \ll T_{\chi_{SR}}$ and one can regard χ_s as restored to a good accuracy.

Since gauge bosons do not obey particle number conservation, their chemical potential is $\mu \equiv 0$. For pure Yang-Mills theory, one thus would not have the rich structure exhibited in figure 2.1, as the “phase diagram” would collapse to the T axis. Still, the confinement-deconfinement transition at the temperature $T_c \approx 265$ MeV remains.⁵ For low temperatures $T < T_c$, the relevant degrees of freedom are color-neutral glueballs, while for high temperatures $T > T_c$, the gluons are deconfined and form a strongly interacting plasma. The $SU(3)$ Yang-Mills confinement-deconfinement phase transition is known to be weakly first order [7]. In the holographic model we will concentrate entirely on the $SU(3)$ Yang-Mills plasma, i.e. on the deconfined phase.

2.2.2. Heavy-Ion Collisions

The main experimental tool for studying the thermodynamics of QCD are heavy-ion collisions performed at SPS, LHC, RHIC⁶ and other facilities. Heavy nuclei are accelerated to energies up to 200 AGeV at SPS (fixed target experiments), or up to 100 AGeV at RHIC (collider experiments), or up to 2.5 ATeV at LHC (collider experiments) and brought to collision. The typical sequence of the relevant stages in the course of a heavy-ion collision is as follows:

After the first collisions of leading-edge nucleons, the constituents of the nuclei interact strongly to very rapidly thermalize and to form a hot and dense QGP “fireball“ in (or nearby) thermal equilibrium. The fireball expands and cools. When the deconfinement transition area as in figure 2.1 is reached, the previously free quarks and gluons confine to form a gas of hadron resonances. After further cooling the resonances freeze out of thermal equilibrium and decay. The decay products are emitted either into the detectors or into the still cooling fireball. In the final stage only hadrons, which interact weakly or electromagnetically among themselves, are left. They may decay, and the decay products are detected. In the course of the collision, also weakly and electromagnetically interacting particles are emitted (the so called direct probes of the fireball).

It might seem to be a surprising fact that the evolution of the fireball from the point of the formation of the thermalized QGP through the phase transition down to the freeze-out of hadronic species can be well described by relativistic hydrodynamics.⁷ After the

⁵Note the rather large difference to $T_c^{QCD} \approx 170$ MeV. Both numerical values are taken from [6].

⁶The acronyms stand for Super Proton Synchrotron, Large Hadron Collider (both at CERN) and Relativistic Heavy Ion Collider (at the Brookhaven National Laboratory), respectively.

⁷This at first glance contra-intuitive insight can be resolved by noting that $l_{QCD} \ll R_{QGP}$: the typical range l_{QCD} of strong interactions is much smaller than the size R_{QGP} of the QGP fireball. Thus, the criterion for the applicability of hydrodynamics is satisfied.

successes of the model of ideal hydrodynamics the analysis was later on refined to first- and second-order viscous hydrodynamics. Hydrodynamics, being an effective theory of long-wavelength excitations, needs input from the microscopic theory of the matter one wants to describe. For ideal hydrodynamics the equation of state $p(e)$ or equivalently $p(T)$ must be supplied.⁸ Here, p denotes the thermodynamic pressure and T stands for the temperature. First-order viscous hydrodynamics needs in addition the input of first order transport coefficients; they are the shear viscosity $\eta(T)$, the bulk viscosity $\zeta(T)$, the heat conductivity $\kappa(T)$ and charge diffusion coefficients. Second order viscous hydrodynamics requires additional second order transport and charge diffusion coefficients.

In heavy ion collisions, the transverse 2-dimensional shape of the fireball is not an ideal sphere. An arbitrary 2-dimensional shape can be decomposed into Fourier modes describing its ellipticity, "triangularity", etc. By determining the Fourier coefficients and fitting the model of viscous hydrodynamic expansion to data, the transport coefficients of the QGP can in principle be "measured" in heavy ion collisions, as they affect the expansion dynamics of the fireball. That means, the equation of state and the transport coefficients of the QGP are important input parameters for the hydrodynamical description of the evolution of the QGP fireball.

2.2.3. Perturbative methods

The QCD β function

Consider the QCD β function (2.7). One recognizes a problem. Ordinary perturbation theory, i.e. a Taylor expansion in the coupling g , is applicable to QCD only at large energies, where the coupling g is supposed to be small. In this regime, perturbation theory has been successfully applied to describe, e.g., deep inelastic scattering, the Drell Yan process etc. At small energies, however, the coupling becomes large and usual perturbation theory is no longer applicable.⁹ Thus, low-energy phenomena of strong interactions like hadron spectra and hadron interactions, stability of hadrons and atomic nuclei, the confinement-deconfinement and chiral phase transitions and the QCD phase diagram can, if at all, only poorly be described by perturbative QCD. Successful effective low-energy models do exist.

⁸Actually $p(T, \mu_B)$ is needed, the same applies to transport coefficients. In the following we drop μ_B , as in the Yang-Mills theory, relevant for us, $\mu_B \equiv 0$ holds.

⁹Some improvements can be achieved by a reorganized perturbation theory.

Results and limitations of perturbation theory applied to QCD thermodynamics

For the details of the following discussion we refer the reader to chapter 8 of [6]. Much effort has been put into the computation of the equation of state of QCD, $p(T)$, using perturbation theory at finite temperature. To zeroth order in the coupling, $p(T)$ is given by the Stefan-Boltzmann limit of the Yang-Mills pressure (B.10) plus the ideal gas contribution of the quarks. The first correction to $p(T)$ comes from Feynman diagrams $\propto g^2$; subsequent corrections are of order g^3 and $g^4 \ln g^2$. In evaluating these corrections one encounters overlapping ultraviolet as well as infrared divergences. Special resummation techniques are used to overcome the latter problem: by resumming diagrams effective electric and magnetic screening masses of gluons are introduced, which regularize the infrared divergences.

It might seem that, in principle, one could calculate $p(T)$ to any desired order in g . However, at order g^6 a problem arises [8]. Consider the $(l + 1)$ -loop gluon diagram exhibited in figure 2.2.

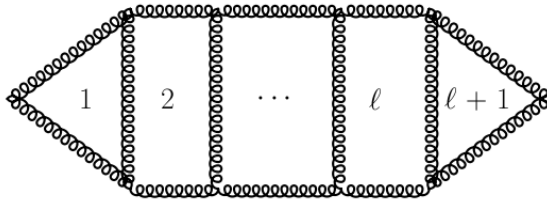


Figure 2.2.: Gluon loop diagram, contributing to $p(T)$.

One can schematically examine its degree of divergence by

$$g^{2l} \left(T \int d^3p \right)^{(l+1)} p^{2l} (p^2 + m^2)^{-3l}, \quad (2.15)$$

where the g^{2l} and p^{2l} factors come from the vertices, the $(T \int d^3p)^{(l+1)}$ factor from the loop integrations, and the $(p^2 + m^2)^{-3l}$ factor stems from the propagators, where an explicit infrared cutoff m was introduced, which will be identified with one of the screening masses introduced above. Place an ultraviolet cutoff equal to the temperature T on the momentum integration to obtain the order of divergence

$$g^{2l} T^4 \quad \text{for } l = 1, 2, \quad (2.16)$$

$$g^6 T^4 \ln(T/m) \quad \text{for } l = 3, \quad (2.17)$$

$$g^6 T^4 (g^2 T/m)^{l-3} \quad \text{for } l > 3. \quad (2.18)$$

For $l \geq 3$ and $m \rightarrow 0$ the diagram is infrared divergent. Consider the magnetic screening mass $m_{mag} \propto g^2 T$ at two-loop order and evaluate (2.18) to obtain $g^6 T^4$ for all $l > 3$. This implies that at order g^6 *all* loops with $l > 3$ contribute to the diagram in figure 2.2. Since it is not known how to sum such diagrams, we conclude that it is impossible to analytically calculate the complete g^6 order correction term to $p(T)$. Thus, the perturbation theory approach to calculating the equation of state $p(T)$ breaks down at $\mathcal{O}(g^6)$ which is the so called perturbation horizon. We show in figure 2.3 the results of perturbative calculations at subsequent orders in g for the pure $SU(3)$ Yang-Mills plasma. One sees that the $\mathcal{O}(g^3)$ and $\mathcal{O}(g^4)$ curves are for $T \rightarrow \Lambda_{\overline{MS}}$ qualitatively wrong.¹⁰ The constant in the last calculable order $g^6 \ln(1/g)$ was chosen to best reproduce the lattice data.

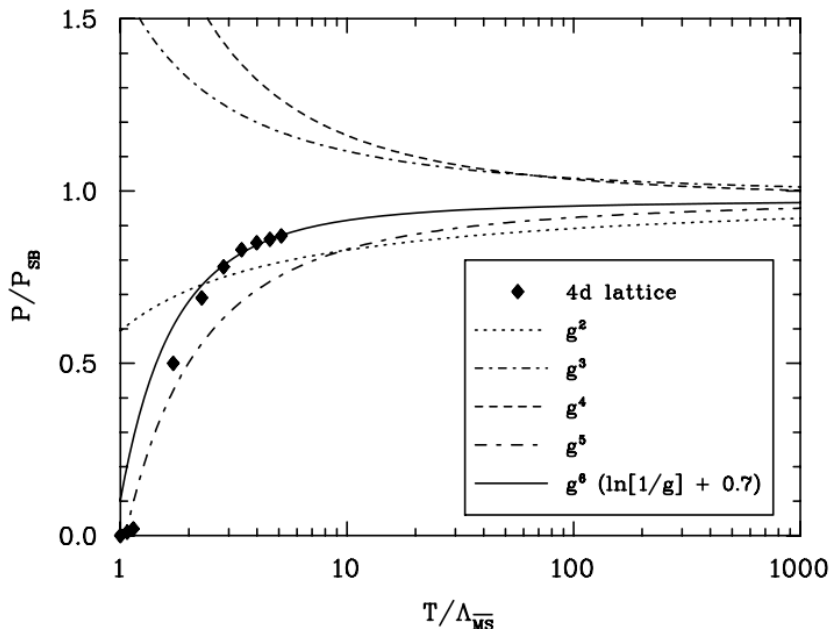


Figure 2.3.: Results of perturbative calculations of the pure Yang-Mills theory equation of state $p(T)$, normalized to the Stefan-Boltzmann limit of the pressure (B.10). Reproduced from [6]. Note that within perturbation theory any deviation from the Stefan-Boltzmann behavior (B.10) is a purely quantum effect.

Conclusions

As is evident from the above discussion, perturbation theory applied to QCD and Yang-Mills theory thermodynamics describes well the high-temperature behavior of the theory. It

¹⁰The quantity $\Lambda_{\overline{MS}}$ is the energy scale of the \overline{MS} regularization scheme. It is of the order of the deconfinement temperature.

reproduces to some extent the lattice calculations of the QGP equation of state in the region $T/T_c^{QCD} \gtrsim 4$, while for the pure gluon plasma, (forgetting the semi-phenomenological result of the g^6 -order) naive perturbation theory is a good description for $T/T_c^{YM} \gtrsim 100$. However, close to the deconfinement transition, $T \approx T_c$, neither the QGP nor the pure Yang-Mills plasma can be well described within perturbation theory. Thus, to understand the mechanism of the confinement-deconfinement transition and the origin, as well as the quantitative form of the trace anomaly, a different description is needed.

2.2.4. Lattice Gauge Theory

Lattice gauge theory has become the standard tool for computations in the strongly coupled regimes of QCD and Yang-Mills theory and is by now a field of science for itself. The basic concept is simple: the spacetime is discretized and the partition function is directly evaluated on a now finite number of the spacetime points. A Wick rotation is performed to ensure the convergence of the path integral. Computing e.g. a Green's function between two spacetime points x_1 and x_2 , all¹¹ paths from x_1 to x_2 are considered. The weighting factor e^{-S} then ensures that shorter paths give a larger contribution. To improve the convergence behavior, the action S is often improved, see chapter 10 of [6]. Finite temperature T is introduced in the usual way by integration of the Wick rotated time τ from 0 to $\beta_\tau = 1/T$. After calculating the relevant observables on different lattice sizes, the continuum extrapolation is carried out to obtain the final prediction.

Lattice gauge theory yields robust results for the equation of state of the Yang-Mills theory, as well as for the QCD phase diagram in the direct vicinity of the T axis. The extraction of viscosities is more difficult since, to employ the Kubo formulae (see section 6.1), an analytic continuation of the Euclidean correlator must be performed. This procedure is ambiguous for a correlator that is computed on a finite number of frequencies. Thus, without additional assumptions, no accurate lattice gauge theory prediction for the viscosities exists up to now.

2.3. The AdS/QCD correspondence

In sections 2.2.3 and 2.2.4 two standard theoretical approaches to the thermodynamics of QCD and Yang-Mills theory were described: the resummed perturbation theory and lattice gauge theory. As discussed in section 2.2.3, perturbation theory suffers from the conceptual problem that contributions of the order g^6 and higher cannot be completely

¹¹Often not all paths are considered, but rather those with a given maximum length.

computed, thus pointing at a manifestly non-perturbative behavior of the theories, which is important already for temperatures $T/T_c \approx 4$ and $T/T_c \approx 100$ for QCD and Yang-Mills theory, respectively. Lattice QCD, although being able to compute some observables in the non-perturbative regime, is an unsatisfactory approach in the sense that the mechanisms underlying in particular confinement and chiral symmetry restoration remain obscured. In addition, lattice QCD has its own problems, most notably the difficulties in calculations with a finite baryochemical potential μ_B of the order of the temperature $\mu_B \propto T$, and, as mentioned in section 2.2.4, the extraction of the transport coefficients of the QGP and Yang-Mills plasma. It is thus desirable to find a theoretical method, which would allow for analytic calculations in the strongly coupled regime. One such method, the AdS/CFT correspondence, was indeed recently discovered by Maldacena [9]. Maldacena conjectured that a certain kind of string theory is dual (i.e. equivalent) to a special quantum field theory. While the full conjecture is certainly theoretically interesting by itself, a simpler version of it provides a valuable new tool for the understanding of strongly coupled field theories. In essence, the statement is that a strongly coupled large- N field theory can be described by a classical theory of gravity, the latter being provided by Einstein's general theory of relativity. The drawback of this method is the $N \rightarrow \infty$ (meaning large- N) limit, which has to be taken to obtain classical instead of quantized string theory, while, in QCD, $N = 3$. Nevertheless, Maldacena's conjecture sparked a by now vast field of research in purely theoretical, as well as in phenomenological physics. We now proceed to sketch the ideas leading to the correspondence, review its "canonical" version and establish the mapping between the gravity and the gauge theories. After briefly discussing the applicability to "realistic" theories like QCD, we will employ the correspondence to understand the equilibrium and near-equilibrium properties of the $SU(3)$ Yang-Mills theory thermodynamics.

3. The AdS/CFT correspondence

It is beyond the scope of this thesis to give a rigorous introduction to superstring theory, within which the AdS/CFT correspondence was derived. We will thus mention the necessary basic facts and give a sketch of the derivation. Readers interested in string theory are referred to [10–12]. In appendix D we list a number of reviews of the correspondence. The following discussion is mainly based on [13].

3.1. String theory and branes

3.1.1. String theory

String theory is one of the candidate theories for quantum gravity.¹ The fundamental concept of string theory is that elementary particles are not pointlike as in today's Standard Model, but are instead 1-dimensional objects: open and closed strings. It is thought that, on energy scales, and thus spatial resolutions available today, the elementary particles appear pointlike and their extended nature can not yet be probed. The basic action principle of string theory is the generalization of the action principle for a pointlike particle in curved space. While the pointlike particles minimize its world-line (i.e. moves along a geodesic), the string minimizes its, now 2-dimensional, world-sheet. The action can straightforwardly be further generalized to membranes, usually called p -branes, (higher dimensional objects of dimension $p > 1$, $p < d$, where d is the space-time dimension) minimizing their world-volume. The Polyakov (also called sigma model) action for a string is given by

$$S = -\frac{1}{2}T_s \int d\sigma d\tau \sqrt{-h} h^{\alpha\beta} \partial_\alpha X_\mu \partial_\beta X^\mu, \quad (3.1)$$

where $X^\mu(\sigma, \tau)$, $\mu = 1, \dots, d$ are the functions embedding the string world-sheet into a curved background spacetime of dimension d , and $h^{\alpha\beta}(\sigma, \tau)$, $\alpha = 1, 2$ is the world-sheet metric. The dimensionful constant $T_s = (2\pi\alpha')^{-1}$ is the string tension, where $\alpha' = l_s^2$ and

¹Since the 4-dimensional Newton constant G_4 is a dimensionful quantity (as seen from (A.1) in 4 dimensions), Einstein's general theory of relativity is non-renormalizable and is thus thought to be a low-energy effective theory of a more fundamental as yet unknown theory of quantum gravity.

l_s denotes the string length. To solve the equations of motion for $X^\mu(\sigma, \tau)$ following from (3.1), boundary conditions need to be specified. For the closed string, one requires periodicity of X^μ in σ ; for the open string one can require Neumann boundary conditions for all μ (no momentum flowing through the ends of the string) or Dirichlet boundary conditions for some $\mu = 1, \dots, d - p - 1$ (the two ends of the open string are fixed in $p - 1$ spatial directions) and Neumann boundary conditions for the remaining $d - p$ spatial coordinates. Neumann boundary conditions respect Poincaré invariance, while Dirichlet boundary conditions break it. The Dirichlet boundary conditions correspond to the ends of the string being attached to an extended dynamical object called Dp -brane, which is a special type of a p -brane mentioned above. With the boundary conditions specified, the equations of motion for X^μ can then be solved in terms of mode expansions of left/right-moving and standing waves for closed and open strings, respectively. With the mode expansion at hand the theory can be quantized, in analogy to the field theory quantization in terms of the plane wave expansion.² One has to make sure to retain only the physical states. They are then labeled by their mass m and angular momentum s , to be identified with a particle of mass m and spin s . Every string theory has a massless spin-2 particle in its closed string spectrum, which is identified with the graviton. String interactions are governed by the string coupling parameter g_s .

The condition of physical states fixes the spacetime dimension to $d = 26$, i.e. 1 time dimension and 25 space dimensions.³ Introduction of supersymmetry⁴ reduces the spacetime dimension of the critical string theory to $d = 10$, which is referred to as superstring theory. The spectrum has to be truncated to ensure consistent supersymmetry. There are different possibilities, depending on the chosen different superstring theories (IIA superstring theory or IIB superstring theory) arise.⁵ Their low-energy effective theories⁶ are type IIA and type IIB supergravity, respectively, which are supersymmetric generalizations of Einstein's classical theory of general relativity. Dp -branes can be consistently added to type IIA or IIB superstring theories. The possible dimensions p of the branes are constrained.

²From the Poisson brackets of X^μ and its canonical momentum conjugate the Poisson brackets for the Fourier coefficients of the modes are obtained. The Poisson brackets are then replaced by commutators. Note that, in string theory, this is the "first" quantization.

³String theory in $d = 26$ dimensions is called critical string theory. There is a possibility for a consistent formulation in $d < 26$, which is called non-critical string theory. This possibility is however often not considered.

⁴We will not explain supersymmetry in detail, but just note that it is a symmetry which interrelates bosons and fermions.

⁵IIA and IIB superstring theories are two of the five different superstring theories. They are distinguished by their string content (open and/or closed), their treatment of left- and right-moving modes (equivalent or non-equivalent) and the chirality of massless fermions (chiral symmetry present or not), see e.g. [12].

⁶One integrates out the massive modes to retain only the massless ones. Then, the limit $\alpha' \rightarrow 0$ is taken. See also section 3.2.

3.1.2. p -branes and Dp -branes

The holographic duality of a theory of quantum gravity and a quantum field theory can be traced back to two different possibilities to describe p -branes.

p -branes in supergravity

On the one hand, p -branes are known as solutions of supergravity theories. They can be viewed as generalizations of the Reissner-Nordström black hole, which is the spherically symmetric solution of the Einstein equations with the energy momentum tensor of electrodynamics. Analogously to the electrically charged Reissner-Nordström black hole, p -branes can carry charge of the non-Abelian fields present in supergravity. The dimension of p -branes is not constrained to two, (as the horizon of the four-dimensional Reissner-Nordström black hole) but is determined by the maximum dimension and type of the supergravity theory under consideration. They can also have planar instead of spherical geometries. As the Reissner-Nordström black hole, p -branes can be “extremal”, i.e. have zero Hawking temperature (B.1).

Dp -branes in superstring theory

On the other hand, Dp -branes can be consistently defined in superstring theory as hypersurfaces on which open strings can end. Their dimension is again determined by the type of superstring theory under consideration. One can consider the dynamics of just the strings attached to one or more Dp -branes; as we will see these are closely related to super-Yang-Mills theory.

It was realized by Polchinski [14] that both viewpoints are actually describing the same object. As we will see, the AdS/CFT correspondence will emerge when we consider D3-branes in IIB string theory and supergravity and compare the appropriate limits on both sides, that is of the 3-brane metric on the supergravity side and of the superstring theory containing D3-branes.

3.2. A sketch of the derivation

The AdS/CFT correspondence, also called gauge/gravity or holographic duality, was first conjectured by Maldacena in [9] for type IIB string theory on $AdS_5 \times S^5$ and $\mathcal{N} = 4$ super-Yang-Mills (SYM) theory in 4 dimensions.⁷

⁷The quantity \mathcal{N} is the number of supersymmetry generators, see e.g. [15].

3.2.1. Supergravity side

Consider the 3-brane solution to the IIB supergravity equations of motion, (see section 1.3.1 of [13] for the derivation) given by the following infinitesimal line element squared

$$ds^2 = f^{-1/2}(-dt^2 + dx_1^2 + dx_2^2 + dx_3^2) + f^{1/2}(dr^2 + r^2 d\Omega_5^2), \quad (3.2)$$

$$f = 1 + \frac{R^4}{r^4}, \quad (3.3)$$

where R is a parameter which determines the "size" of the 3-brane. Here, t, x_1, x_2, x_3 are the coordinates on the 3-brane; r is the "radial" coordinate perpendicular to the brane, and Ω_5 is a 5-sphere. Consider the limit of the geometry far from the branes, $r \gg R$; in this case, $f \approx 1$. Then one has

$$ds^2 = -dt^2 + dx_1^2 + dx_2^2 + dx_3^2 + dr^2 + r^2 d\Omega_5^2, \quad (3.4)$$

i.e. a 10-dimensional Minkowski space. Now consider the limit $r \ll R$, i.e. close to the branes (this region is referred to as the "throat region"). In this case $f \approx R^4/r^4$ and one gets

$$ds^2 = \frac{r^2}{R^2}(-dt^2 + dx_1^2 + dx_2^2 + dx_3^2) + \frac{R^2}{r^2}dr^2 + R^2 d\Omega_5^2. \quad (3.5)$$

The metric (3.5) is $AdS_5 \times S^5$, i.e. a product of a 5-dimensional anti-deSitter space in Poincaré coordinates and a 5-sphere. Both have the "radius" R . Perform a coordinate transformation $r/R = R/z$ to transform into Fefferman-Graham coordinates:

$$ds^2 = \frac{R^2}{z^2}(-dt^2 + dx_1^2 + dx_2^2 + dx_3^2 + dz^2) + R^2 d\Omega_5^2. \quad (3.6)$$

Return to the metric given by (3.2) and consider low-energy excitations with respect to an observer at infinity, i.e. at $r = \infty$. These can be massless excitations in the Minkowski region (3.4) or, due to the redshift factor $f^{-1/4}$, excitations of any energy E_r in the throat region (3.5).⁸ One thus has superstring theory in the throat region and supergravity in the Minkowski region. The two theories decouple: The low-energy excitations of the Minkowski region cannot be absorbed by the brane as their wavelength is much greater than the "size" R of the brane; the excitations close to the brane are confined to the throat region due to the gravitational potential.

One has thus two decoupled theories: IIB supergravity theory in Minkowski space (3.4) and IIB superstring theory on $AdS_5 \times S^5$ (3.5) close to the branes.

⁸Denoting by E the energy of the latter ones measured at infinity one has $E = f^{-1/4}E_r$.

3.2.2. String theory side

It is possible to consistently define the limit of N coincident D3-branes. Type IIB superstring theory in 10 dimensions with N coincident D3-branes extended in 4 dimensions (one time, three spatial) contains open strings with ends on the D3-branes and closed strings. The open strings describe the excitations of the branes, and the closed strings describe the excitations of empty space. Integrating out the massive string modes one obtains the effective low-energy theory which contains only massless strings. The action of the low-energy theory is given schematically by

$$S = S_{bulk} + S_{brane} + S_{int}, \quad (3.7)$$

with

$$S_{bulk} = S_{IIB \text{ Sugra}} + S_{c,corr}, \quad (3.8)$$

$$S_{brane} = S_{SYM} + S_{o,corr}. \quad (3.9)$$

Here, S_{bulk} is the action describing the closed string dynamics in empty space; it contains $S_{IIB \text{ Sugra}}$, i.e. IIB supergravity, and higher derivative closed strings corrections $S_{c,corr}$. The action on the branes S_{brane} gives rise to a $\mathcal{N} = 4$ $SU(N)$ ⁹ super-Yang-Mills theory S_{SYM} with higher derivative corrections $S_{o,corr}$ due to open string dynamics. The corrections $S_{c,corr}$ and $S_{o,corr}$, as well as the interaction between the branes and the bulk, S_{int} , are proportional to powers of α' . Take the limit $\alpha' \rightarrow 0$ keeping fixed all dimensionless parameters, including g_s and N . The corrections terms as well as the bulk-brane interaction terms vanish and one is left with two decoupled theories: the 4-dimensional SYM theory on the branes and the IIB supergravity theory.

3.3. The correspondence

We have seen that, from the point of view of supergravity as well as from the point of view of superstring theory, one obtains two decoupled theories when considering the low-energy limit of the 3-brane theories. In the first case, one has free IIB supergravity in the Minkowski region and the full IIB superstring theory on $AdS_5 \times S^5$; in the second case one has free IIB supergravity in the bulk and the SYM theory on the branes. The free theory

⁹Actually, the gauge group of the SYM theory is $U(N)$, which is locally equivalent to a free $U(1)$ vector multiplet times a $SU(N)$ gauge theory. The $U(1)$ multiplet describes the center of mass motion of the branes and one generally regards it as decoupled. See however the discussion on page 58 of [13].

in both cases is supergravity in flat space. Maldacena's conjecture was to identify the two theories close to and on the branes. The statement is thus [9]:

Type IIB superstring theory on $AdS_5 \times S^5$ is equivalent (i.e. dual) to $\mathcal{N} = 4$ $SU(N)$ super-Yang-Mills theory in 4 dimensions.

3.3.1. Regimes of validity

The parameter R in the IIB supergravity 3-brane solution (3.2) is related to the superstring theory parameters by

$$R^4 = 4\pi g_s \alpha'^2 N. \quad (3.10)$$

The string coupling g_s is related to the SYM coupling constant by

$$g_{YM}^2 = 4\pi g_s \quad (3.11)$$

which gives with (3.10)

$$R^4 = \alpha'^2 g_{YM}^2 N. \quad (3.12)$$

The conjecture stated above was in its strongest form: The full quantized IIB superstring theory is dual to $\mathcal{N} = 4$ $SU(N)$ super-Yang-Mills theory for any value of the respective parameters. By taking appropriate limits one can deduce its weaker forms.

Keep $g_s N$ fixed and take the limit $g_s \rightarrow 0$. This corresponds to the large- N (called t'Hooft) limit of quantum field theory and yields classical instead of quantized¹⁰ superstring theory. The quantum field theory coupling (often called t'Hooft coupling) in the large- N limit is $\lambda \equiv g_{YM}^2 N$. The conjecture now becomes:

Type IIB classical superstring theory on $AdS_5 \times S^5$ is equivalent (i.e. dual) to the large- N limit of $\mathcal{N} = 4$ $SU(N)$ super-Yang-Mills theory in 4 dimensions.

To obtain the supergravity limit from classical string theory let further be $\alpha'/L^2 \rightarrow 0$, where L denotes the typical curvature scale of a spacetime. Equation (3.12) yields

$$\frac{\alpha'^2}{R^4} = \frac{1}{g_{YM}^2 N} \rightarrow 0, \quad (3.13)$$

¹⁰The parameter N in equation (3.10) is actually a quantum of charge of a 5-index antisymmetric field F_5 , appearing in IIB superstring theory (see section 1.3.1 of [13] and references therein). It is not known how to quantize IIB string theory on a curved spacetime with $F_5 \neq 0$.

and consequently

$$\lambda = g_{YM}^2 N \rightarrow \infty. \quad (3.14)$$

The correspondence becomes now:

Type IIB supergravity on $AdS_5 \times S^5$ is equivalent (i.e. dual) to the large- N , strongly coupled limit of the $\mathcal{N} = 4$ $SU(N)$ super-Yang-Mills theory in 4 dimensions.

From (3.13) one learns an important fact: The supergravity approximation is valid when the super-Yang-Mills theory is strongly coupled. Supergravity thus yields a new method to do calculations in super-Yang-Mills theory. The big advantage is the fact that the supergravity description is valid at strong coupling. In this sense, it is complementary to perturbation theory and provides a tool for the solution of large- N quantum field theory in a regime where no analytical methods were previously known. One could also use the conjecture the other way around to describe strongly coupled string theory by means of a weakly coupled quantum field theory. Equation (3.13) is also the reason why the conjecture is called a duality: strong coupling of one theory translates into weak coupling of the other.¹¹ This fact makes the conjecture difficult to test: when one side is weakly coupled and calculable, the other side is strongly coupled and difficult to compute.

Looking at equation (3.13) one might be tempted to keep N fixed and let $g_s \propto g_{YM}^2 \rightarrow \infty$, i.e. perform a limit, which would be better suited for QCD. In this limit however a weakly coupled supergravity approximation is not possible, see page 60 of [13].

Note that in the strongest form of the conjecture, the spacetime is required to be $AdS_5 \times S^5$ only asymptotically. This is the analogue of the condition of asymptotic flatness.

3.3.2. Tests of the correspondence

Here, we briefly summarize the evidences for the validity of the correspondence. As the foregoing discussion suggests, one should compare properties that do not depend on the coupling, since it is not clear how to compare a gauge theory quantity calculated on the one hand within perturbation theory at weak coupling and on the other hand within the supergravity theory at strong coupling. We list two properties and refer the reader to [13] for further properties and details.

¹¹On the gravity side, weak coupling means that the curvature of the spacetime is small. In the context of string theory this means that, as expressed by equation (3.13), the string corrections to the Einstein gravitational theory are negligible.

- The global symmetry groups of both the $\mathcal{N} = 4$ SYM theory and the IIB supergravity on $AdS_5 \times S^5$ coincide. In addition to Poincaré symmetry, $AdS_5 \times S^5$ is invariant under the full conformal symmetry group.¹² On the gauge theory side this is reflected by the vanishing of the β function of the $\mathcal{N} = 4$ SYM theory.
- Some supersymmetric SYM operators are "protected" from renormalization as their masses and spins are exactly related to invariants of the supersymmetry group. The spectra of these on both sides were successfully matched.

3.3.3. AdS_5/CFT_4 correspondence

One can conformally compactify the d -dimensional AdS_d space. The boundary is then a $(d - 1)$ -dimensional space, identical to the conformal compactification of a $(d - 1)$ -dimensional Minkowski space.¹³ This identity leads to the picture that, in the context of the AdS/CFT correspondence, the 4-dimensional SYM theory "lives" on the boundary of AdS_5 . It is thus natural to decompose the fields on the whole $AdS_5 \times S^5$ spacetime into spherical harmonics on S^5 . This procedure (referred to as "Kaluza-Klein compactification") introduces effective masses (dependent on the harmonic) of fields, which now "live" only on AdS_5 . This leads to an important variant of the duality: Gravity on AdS_5 is dual to a 4-dimensional conformal field theory, the latter "living" on the boundary of AdS_5 in the sense just described. This form of the conjecture can be viewed as a manifestation of the holographic principle.¹⁴ It can further be motivated by

- Non-critical string theory on AdS_5 .
- "Geometrizing" the renormalization group (RG) flow [17]. The 5th (often referred to as "radial" or "holographic") coordinate of the AdS_5 is viewed as the inverse of the RG energy scale μ , the latter introduced in 2.1.2. One merges the ordinary spacetime dynamics with the RG dynamics of a gauge theory into a unified description. This unification is manifest on the gravity side, since the gravity equations of motion treat all coordinates equally. A concrete ansatz for the metric will however reflect the special role of the holographic coordinate.

¹²The conformal transformations include the Poincaré transformations and in addition the scalings and special conformal transformations.

¹³The compactified Minkowski space is invariant under the full conformal group, see e.g. [16].

¹⁴See the last paragraph of appendix B.1 and references therein.

3.4. Mapping between AdS and CFT

The mapping between the gravity theory and the field theory can be formulated without the use of string theory or supersymmetry. We will thus only consider “standard“ field theory operators and correlators; in particular the operators $\text{Tr}(F_{\mu\nu}F^{\mu\nu})$, J^μ and $T^{\mu\nu}$, where $F^{\mu\nu}$ is the gauge field strength tensor, J^μ is a conserved gauge theory current and $T^{\mu\nu}$ is the gauge theory energy momentum tensor. The gravity theory relevant for us will be the general theory of relativity, see appendix A.1.¹⁵

3.4.1. Field-Operator Correspondence

The general prescription

From the discussion of section 3.1.2 and from the analogy with the Reissner-Nordström black hole it is straightforward to motivate the prescription that the gravity field dual to a given field theory operator is its conjugated field. When constructing the correlators in the next section we will explicitly make use of this prescription. The gauge theory operator has to be local and gauge invariant. One thus has:

- $T^{\mu\nu}$ is dual to the gravity theory metric tensor $g_{\mu\nu}$,
- $\text{Tr}(F_{\mu\nu}F^{\mu\nu})$ is dual to a scalar field ϕ in the gravity theory,¹⁶
- J^μ is dual to a gauge field A_μ in the gravity theory.

When considering other fields than the metric $g_{\mu\nu}$ within the gravity theory one has two options:

1. The fields interact with the metric and thus change the geometry of spacetime.
2. The metric is static and the fields “live” on the fixed background spacetime.

Within Einstein’s general theory of relativity the first possibility amounts to including the desired fields into the energy momentum tensor and solving the Einstein equations, whereas the second possibility does not require a solution of the Einstein equations but, instead, changes the equations of motions of the fields in question. For example, the differential operator in the Klein-Gordon equation for a scalar field ϕ will depend on the metric via $D_\mu D^\mu \phi = (\sqrt{-g})^{-1} \partial_\mu (\sqrt{-g} \partial^\mu \phi)$. It depends on the application which of the two options should be used, see also section 3.5.2.

¹⁵In some applications classical strings are used, see e.g. section 7.1 of [17].

¹⁶Every string theory contains a scalar field in its spectrum, usually referred to as dilaton. It plays the role of the string coupling constant g_s , where a non-trivial dilaton profile leads to a variable string coupling g_s .

3.4.2. A massive scalar field Φ on AdS_5

Consider for the purpose of illustration a free scalar field $\Phi(X) = \Phi(z, x^\mu)$ of mass M in AdS_5 . For definiteness, we use the Fefferman-Graham coordinates for AdS_5 . The action for Φ is given by

$$S = -\frac{1}{2} \int d^5 X \sqrt{-g} \left[\partial_N \Phi \partial^N \Phi + M^2 \Phi^2 \right]. \quad (3.15)$$

Introduce the Fourier transform $\Phi(z, k^\mu)$ with respect to the x^μ -coordinates by

$$\Phi(z, k^\mu) = \int \frac{d^4 x}{(2\pi)^4} e^{-ikx} \Phi(z, x^\mu), \quad (3.16)$$

where $kx \equiv \eta_{\mu\nu} k^\mu x^\nu$ is the scalar product in Minkowski space and $k^\mu = (\omega, \vec{k})$. The equation of motion for a Fourier mode $\Phi(z, k^\mu) \equiv \Phi_k(z)$, following from the action (3.15) is

$$z^5 \partial_z (z^{-3} \partial_z \Phi_k) + \mu^2 z^2 \Phi_k - M^2 L^2 \Phi_k = 0, \quad (3.17)$$

where we have defined the 4-dimensional invariant mass $\mu^2 \equiv -k^\mu k_\mu$ and L is the "radius" of AdS_5 . The solution of (3.17) is given by

$$\Phi_k(z) = C_1(k) z^2 Y_\nu(\mu z) + C_2(k) z^2 J_\nu(\mu z), \quad (3.18)$$

where J_ν and Y_ν are Bessel functions of respectively the first and second kind, $C_1(k)$ and $C_2(k)$ are integration constants and

$$\nu = \sqrt{4 + M^2 L^2}. \quad (3.19)$$

Expanding equation (3.18) around $z = 0$ one obtains^{17,18}

$$\Phi_k(z) = A(k) z^{2-\nu} + B(k) z^{2+\nu}, \quad (3.20)$$

where $A(k)$ and $B(k)$ are combinations of $C_1(k)$ and $C_2(k)$. Fourier transforming back into position space one has for $z \rightarrow 0$

$$\Phi(z, x^\mu) = A(x) z^{2-\nu} + B(x) z^{2+\nu}. \quad (3.21)$$

¹⁷The expansion in (3.20) is valid for $\nu \notin \mathbb{Z}$. For $\nu \in \mathbb{Z}$, the expansion of Y_ν contains terms $\propto \ln z$. See e.g. [18].

¹⁸Equation (3.20) can also be obtained directly by solving the equation (3.17) after neglecting the $\mu^2 z^2 \Phi_k$ term.

Define

$$\Delta_{\pm} = 2 \pm \nu = 2 \pm \sqrt{4 + M^2 L^2} \quad (3.22)$$

to rewrite equation (3.22) as

$$\Delta(\Delta - 4) = M^2 L^2, \quad (3.23)$$

where Δ_+ and Δ_- are the respective larger and smaller roots of (3.23). We define Δ as

$$\Delta \equiv \Delta_+. \quad (3.24)$$

Equation (3.21) can be rewritten as

$$\Phi(z, x^\mu) = A(x)z^{4-\Delta} + B(x)z^\Delta. \quad (3.25)$$

Equation (3.22), or equivalently (3.23), is referred to as mass-dimension relation. The form stated is valid only for scalar fields; for the mass-dimension relations of vectors, tensors, etc., see page 85 of [13].

The limit $\Phi(z \rightarrow 0, \mathbf{x}) = \Phi_0(\mathbf{x})$

Note from equation (3.25) that, in order to have a well-defined constant value $\Phi_0(x) \equiv A(x)$ on the boundary $z = 0$, one has to modify the boundary conditions to

$$\Phi_0(x) \equiv \Phi(0, x) = \lim_{z \rightarrow 0} z^{\Delta-4} \Phi(z, x). \quad (3.26)$$

For a massless scalar field, equation (3.19) yields $\Delta = 4$ and the limit of (3.26) becomes trivial.

Breitenlohner-Freedman bound

It is evident from equation (3.19) that the exponents of equation (3.21) are real if

$$M^2 L^2 \geq -4. \quad (3.27)$$

The inequality (3.27) is known as the Breitenlohner-Freedman (BF) bound. It was shown in [19,20] that, as long as the scalar field Φ of mass M satisfies the bound (3.27), the theory is stable (i.e. it does not contain modes which grow exponentially with time). Thus, $M^2 < 0$ is allowed, as long as (3.27) is satisfied.

Normalizable and non-normalizable modes

Define the scalar product in AdS_5 by

$$\langle \Phi_1 \Phi_2 \rangle = -i \int_{\Sigma_t} d^5 X \sqrt{-g} g^{tt} \left(\Phi_1^* \partial_t \Phi_2 - \Phi_2 \partial_t \Phi_1^* \right), \quad (3.28)$$

where Σ_t is a constant time slice. Inserting the asymptotic behavior (3.25) one sees that

- for $\Delta > 2$ the solution $\propto B(x)$ is normalizable, while the solution $\propto A(x)$ is non-normalizable,
- for $1 \leq \Delta \leq 2$ both solutions are normalizable.

Since a non-normalizable mode should not correspond to a physical state, one concludes (due to the lack of other options) that it acts as a source for the dual operator \mathcal{O} of the boundary gauge theory. One thus has

$$S_{GAUGE} \rightarrow S_{GAUGE} + \int d^4 x A(x) \mathcal{O}(x), \quad (3.29)$$

where

$$A(x) \equiv \Phi_0(x) = \lim_{z \rightarrow 0} z^{\Delta-4} \Phi(z, x), \quad (3.30)$$

as defined by equation (3.26).

The normalizable mode $\propto B(x)$ is an element of the AdS_5 -theory Hilbert space. Since, if the gauge theory is to be equivalent to the gravity theory, their Hilbert spaces should be isomorphic (see section 3.4 of [13]), one concludes that the mode $\propto B(x)$ describes a state of the boundary theory. In fact, (see appendix C of [17] and references therein) $B(x)$ determines the expectation value of the operator \mathcal{O} dual to Φ in the presence of a source Φ_0 as

$$\langle \mathcal{O}(x) \rangle_{\Phi_0} = 2\nu B(x). \quad (3.31)$$

For $A(x) \equiv \Phi_0(x) = 0$, equation (3.31) yields the expectation value $\langle \mathcal{O}(x) \rangle$. With equations (3.30) and (3.31) one can now rewrite equation (3.25) as

$$\Phi(z, x) = \frac{\langle \mathcal{O}(x) \rangle_{\Phi_0}}{2\nu} z^\Delta + \Phi_0(x) z^{4-\Delta}. \quad (3.32)$$

Equations (3.29), (3.31) and (3.32) imply that Δ is the scaling dimension of the operator \mathcal{O} , see section 5.1.5 of [17], thus justifying the term “mass-dimension relation” for equation (3.23).

In the case when $1 \leq \Delta \leq 2$, both modes of Φ are normalizable. In this case, either of the modes can be used to build the Hilbert space of the boundary theory [21]. We will not consider this case and assume instead that $\Delta > 2$.

3.4.3. Correlators

The general prescription

The holographic calculation of the correlators was established in [22, 23]. The correlators are constructed within the path-integral formulation of quantum field theory. We assume the AdS_5/CFT_4 -form of the correspondence (see section 3.3.3), and perform a Wick rotation to work in Euclidean AdS space. We use Fefferman-Graham coordinates for AdS_5 . The partition functions of the string theory and of the gauge theory are identified:

$$\mathcal{Z}[\Phi(z, x); \lim_{z \rightarrow 0} \Phi(z, x) = \Phi_0(x)]_{STRING} = \mathcal{Z}[\Phi_0(x)]_{GAUGE}. \quad (3.33)$$

Here, $\Phi_0(x)$ stands for a source of the corresponding gauge theory operator \mathcal{O} , the limit $\lim_{z \rightarrow 0} \Phi(z, x) = \Phi_0(x)$ is to be understood as in (3.26) and

$$\mathcal{Z}[\Phi_0]_{GAUGE} = \int \mathcal{D}\mathcal{O} e^{-S[\mathcal{O}] + \int d^4x \Phi_0 \mathcal{O}}. \quad (3.34)$$

From (3.34) n-point correlation functions G_n of \mathcal{O} are obtained via

$$\begin{aligned} G_n(x_1, \dots, x_n) &\equiv \int \mathcal{D}\mathcal{O} e^{-S[\mathcal{O}]} \mathcal{O}(x_1) \dots \mathcal{O}(x_n) \\ &= \frac{\delta^n}{\delta \Phi_0(x_1) \dots \delta \Phi_0(x_n)} \mathcal{Z}[\Phi_0]_{GAUGE} \Big|_{\Phi_0(x_i)=0}. \end{aligned} \quad (3.35)$$

In the weakest form of the correspondence, the quantized string theory becomes a classical gravity theory, and the steepest descent approximation is used to obtain

$$\mathcal{Z}[\Phi]_{STRING} \approx \mathcal{Z}[\Phi]_{GRAV,cl} = e^{-S_{GRAV}[\Phi_{cl}(z, x_i); \Phi_0(x_i)]}, \quad (3.36)$$

where $S_{GRAV}[\Phi_{cl}(z, x_i); \Phi_0(x_i)]$ is the action of the gravity theory evaluated on the classical solution $\Phi_{cl}(z, x)$ with the boundary condition $\Phi_{cl}(z \rightarrow 0, x_i) = \Phi_0(x_i)$. Insert (3.36) into (3.35) using the identification (3.33) to obtain¹⁹

$$G_n(x_1, \dots, x_n) = \frac{\delta^n}{\delta \Phi_0(x_1) \dots \delta \Phi_0(x_n)} e^{-S_{GRAV}[\Phi(X_i); \Phi_0(x_i)]} \Big|_{\Phi_0(x_i)=0}. \quad (3.37)$$

¹⁹From now on, we drop the subscript, $\Phi \equiv \Phi_{cl}$.

Equations (3.33) and (3.37) have a nice heuristic interpretation exhibited in figure 3.1. A correlation between two spacetime points of the 4d boundary field theory (i.e. along the circle in figure 3.1) can be calculated in the 5d bulk gravity theory (i.e. in the interior of the circle in figure 3.1). A quantum gravity correction to the correlator would correspond to a closed loop in an interior line or in a vertex in figure 3.1.



Figure 3.1.: Witten diagrams: empty AdS, tree-level 2-point, 3-point, and two 4-point correlators (from left to right). Reproduced from [15].

Evaluation of S_{GRAV}

The action $S_{GRAV}[\Phi]$ is evaluated as follows:

1. The equations of motion following from $S_{GRAV}[\Phi, \Phi_0]$ are solved. The boundary conditions that need to be imposed are:
 - close to the boundary, i.e. for $z \rightarrow 0$, $\Phi(z, x) \rightarrow \Phi_0(x)$ as defined by equation (3.26),
 - in the interior of AdS_5 , i.e. for $z \rightarrow \infty$, $\Phi(z, x)$ is to be regular.

The solution $\Phi(z, x)$ can be obtained in two equivalent ways:

- Define the bulk-to-boundary propagator $K(z, x; x')$ by

$$\lim_{z \rightarrow 0} D_\Phi K(z, x; x') = \delta^{(4)}(x - x'), \quad (3.38)$$

where D_Φ denotes schematically the differential operator following from the Euler-Lagrange equations of $S_{GRAV}[\Phi, \Phi_0]$. Calculate $K(z, x; x')$. The solution is given by

$$\Phi(z, x) = \int d^4 x' K(z, x; x') \Phi_0(x'). \quad (3.39)$$

- Determine the general solution of the equations of motion. The integration constants are fixed by the boundary conditions.

2. Using integration by parts $S_{GRAV}[\Phi, \Phi_0]$ is rewritten as a sum of terms vanishing upon the use of the equations of motion, and total derivatives vanishing in all directions except in the direction of the radial coordinate. Since the AdS_5 metric diverges at the boundary, a cutoff ϵ is introduced for the radial coordinate, i.e. one replaces $z \rightarrow 0$ with $z = \epsilon$. The resulting expression is evaluated using (3.39) and keeping only leading terms in ϵ . The correlator is then given by employing (3.37) and subsequently taking the limit $\epsilon \rightarrow 0$.
3. When performing the second step one potentially encounters divergences which, in general, have to be regularized using the procedure of "holographic renormalization", see [24]. Local counterterms are added to obtain the renormalized action $S_{GRAV}^{[ren]} = S_{GRAV} + S_{ct}$, where $S_{GRAV}^{[ren]}$ is now free of divergences in the limit $z \rightarrow 0$.

Remarks

- See appendix C of [17] and section 4.4 of [25] for a calculation of $\langle \mathcal{O}(x)\mathcal{O}(y) \rangle$, where \mathcal{O} is dual to a scalar field Φ .
- Note that, within the path-integral formalism, the expectation value of an operator in the presence of a source Φ_0 is given by

$$\langle \mathcal{O}(x) \rangle_{\Phi_0} \equiv \frac{\delta S_{GAUGE}^{[ren]}[\Phi_0]}{\delta \Phi_0} = \lim_{z \rightarrow 0} z^{4-\Delta} \frac{\delta S_{GRAV}^{[ren]}[\Phi(z, x), \Phi_0]}{\delta \Phi(z, x)}. \quad (3.40)$$

Thus, one concludes that, as one might intuitively expect from equation (3.25) or (3.32), given the source Φ_0 , i.e. the leading behavior of $\Phi(z, x)$ for $z \rightarrow 0$, one can obtain the expectation value $\langle \mathcal{O}(x) \rangle_{\Phi_0}$, i.e. the sub-leading $z \rightarrow 0$ behavior of $\Phi(z, x)$, by functional differentiation as defined by (3.40).

3.5. Application to Yang-Mills theory

3.5.1. Limitations

The AdS/CFT correspondence, though conceptually interesting by itself, cannot be directly applied to QCD or Yang-Mills theory. The limitations arise from the correspondence and from the specific properties of the $\mathcal{N} = 4$ SYM theory.

Two limitations arise from the correspondence itself:

1. To perform calculations within classical string theory or gravity the $N \rightarrow \infty$ limit of the gauge theory is needed, while in QCD one has $N = N_c = 3$.

Since string theory has not yet been consistently quantized on curved spaces, one has to rely on the large- N limit, hoping that an extrapolation to finite N makes sense.²⁰

2. The gravity approximation is strictly valid in the limit of infinite t'Hooft coupling $\lambda \rightarrow \infty$, while one might want to perform calculations at large but finite coupling. As mentioned in section 2.2.1, the QGP phase of QCD is a strongly coupled near-ideal liquid, i.e. the coupling g is large even at temperatures of the order $T \approx T_c \approx 170$ MeV. Therefore, the $\lambda \rightarrow \infty$ limit is regarded as a good approximation. Finite coupling corrections correspond to higher order curvature corrections²¹ of the Einstein-Hilbert action (A.1). These can be partially motivated by supergravity (see [27], and references therein) and/or systematically studied in a general setting [26].

Two specific properties of the $\mathcal{N} = 4$ SYM theory preventing direct applications to QCD and Yang-Mills theory are (see section 4.3.1 of [13]):

1. Because of the vanishing of the SYM theory β function it is conformally invariant, while QCD and Yang-Mills theory have non-trivial β functions as mentioned in section 2.1.2.

Conformal invariance can be broken by deforming the $\mathcal{N} = 4$ SYM theory by a relevant²² operator. On the gravity side this corresponds to deforming the pure AdS_5 space by a matter field.

2. The SYM theory is supersymmetric in contrast to QCD and Yang-Mills theory. Supersymmetry can be broken by compactifying the 10-dimensional supergravity theory on a circle of radius R with supersymmetry-breaking boundary conditions. This introduces a scale R into the theory, above which supersymmetry is still present. A "phenomenological" solution to this problem is to use the non-supersymmetric Einstein's theory of general relativity.

3.5.2. Top-down and bottom-up models

Despite the problems discussed above, the AdS/CFT correspondence was used to gain new insights into QCD and Yang-Mills theory, the holographic models being usually referred to as AdS/QCD. Two different approaches have emerged. Top-down models take the original AdS/CFT correspondence and deform the theory as described in the last

²⁰See however [26], where finite- N corrections were calculated within an effective (effective with respect to string theory) supergravity description.

²¹These are e.g. invariants of the form $R_{\mu\nu\rho\sigma}R^{\mu\nu\rho\sigma}$ or $C_{\mu\nu\rho\sigma}C^{\mu\nu\rho\sigma}$ and higher order contractions, where $R_{\mu\nu\rho\sigma}$ and $C_{\mu\nu\rho\sigma}$ are respectively the Riemann and Weyl curvature tensors.

²²A relevant operator is one with scaling dimension $\Delta < 4$.

subsection, or start from a different brane system to obtain a more "QCD-like" theory on the gauge theory side of the duality. Bottom-up models assume that a gravity dual to QCD or pure Yang-Mills theory exists, and that its leading behavior is given by Einstein gravity. In the context of the correspondence the top-down models can be regarded as more rigorous: They start from the full classical superstring theory or supergravity, consistently break supersymmetry, introduce extra branes to model matter fields in the fundamental representation of the gauge group,²³ etc. Bottom-up models are in this sense more phenomenological: The emphasis lies not so much on a string theoretically consistent construction of the model, but rather on the reproduction or prediction of one or more QCD or Yang-Mills theory properties. Thus, for bottom-up models, the theory of gravity in question is usually Einstein's general theory of relativity, the metric interacting with or acting as a background for matter fields. Top-down models usually use the full 10-dimensional formulation of the conjecture, while bottom-up models usually work with the 5-dimensional form described in section 3.3.3.

See [28] for the successful Sakai-Sugimoto top-down model. See e.g. [29] for the soft-wall bottom-up model. See [30] for a top-down oriented review on mesons in AdS/QCD, see [17] for an extensive review on AdS/QCD applications.

Since string theory is an important candidate, but not yet a fully established theory of quantum gravity²⁴, it cannot be said that one approach is better than the other; both directions are worth pursuing.

3.5.3. Yang-Mills plasma thermodynamics and the large- N limit

The discussion in section 3.5.1 brings up an important question. While, as mentioned above, the approximation of strong coupling should be a minor problem, the $N \rightarrow \infty$ limit of the $SU(N)$ Yang-Mills theory plasma might have little in common with the $N = 3$ plasma one wants to describe. An exact answer to this question is not known; there is however evidence that a calculation in the large- N limit can indeed reproduce the features of the $SU(3)$ Yang-Mills plasma. Consider the lattice calculations exhibited in figures 3.2 and 3.3.²⁵ One sees that, once normalized to their respective Stefan-Boltzmann limits, the thermodynamic quantities show little dependence on the rank of the $SU(N)$ gauge group. Moreover, as seen from figure 3.3, the extrapolation to the large- N limit preserves the qualitative dependences. The holographic approach to the Yang-Mills plasma thermo-

²³This is necessary, since in the $\mathcal{N} = 4$ $SU(N)$ SYM theory the fermions transform in the adjoint representation of the gauge group, while in QCD they transform in the fundamental representation.

²⁴See [16] for arguments against string theory as quantum gravity and alternative theories; see also [31].

²⁵In our nomenclature the interaction measure is denoted by I and Δ denotes the scaling dimension of an operator.

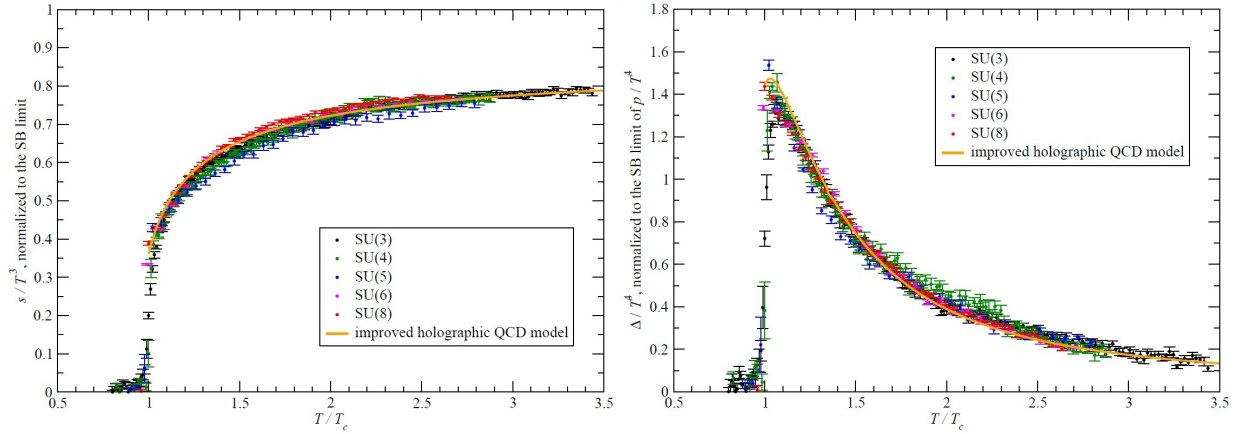


Figure 3.2.: Lattice calculations [32] of the $SU(N)$ Yang-Mills equation of state for $N = 3, 4, 5, 6$ and 8 (symbols) and the Improved Holographic QCD model (curves, [33]). Left panel: scaled entropy density, normalized to its Stefan-Boltzmann limit (B.9). Right panel: scaled interaction measure, normalized to the Stefan-Boltzmann limit of the pressure (B.10).

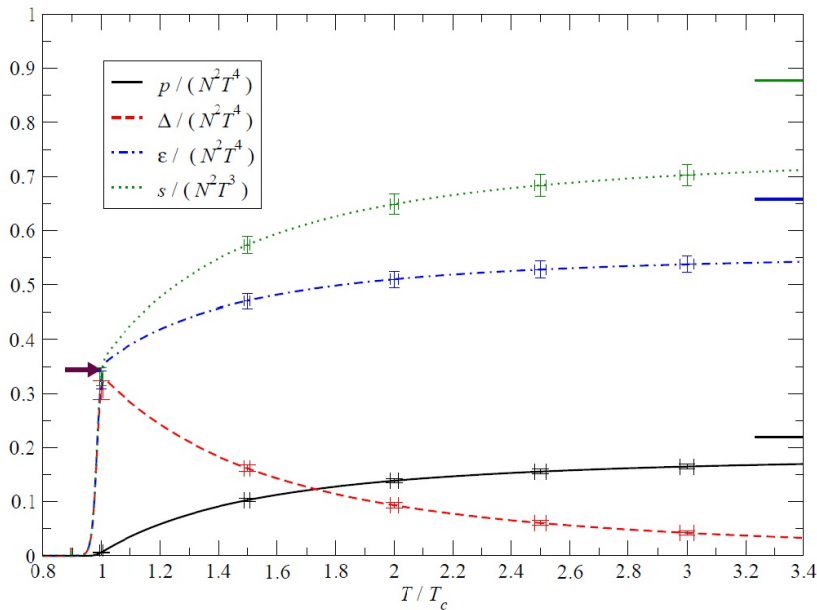


Figure 3.3.: Extrapolation of the $SU(N)$ Yang-Mills equation of state to the large- N limit [32]. The error bars show systematic and statistical uncertainties. The arrow denotes the large- N limit of the latent heat. The vertical bars on the right denote the Stefan-Boltzmann limits of p , $e \equiv \epsilon$ and s , from bottom to top. See [32] for the details of the extrapolation procedure.

dynamics works ”the other way round“: a calculation in the large- N limit is extrapolated to finite N . We take the figures 3.2 and 3.3 as an affirmation that the simple setting of Einstein gravity coupled to a scalar field, see section 4.1, is sufficient for the quantitative

description of the $SU(3)$ Yang-Mills plasma equation of state.

While the above discussion of the equation of state is encouraging, the situation concerning the viscosities is slightly worse. It is by now a well-known result, that in a large class of holographic models [34], including the action (cf. equation (4.1) below) used by us, the shear viscosity to entropy density ratio is given by

$$\frac{\eta}{s} = \frac{1}{4\pi}. \quad (3.41)$$

A different $\eta(s)$ dependence can be achieved, e.g. by considering higher-order curvature corrections in the action [26,27]. Thus, to connect with the present (albeit not very reliable) calculations of η/s , one would need a more complicated model which reproduces the trends exhibited in figure 3.4.

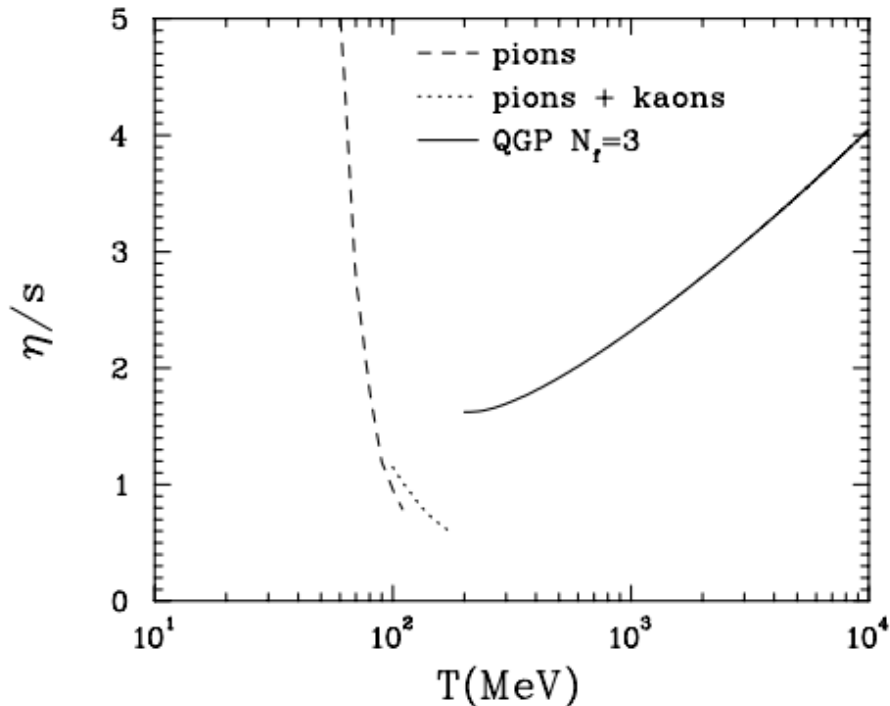


Figure 3.4.: Results of calculations of the η/s ratio for strongly interacting matter, reproduced from [35]. Dashed and dotted curves: hadron resonance gas model. Solid line: perturbative QGP. See [35] for details.

4. Holographic Yang-Mills plasma thermodynamics

We now introduce the bottom-up AdS/QCD model for the thermodynamics of the pure gluon plasma ($SU(3)$ Yang-Mills theory). The setup is five-dimensional Einstein gravity coupled to a scalar field ϕ with a non-trivial potential $V(\phi)$. The basic idea, described in detail below, is to translate the breaking of the conformal invariance of the pure gluon plasma due to quantum fluctuations into the deformation of the conformally invariant AdS space due to a non-trivial scalar field profile. The model is "bottom-up" in the sense that, as we will shortly see, additional information has to be supplied to close the system of equations. This affects the form of one of the unknown functions, as well as the parameters of the specific ansatz. Concretely, in chapter 5, we will adopt the form of the potential considered by Gubser et al. in [2] and use the lattice gauge theory data [36] of the $SU(3)$ Yang-Mills equation of state $s(T)$ to fix the parameters.

4.1. The general setup

The holographic model describing the thermodynamics of the Yang-Mills theory is given by the following action

$$S = \frac{1}{16\pi G_5} \int d^5x \sqrt{-g} \left(R - \frac{1}{2} \partial_\mu \phi \partial^\mu \phi - V(\phi) \right), \quad (4.1)$$

where G_5 is the "Newton constant" related to the Einstein constant κ_5 , $8\pi G_5 = \kappa_5^2$, in a five dimensional pseudo-Riemannian space with the metric fundamental tensor $g_{\mu\nu}$; $-g$ is the negative determinant of the metric tensor $g_{\mu\nu}$, R denotes the Ricci scalar and ϕ is a scalar field with a standard kinetic term and a potential $V(\phi)$ to be specified below.¹ We omitted the Gibbons-Hawking term in (4.1) (see A.1). The action (4.1) serves as the generic AdS/QCD model for the Yang-Mills theory thermodynamics. The ansatz for the

¹In a quantized theory, one would refer to $V(\phi)$ as "self-interaction", we follow the literature and use the term "potential".

metric tensor is encoded in the infinitesimal line element squared

$$ds^2 = e^{2A} \left(-f dt^2 + d\vec{x}^2 + \frac{dz^2}{f} \right). \quad (4.2)$$

The quantities A , f and ϕ are functions of the z -coordinate only, as we demand $SO(3)$ invariance in the x_i -directions. Here, $A(z)$ is a deformation of the black hole AdS space (as long as $A(z) \neq \ln(L/z)$) and $f(z; z_h)$ is the "black hole function", (or blackness function) defining a black hole horizon by $f(z_h) = 0$. There are three independent Einstein equations: the (tt) , $(x_1x_1) = (x_2x_2) = (x_3x_3) \equiv (xx)$ and (zz) components.² Linear combinations of these lead to more tractable equations (a prime denoting d/dz):

$$6A'^2 - 6A'' - \phi'^2 = 0, \quad (4.3)$$

$$3A'f' + f'' = 0, \quad (4.4)$$

$$f(9A'^2 + 3A'') - f'' + e^{2A}V = 0. \quad (4.5)$$

(from the components $(tt)/f^2 + (zz)$; $(tt)/f + (xx)$; $(zz)f/2 - 3/2(tt)/f - (xx)$, respectively). The equation of motion of ϕ following from $T^{\mu\nu}{}_{;\nu} = 0$ as the integrability condition of the Einstein equations is

$$3A'\phi'^2 + \phi'\phi'' - e^{2A}V' = 0. \quad (4.6)$$

It also follows from (4.5) by differentiating and using (4.3) and (4.4), i.e. it does not contain additional information.

In the metric (4.2), the range of the z -coordinate is $0 \leq z \leq z_h$, where $z = 0$ is the location of the boundary, $z \gtrsim 0$ is the asymptotic AdS (aAdS) region, and $z = z_h$ defines the location of the black hole horizon.

According to the AdS/CFT correspondence, the aAdS boundary conditions at $z \rightarrow 0$ must be required:

$$A = \ln \frac{L}{z}, \quad (4.7)$$

$$f = 1, \quad (4.8)$$

$$V = -\frac{12}{L^2} + \frac{M^2}{2}\phi^2, \quad (4.9)$$

$$\phi = (\Lambda z)^{4-\Delta}. \quad (4.10)$$

²The Einstein equations follow from the action (4.1) as $R_{\mu\nu} - \frac{1}{2}Rg_{\mu\nu} = T_{\mu\nu}$ with $T_{\mu\nu} = -\frac{1}{2}g_{\mu\nu}(\frac{1}{2}\partial_\mu\phi\partial^\mu\phi + V) + \frac{1}{2}\partial_\mu\phi\partial_\nu\phi$.

The $-12/L^2$ term in the potential (4.9) is the negative cosmological constant (already expressed through the AdS_5 “radius” L). For $\phi \equiv 0$, thus $V = -12/L^2$, the Einstein equations yield the pure AdS_5 metric, where A and f are given by equations (4.7) and (A.19), respectively; see appendix A.2. Equation (4.10) is the analogue of equation (3.32) and means a deformation of the boundary theory by a source Λ . The $M^2\phi^2/2$ term in (4.9) ensures that asymptotically one has the action (3.15) for a massive scalar field on AdS_5 , see section 3.4.2. Further, as in equation (3.23), Δ is the larger root of

$$\Delta(\Delta - 4) = M^2L^2. \quad (4.11)$$

With the boundary conditions $f(z_h) = 0$ and $f(0) = 1$ equation (4.4) can be integrated to yield

$$f(z; z_h) = 1 - \frac{\int_0^z dx e^{-3A}}{\int_0^{z_h} dx e^{-3A}}, \quad (4.12)$$

where we emphasize the parametric dependence on z_h . We will use an abbreviation for the denominator:

$$f_h \equiv f_h(z_h) = \int_0^{z_h} dx e^{-3A} \quad (4.13)$$

Using (B.1) and (B.2) the temperature and the entropy density are given in this metric by

$$T(z_h) = \frac{f'}{4\pi} \Big|_{z_h} = \frac{e^{-3A(z_h)}}{4\pi \int_0^{z_h} dx e^{-3A(x)}}, \quad (4.14)$$

$$s(z_h) = \frac{e^{3A(z_h)}}{4G_5}. \quad (4.15)$$

Equations (4.14) and (4.15) define the equation of state $s(T)$ by the parametric dependence on z_h .

It is a property of the AdS/QCD thermodynamics model defined by the action (4.1) that four functions

$$A(z), f(z), \phi(z), V(\phi) \quad (4.16)$$

have to be related by three independent equations (4.3-4.6). To close the system of equations one needs to supply additional information. Two approaches have been considered so far:

1. the AdS deformation $A(z)$ is specified, or
2. the potential $V(\phi)$ is specified.

The first approach is inspired by the successes of the AdS/QCD soft-wall model [29]. Note however an important difference: in the soft-wall model the metric as well as the scalar field profile are prescribed in an ad hoc manner, i.e. they are not found as self-consistent solutions of the Einstein equations (although an action and the potential leading to the desired profiles was found in [37]).

The second approach is inspired by the following line of thought: The scale invariance of the classical Yang-Mills theory is broken by quantum fluctuations as evidenced by the non-vanishing β function, equation (2.10). On the other hand, the field-operator correspondence, section 3.4.1, states that the energy-momentum tensor $T_{YM}^{\mu\nu}$ of the Yang-Mills theory is dual to the AdS metric $g_{\mu\nu}$, while $\text{Tr}(F_{\mu\nu}F^{\mu\nu})$ is dual to a scalar field ϕ in AdS, which interacts with $g_{\mu\nu}$. The idea is to map the breaking of the conformal invariance in the Yang-Mills theory (due to the β function) to a deformation of the metric from the conformally invariant black hole AdS one (due to the interaction with the scalar field ϕ in AdS). One thus models the running coupling in (2.10) by a non-trivial scalar field profile, mapping the β function on the scalar field potential V . This idea was effectively pursued by Kiritsis and collaborators, resulting in the Improved Holographic QCD (IHQCD) model [33]. In [33] one can find the exact formulation of the mapping just described.

We make a rather obvious, albeit important remark. Since one of the functions $A(z)$, $f(z)$, $\phi(z)$, $V(\phi)$ has to be supplied by an additional relation, one needs extra input “from outside the model”. It is perfectly reasonable to take some Yang-Mills theory information like the β function etc., however, within equilibrium thermodynamics, the only new thing that we learn this way is that the AdS/CFT language is indeed appropriate for describing strongly coupled Yang-Mills theory or QCD. Though important by itself, this insight does not lead us to new predictions for Yang-Mills theory. With this in mind we take the following point of view, analogous to [38]: the parameters of the holographic thermodynamics model will be fixed by fitting to some quantitatively well accessible Yang-Mills observable. After achieving this, we will take a step further and compute observables beyond equilibrium thermodynamics that are easily accessible in the holographic setup, being at the same time not so straightforwardly computed with other methods. Concretely, we will fix $A(z)$ or $V(\phi)$ to the equation of state $s(T)$ of the $SU(3)$ Yang-Mills theory computed on the lattice [36, 39, 40], concentrating on the most recent high precision data of [36] and, with this input, subsequently compute the shear and bulk viscosities $\eta(T)$ and $\zeta(T)$.

We conclude this section with a remark about the compatibility of the two approaches: At first sight it might seem that, besides the fact that one specifies a different function, the

two approaches are completely equivalent. For instance given $V(\phi)$ one can, knowing the solutions of the Einstein equations, immediately obtain $A(z)$ of the other approach and vice versa. However, consider equation (4.5) with the z_h -dependence of f (4.12) emphasized:

$$f(z; z_h)(9A'^2 + 3A'') - f(z; z_h)'' + e^{2A}V = 0. \quad (4.17)$$

We see from (4.12) that the profile of f changes for different values of z_h , the latter being a parameter of the solutions, which defines the temperature via (B.1). Thus, computing the equation of state $s(T)$ one has to vary z_h to scan a range of temperatures. Since it is not possible to eliminate f_h from (4.17) we conclude: if one specifies a z_h -independent profile $V(\phi)$ of the potential, then $A(z; z_h)$ depends on z_h ; conversely, if a z_h -independent $A(z)$ is specified, then the potential depends on z_h : $V(\phi(z); \phi(z_h))$. It is thus not possible to directly compare the two approaches. One would need a family of solutions parametrized by z_h in one approach as an input for the other one.

4.2. Approach by Huang et al.

Huang et al. [1] made the ansatz

$$e^{2A} = \frac{L^2}{z^2} e^{2A_s - \frac{2}{\sqrt{6}}\phi}, \quad (4.18)$$

where the pure AdS part L^2/z^2 is factored out. The motivation for the specific ansatz (4.18) is due to the fact that the numerical factor $2/\sqrt{6}$ in front of ϕ ensures the cancellation of the ϕ'^2 -term in equation (4.3). Thus the equation (4.3) for ϕ becomes a *linear* differential equation.

Einstein equations

Equations (4.3), (4.4) and (4.5) with the ansatz (4.18) become

$$\phi'' - \phi' \left(2A'_s - \frac{2}{z} \right) - \sqrt{6} \left(A''_s - A_s'^2 \right) - 2\sqrt{6} \frac{A'_s}{z} = 0, \quad (4.19)$$

$$f'' + f' \left(3A'_s - \frac{\sqrt{6}}{2} \phi' - \frac{3}{z} \right) = 0, \quad (4.20)$$

$$V = -\frac{z^2}{L^2} e^{-2A_s + \frac{2}{\sqrt{6}}\phi} \left(f'' + f \left(12A''_s - 2\sqrt{6}\phi'' + \frac{3}{2}\phi'^2 + \frac{12}{z^2} \right) \right). \quad (4.21)$$

Boundary conditions

Imposing the aAdS boundary conditions (4.7-4.10) in the asymptotic region $z \rightarrow 0$ for the specific ansatz (4.18) amounts to:

$$A_s \rightarrow 0, \quad (4.22)$$

$$\phi \rightarrow 0. \quad (4.23)$$

Solutions

One can integrate the two equations (4.19) and (4.20) with the result

$$\phi(z) = \sqrt{6} \left(A_s(z) + \int_0^z dx \frac{e^{2A_s(x)}}{x^2} \int_0^x dy y^2 e^{-2A_s(y)} A_s'(y)^2 \right) \quad (4.24)$$

and

$$f(z; z_h) = 1 - \frac{\int_0^z dx x^3 e^{\frac{\sqrt{6}}{2}\phi(x) - 3A_s(x)}}{f_h}, \quad (4.25)$$

with

$$f_h = \int_0^{z_h} dx x^3 e^{\frac{\sqrt{6}}{2}\phi(x) - 3A_s(x)}. \quad (4.26)$$

The temperature and the entropy density can now be calculated. Equations (4.14) and (4.15) yield, with A given by equation (4.18),

$$T = \frac{z_h^3 e^{\frac{\sqrt{6}}{2}\phi(z_h) - 3A_s(z_h)}}{4\pi \int_0^{z_h} dx x^3 e^{\frac{\sqrt{6}}{2}\phi(x) - 3A_s(x)}}, \quad (4.27)$$

$$s = \frac{1}{4G_5} \frac{L^3}{z_h^3} e^{3A_s(z_h) - \frac{\sqrt{6}}{2}\phi(z_h)}. \quad (4.28)$$

In the asymptotic region $z \leq z_h \ll 1$, the exponentials become $\mathcal{O}(1)$ and the conformal behavior of T and s according to (B.3) and (B.4) is recovered, i.e. $s/T^3 = \text{const}$.

To summarize, once $A_s(z)$ is given it is straightforward to obtain ϕ and f_h by performing the integrals (4.24) and (4.26) and, using equations (4.27) and (4.28), to arrive at the equation of state $s(T)$. The potential $V(z; z_h)$ is a byproduct. Due to the dependence on z_h it looks like an effective, temperature dependent interaction term.

4.3. Approach by Gubser et al.

A different ansatz for the infinitesimal line element squared, more convenient for the specification of a potential $V(\phi)$, is used by Gubser et al. [2]:

$$ds^2 = e^{2A}(-f dt^2 + d\vec{x}^2) + L^2 e^{2B} \frac{d\phi^2}{f}. \quad (4.29)$$

Here, the profile of the scalar field ϕ itself is used as the radial coordinate. Since the scalar field ϕ has mass dimension zero, a scale needs to be introduced. The metric (4.29) follows from (4.2) by a coordinate transformation:

$$dz^2 = \frac{1}{L^2} \frac{dz^2}{d\phi^2} L^2 d\phi^2, \quad (4.30)$$

i.e.

$$ds^2 = e^{2A} \left(-f dt^2 + d\vec{x}^2 + \frac{dz^2}{f} \right) \quad (4.31)$$

$$= e^{2A}(-f dt^2 + d\vec{x}^2) + e^{2A} \frac{dz^2}{L^2 d\phi^2} L^2 \frac{d\phi^2}{f}. \quad (4.32)$$

Defining

$$e^{2B} \equiv e^{2A} \frac{dz^2}{L^2 d\phi^2} \quad (4.33)$$

one arrives at (4.29).

Einstein equations

The Einstein equations following from the metric (4.29) are (where a prime now denotes $d/d\phi$):

$$A'' - A'B' + \frac{1}{6} = 0, \quad (4.34)$$

$$f'' + f'(4A' - B') = 0, \quad (4.35)$$

$$6A'f' + f(24A'^2 - 1) + 2e^{2B}L^2V = 0. \quad (4.36)$$

(from the components $(\phi\phi) + (tt)e^{2(B-A)}/f^2$, $e^{2(B-A)}((tt)/f + (xx))$ and $(\phi\phi)$, respectively).

The equation of motion of ϕ following from $T^{\mu\nu}{}_{;\nu} = 0$ is

$$4A' - B' + \frac{f'}{f} - \frac{e^{2B}}{f} L^2 V' = 0. \quad (4.37)$$

It also follows from (4.34-4.36) and their derivatives, i.e. it does not contain new information.

Boundary conditions

We transform now the boundary conditions (4.7-4.10) into the coordinate system characterized by (4.29). First, note that (4.10) implies that $0 \leq z \leq z_h$ translates into $0 \leq \phi \leq \phi_h$. aAdS now means $\phi \rightarrow 0$, and (4.7) with (4.10) lead to

$$\phi = (\Lambda L)^{4-\Delta} e^{(\Delta-4)A} \quad (4.38)$$

rending

$$A = \frac{\ln \phi}{\Delta - 4} + \ln(\Lambda L). \quad (4.39)$$

Equation (4.38) with $A = \ln \frac{L}{z}$ yields

$$z = \phi^{1/(4-\Delta)} L (\Lambda L)^{-1} \quad (4.40)$$

and

$$\frac{dz}{d\phi} = \frac{1}{4-\Delta} \phi^{1/(4-\Delta)-1} L (\Lambda L)^{-1}. \quad (4.41)$$

Combining (4.33), (4.39) and (4.41) one obtains

$$B = -\ln((4-\Delta)\phi). \quad (4.42)$$

The boundary conditions for f are as in equation (4.12), and the horizon is now defined by ϕ_h . Integrating (4.35) one obtains

$$f(\phi; \phi_h) = 1 - \frac{\int_0^\phi d\tilde{\phi} e^{-4A(\tilde{\phi})+B(\tilde{\phi})}}{\int_0^{\phi_h} d\tilde{\phi} e^{-4A(\tilde{\phi})+B(\tilde{\phi})}}. \quad (4.43)$$

Equations (4.43) and (4.33) reproduce (4.12).

The to-be-specified potential $V(\phi)$ should be of the form (4.9) for small values of ϕ .

Solution technique

To solve the system (4.34-4.36), given a potential $V(\phi)$, one has two possibilities:

1. integrate the system of equations directly, or
2. compute A' from V and its derivatives and integrate equations (4.34) and (4.35).

In [2] the second option is used, and we employ the same technique. Manipulations of equations (4.36) and (4.37) (the goal is to eliminate f and B by combining the two equations and/or taking derivatives) and subsequent use of (4.34) and (4.35) lead to

$$A''' - \frac{U + 3A'}{A'(U + A')} A''^2 - \frac{U^2(24A'^2 + 1) + 3A'U(8A'^2 + 1) + 2A'^2 - 6A'^2U'}{6A'U(U + A')} A'' = 0, \quad (4.44)$$

where we have defined

$$U \equiv \frac{V}{3V'}. \quad (4.45)$$

This form points on a dependence on U and U' , rather than a dependence solely on V . Equation (4.44) coincides with equation (34) in [2] after the execution of the ϕ derivative. It is a second-order nonlinear differential equation for A' . Thus, we need to specify two initial conditions. Consider equations (4.36) and (4.37) at the horizon $\phi = \phi_h$ where $f(\phi_h; \phi_h) = 0$:

$$L^2V = -3A'f'e^{-2B}, \quad (4.46)$$

$$L^2V' = f'e^{-2B}. \quad (4.47)$$

Divide (4.46) by (4.47) to obtain

$$A'(\phi_h) = -\frac{V}{3V'} \Big|_{\phi_h}. \quad (4.48)$$

Using equations (4.46) and (4.47) one can develop a power series around ϕ_h to $\mathcal{O}(\phi - \phi_h)$ and obtain the initial conditions for $A'(\phi_h)$ and $A''(\phi_h)$:

$$A' = -\frac{V}{3V'} \Big|_{\phi_h} + \frac{1}{6} \left(\frac{VV''}{V'^2} - 1 \right) \Big|_{\phi_h} (\phi - \phi_h), \quad (4.49)$$

$$A'' = \frac{1}{6} \left(\frac{VV''}{V'^2} - 1 \right) \Big|_{\phi_h}. \quad (4.50)$$

With these initial conditions we can numerically integrate equation (4.44) from ϕ_h to some small $\phi_0 \approx 0^+$ (A' diverges at $\phi = 0$ as seen with (4.39)) and obtain $A'(\phi)$. Now we can compute A and B using (4.34) and (4.39), (4.42) for the integration constants:

$$A = \frac{\ln \phi_0}{\Delta - 4} + \ln(\Lambda L) + \int_{\phi_0}^{\phi} d\tilde{\phi} A', \quad (4.51)$$

$$B = -\ln((4 - \Delta)\phi_0) + \int_{\phi_0}^{\phi} d\tilde{\phi} \frac{A'' + 1/6}{A'}. \quad (4.52)$$

We choose $\phi_0 = 10^{-3}$. With A and B , f is immediately given by (4.43).

Having calculated all metric coefficients we now can obtain the entropy density and the temperature for the metric (4.29) via (B.1) and (B.2) and determine the equation of state with (4.43):

$$TL = -\frac{f'}{4\pi} e^{A-B} \Big|_{\phi_h} = \frac{e^{-3A(\phi_h)}}{4\pi \int_0^{\phi_h} d\tilde{\phi} e^{-4A+B}}, \quad (4.53)$$

$$sG_5 = \frac{e^{3A(\phi_h)}}{4}. \quad (4.54)$$

Using the coordinate transformation (4.40) together with the asymptotic formulas (B.3) and (B.4) one obtains for $\phi_h \rightarrow 0$:

$$LT = \frac{\Lambda L}{\pi} \phi_h^{1/(\Delta-4)}, \quad (4.55)$$

$$G_5 s = \frac{1}{4} (\Lambda L)^3 \phi_h^{3/(\Delta-4)}. \quad (4.56)$$

Following Gubser [2], we from now on set

$$\Lambda L \equiv 1. \quad (4.57)$$

5. The equation of state

5.1. Approach by Huang et al. - Analysis of the model

We first follow [1] and consider the ansatz

$$A_s(z) = \pm k^2 z^2. \quad (5.1)$$

This ansatz is similar in spirit to the soft-wall AdS/QCD model, where a quadratic scalar field profile is postulated. The ansatz (5.1) can be seen as an extension of the soft-wall model. Instead of specifying the profile of the scalar field, one specifies the deformation of the AdS space. Since the parameter k has the dimension of energy (or inverse length) it introduces a scale into the model. To study the behavior of ϕ , expand (4.24) around $z = 0$:

$$\phi(z) = \sqrt{6} \left(\pm k^2 z^2 + \frac{1}{5} k^4 z^4 + \dots \right). \quad (5.2)$$

We see that ϕ is quadratic for $z \rightarrow 0$, but will have a more complicated form for larger z . Comparing with the asymptotic behavior following from the field-operator correspondence (4.10) we see that

$$\Delta = 2, \quad (5.3)$$

$$\Lambda = 6^{1/4} k, \quad (5.4)$$

and conclude that a specification of A_s automatically fixes the scaling dimension Δ and the $z \rightarrow 0$ limit Λ of ϕ .

Having specified A_s we proceed as described at the end of section 4.2 to obtain the equation of state $s(T)$ and other thermodynamic quantities. With the ansatz (5.1) one obtains the equations of state exhibited in figure 5.2.

One recognizes in figure 5.1 for $kz_h \lesssim 0.5$ the asymptotic behaviors of s and T according to equations (B.4) and (B.3). The entropy density sG_5 is a monotonously decreasing function of z_h , while the temperature T reaches a minimum and then increases, leading

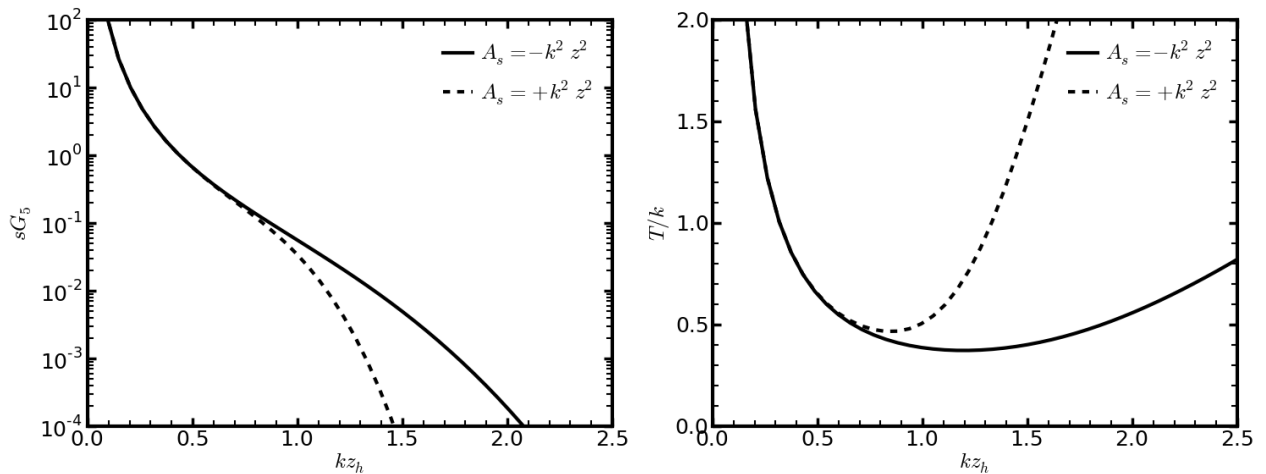


Figure 5.1.: Entropy density and temperature as functions of z_h for the ansatz (4.18) with $k = 0.7$ GeV and $L \equiv 1$. Left panel: entropy density sG_5 . Right panel: temperature T/k .

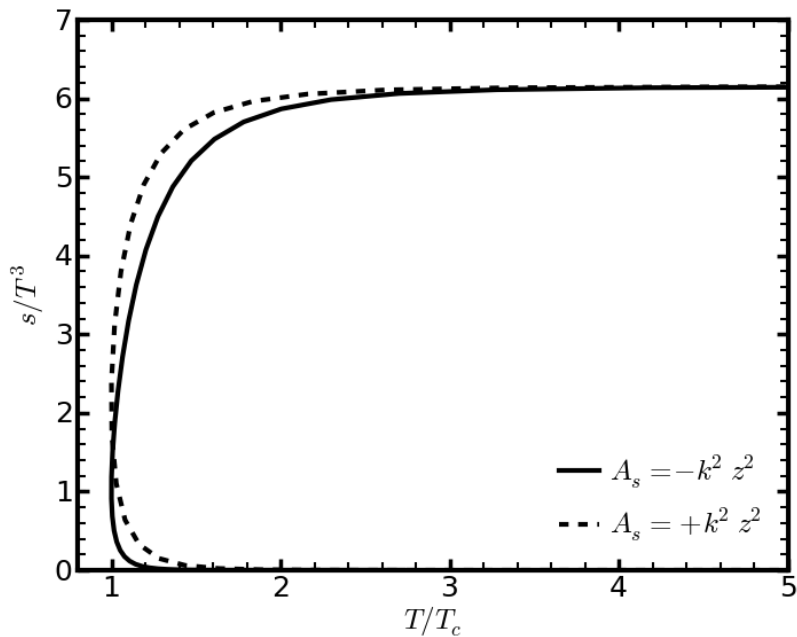


Figure 5.2.: Scaled entropy density as a function of T/T_c for the ansatz (5.1) with $k = 0.7$ GeV, $L \equiv 1$ and $G_5/L^3 = 1.26$.

to the equation of state exhibited in figure 5.2. The scaled entropy density s/T^3 rapidly approaches the conformal behavior, i.e. $s/T^3 = \text{const}$, according to equation (B.5). For $k = 0.7$ GeV one obtains $T_c = 0.326$ GeV and $T_c = 0.260$ GeV for respectively the positive and the negative sign in the ansatz (5.1), where the deconfinement temperature T_c is

defined as the minimum of $T(z_h)$.¹

Rewrite equations (4.27) and (4.28) in terms of the dimensionless variable $\tilde{z} \equiv kz$ to obtain:

$$T = \frac{k\tilde{z}_h^3 e^{\frac{\sqrt{6}}{2}\phi(\tilde{z}_h) - 3A_s(\tilde{z}_h)}}{4\pi \int_0^{\tilde{z}_h} d\tilde{x} \tilde{x}^3 e^{\frac{\sqrt{6}}{2}\phi(\tilde{x}) - 3A_s(\tilde{x})}}, \quad (5.5)$$

$$s = \frac{1}{4G_5} \frac{(kL)^3}{\tilde{z}_h^3} e^{3A_s(\tilde{z}_h) - \frac{\sqrt{6}}{2}\phi(\tilde{z}_h)}. \quad (5.6)$$

One sees from the equations (5.5) and (5.5), that the scaled entropy density s/T^3 is independent of the scale k . Thus, k can be chosen such that the value of T_c reproduces that of the $SU(3)$ Yang-Mills plasma. The choice $k = 0.7$ GeV leads to $T_c = 0.260$ GeV for the negative sign in the ansatz (5.1), which coincides with the value $T_c \approx 265$ MeV computed on the lattice.² To better reproduce the $SU(3)$ Yang-Mills plasma equation of state, one needs to modify the ansatz (5.1) for A_s by e.g. adding powers of \tilde{z} or considering a power-law dependence $A_s = \tilde{z}^\alpha$. We will not follow in this direction and instead from now on concentrate on the model by Gubser et al. which was introduced in section 4.3.

5.2. Approach by Gubser et al. - Analysis of the model

In [2], Gubser et al. considered the potential

$$V(\phi) = -\frac{12}{L^2} \cosh(\gamma\phi) + \frac{b}{L^2} \phi^2. \quad (5.7)$$

The potential (5.7) was shown to well reproduce the squared speed of sound of $2 + 1$ flavor QCD, see figure 3 of [2]. Expanding the cosh around $\phi = 0$ and comparing to the asymptotic form (4.9) we obtain

$$\Delta(\Delta - 4) = M^2 L^2 = 2b - 12\gamma^2. \quad (5.8)$$

According to the AdS/CFT prescription, Δ is the larger root of equation (5.8). Employing the solution technique described in section 4.3 we calculate the equation of state $s(T)$ and other thermodynamic quantities. Already by varying the parameters γ and b one obtains a variety of qualitatively different equations of state.

We exhibit the $T(\phi_h)$, $s(\phi_h)$, $s/T^3(\phi_h)$ and $s/T^3(T/T_c)$ dependences for different values of

¹See section 5.2 for a discussion concerning the definition of T_c . The behavior of $T(z_h)$ is analogous to the $T(\phi_h)$ -behavior referred to as a first order phase transition in section 5.2.

²The ansatz (5.1) with $G_5/L^3 = 1.26$ yields an equation of state s/T^3 which is already qualitatively similar to the equation of state of the $SU(3)$ Yang-Mills plasma, see figures 3-7 of [1].

γ and b , summarized in table 5.1. The potential (5.7) is exhibited in figure 5.3 for values of γ and b as listed in table 5.1. The first three parameter values were used in [2], the last in [41].

One recognizes in figure 5.3 the negative cosh behavior for large values of ϕ , while for smaller values of ϕ the quadratic term in the Taylor expansion of the cosh can be compensated by the $(b/L^2)\phi^2$ -term in (5.7). With the decreasing of the quadratic, i.e. M^2L^2 term the potential becomes flatter and almost quartic and shifts to the right as a whole. For a fixed value of M^2L^2 , one can still “tune“ the potential, as represented by the curves 1 and 2. Since the equation (4.44) depends on U and U' , we exhibit these quantities in figure 5.4. One sees that, while the potential V itself is relatively featureless, the quantities U and U' have an interesting structure. The quantity U diverges for $\phi \rightarrow 0$, since then $V' \rightarrow 0$, and exhibits a minimum at $\phi \approx 4$, which shifts to the right with increasing Δ . Note that for the curve 4, representing the case $\Delta \rightarrow 4$, U is for small values of $\phi \lesssim 2$ almost an order of magnitude larger than for the curves 1, 2 and 3 with $\Delta \lesssim 3.4$. Since $U' \propto 1/V'^2$ for small values of ϕ , it takes large negative values for $\phi \rightarrow 0$. Consistent with the minimum of U , U' has a root at $\phi \approx 4$, which shifts to the right with increasing Δ .

#	γ	b	$-M^2L^2$	Δ	ϕ_h^c	T_cL	T_c -type	Phase transition
1	$\sqrt{3/4}$	3.0	3.0	3.0	≈ 1.67	≈ 0.304	minimum	1st order
2	$\sqrt{7/12}$	2.0	3.0	3.0	≈ 2.67	≈ 0.210	minimum	1st order
3	$\sqrt{1/2}$	1.942	2.116	≈ 3.373	≈ 4.27	≈ 0.157	inflection	2nd order
4	0.606	2.057	≈ 0.293	≈ 3.925	≈ 4.36	≈ 0.704	inflection	crossover

Table 5.1.: Different parameters of the potential (5.7) following [2,41] and the resulting deconfinement temperatures T_c .

As seen in figure 5.5, the temperature $T(\phi_h)$ may be sorted into three different classes depending on the values of the parameters γ and b . These possibilities are:

1. $T(\phi_h)$ decreases monotonously for all values of ϕ_h , as represented by the curves 3 and 4,
2. $T(\phi_h)$ reaches a minimum value T_{min} at some value ϕ_{min} and then increases, as represented by curve 1,
3. $T(\phi_h)$ reaches a minimum value T_{min} at some value ϕ_{min} , increases, reaches a maximum and then decreases again, as represented by curve 2 in figure 5.6.

The entropy density sG_5 and the scaled entropy density s/T^3 , in contrast, are decreasing functions of ϕ_h , see figure 5.7. The three possible forms of $T(\phi_h)$ are reflected in the scaled

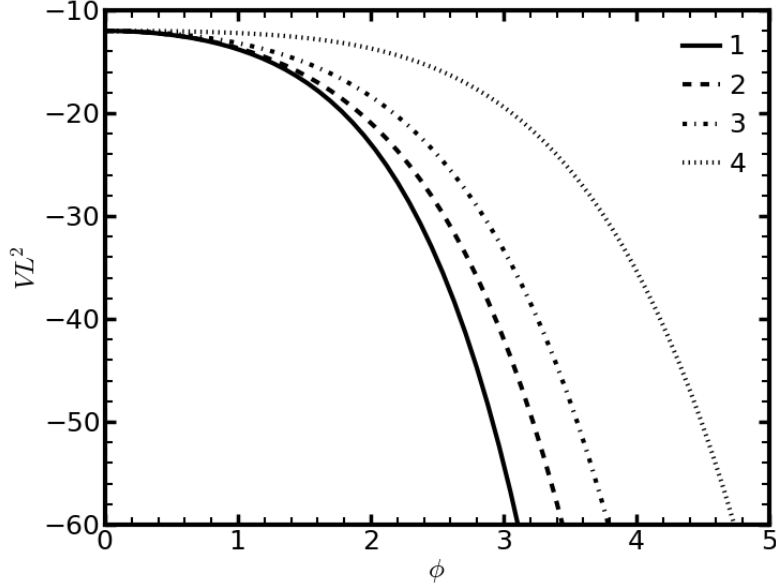


Figure 5.3.: The potential $V(\phi)$ according to (5.7) for the parameter values of table 5.1.

entropy density s/T^3 as a function of T/T_c , see figure 5.8. The value of $s/T^3 G_5/L^3$ at $T/T_c = 1$ can vary in a large interval; for the displayed examples it ranges from 1 to 4. For small values of ϕ_h , one recognizes from the right panel of figure 5.5 and from the left panel of figure 5.7 the asymptotic power law behaviors (4.55) and (4.56), whereas for large values, $\phi_h \gtrsim 4$, the exponential Chamblin-Reall behavior, i.e. $T \propto e^{\phi_h}$, $s \propto e^{\phi_h}$ (see appendix C, equations (C.2) and (C.3)) is recognized.³

The different cases of the behavior of s/T^3 as a function of T/T_c are exhibited in figure 5.8. Curves 1 and 2 are double valued, while 3 and 4 are single valued. Moreover, curves 3 and 4 continue to $T/T_c < 1$. One may attribute these different patterns to a general discussion of phase transitions in the AdS/CFT setting. Here, we will not go into detail and instead follow the nomenclature of Gubser et al. [2]. Thus, we distinguish the following cases:

1. We refer to the case when the temperature T as a function of ϕ_h reaches a minimum and then increases (as for the curves 1 and 2 in figure 5.5), as a first order phase transition.

The specific heat C (5.9), and the squared speed of sound c_s^2 (5.13) become negative after $T(\phi_h)$ passes its minimum, indicating a thermodynamical instability (see [2] and references therein). It is thought that, in this case, the spacetime undergoes a first-

³Note however, that due to the $b\phi^2$ -term the quantity U does not become constant for larger values $\phi \gtrsim 4$ but rather shows a linear behavior as exhibited in figure 5.4.

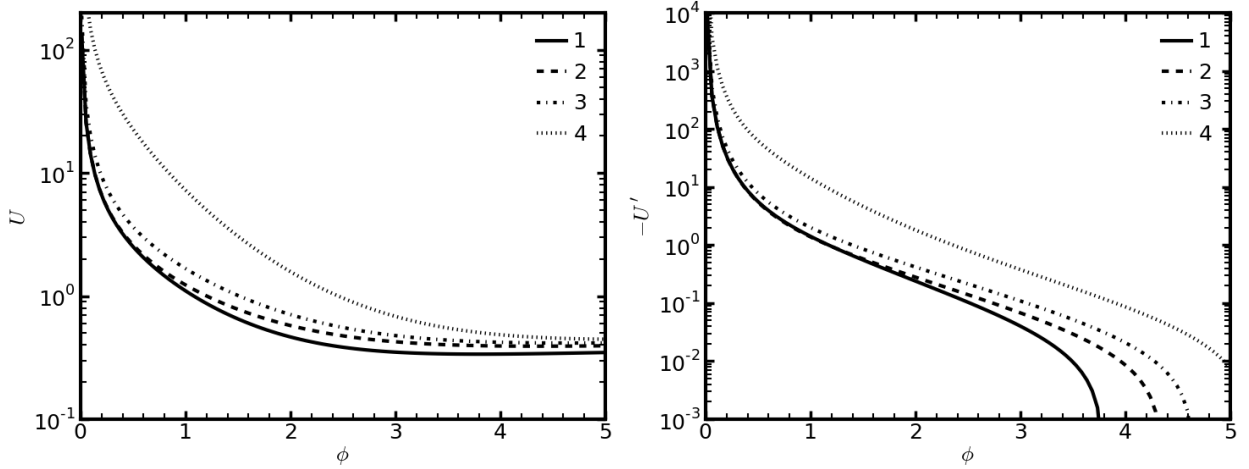


Figure 5.4.: The quantities $U = V/(3V') = -A'|_{\phi_h}$ and $U' = 1/3(1 - VV''/V'^2)$ according to equation (4.45) for the parameter values of table 5.3. Left panel: $U(\phi)$. Right panel: $U'(\phi)$.

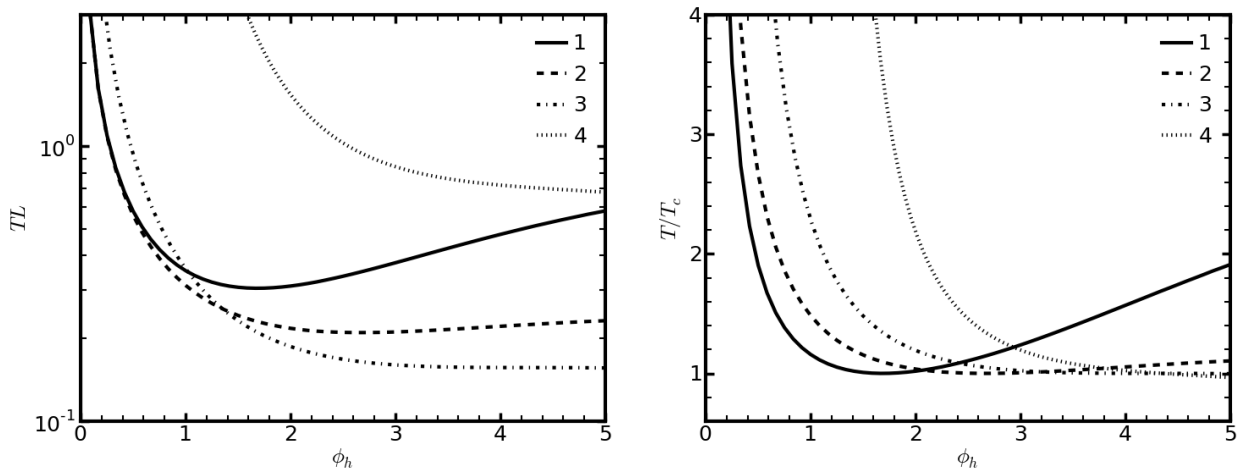


Figure 5.5.: Temperature as a function of ϕ_h for the parameter values of table 5.1. Left panel: temperature TL . Right panel: scaled temperature T/T_c .

order Hawking-Page phase transition [42] to a geometry without a black hole.⁴ This point of view is supported by the IHQCD model [33]. Note that this is consistent with the behavior of the $SU(3)$ Yang-Mills plasma: the deconfinement phase transition is first-order and, also, the entropy density scales as N^2 in the deconfined phase (cf. equations (B.2) and (C.9)) and as N^0 in the confined phase.

⁴The curve 2, figure 5.6, will actually eventually drop below its local minimum and consequently s/T^3 will decrease to low temperatures (see figure 6 of [2]). One could thus also have a first-order transition between two black hole phases.

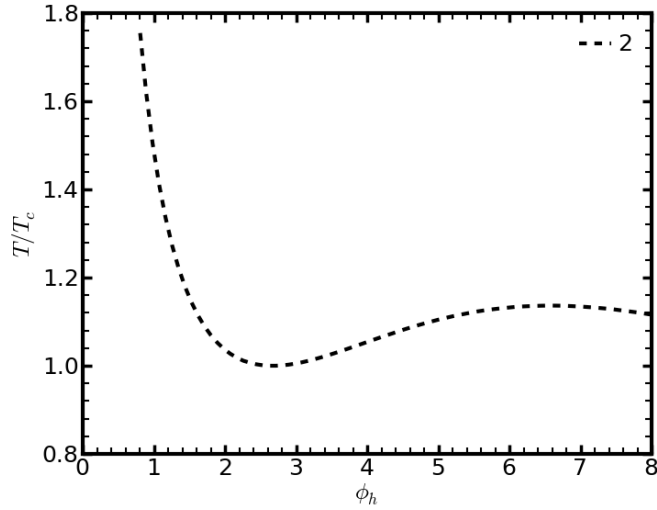


Figure 5.6.: Scaled temperature T/T_c for case #2 (see table 5.1) for a larger range of ϕ_h with a local maximum at $\phi_h \approx 6.6$.

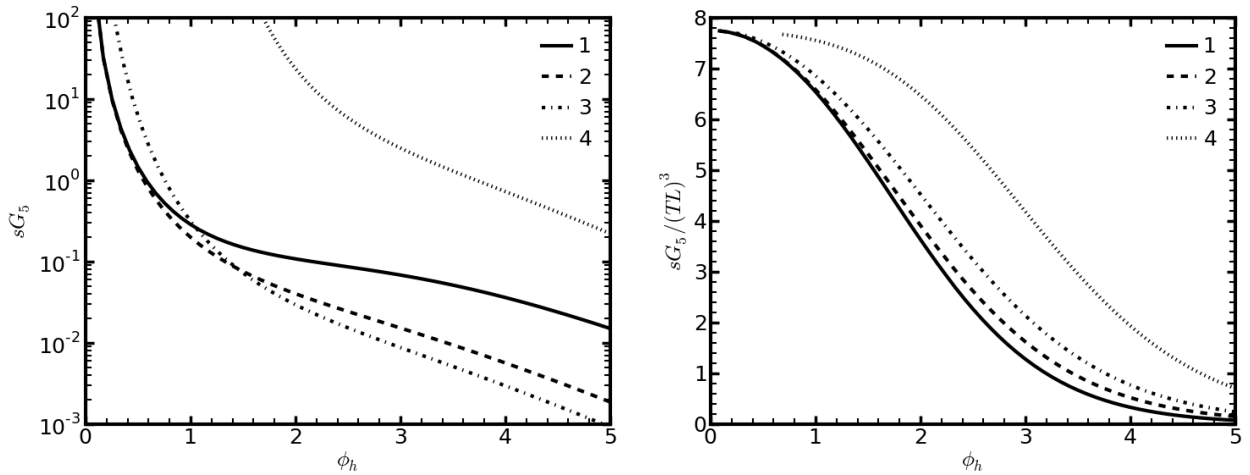


Figure 5.7.: Entropy density as a function of ϕ_h for the parameter values of table 5.1. Left panel: entropy density sG_5 . Right panel: scaled entropy density $sG_5/(TL)^3$.

2. We refer to the case when the temperature T is a monotonously decreasing function of ϕ_h and its derivative goes to zero as $\phi_h \rightarrow \infty$ (as for the curve 3 in figure 5.5) as a second order phase transition.

In this case, the T -derivative of the entropy density s exhibits a singularity at $T = T_c$ (see below) and the squared speed of sound c_s^2 as a function of the temperature T exhibits a kink (see the right panel of figure 7 in [2]).

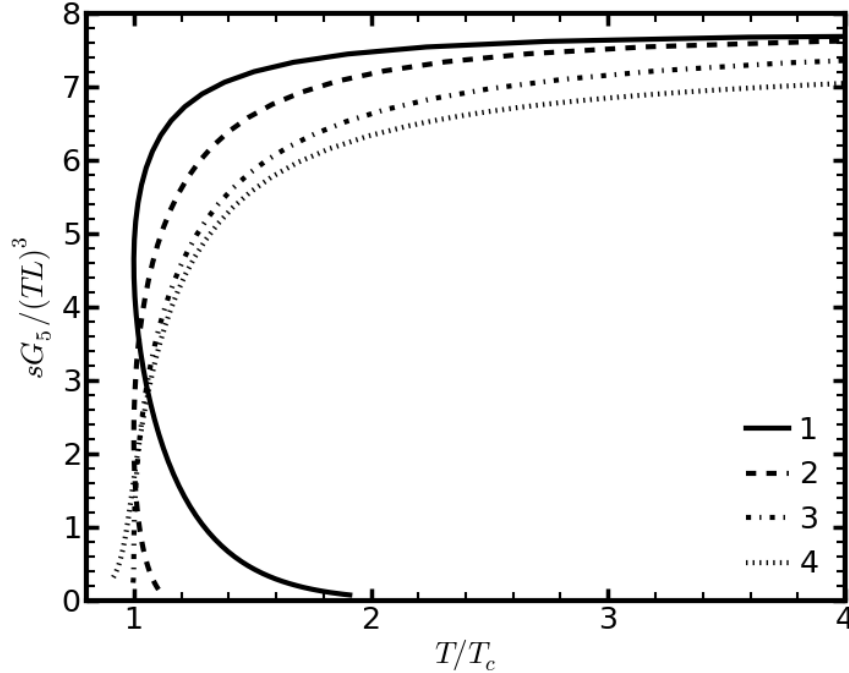


Figure 5.8.: Scaled entropy density as a function of T/T_c for the parameter values of table 5.1.

3. We refer to the case when the temperature T is a monotonously decreasing function of ϕ_h and its derivative stays finite for $\phi_h \rightarrow \infty$ (as for the curve 4 in figure 5.5) as a crossover.

In this case, the T -derivative of the scaled entropy density s/T^3 reaches a maximum at $T = T_c$ (see below) but stays finite, and consequently the specific heat C and the squared speed of sound c_s^2 do not exhibit singular behavior.

The three different types of the phase transition arise with the potential (5.7) for a fixed value of γ and varying values of b . This is shown in table 5.2 and figures 5.10, 5.11 and 5.12. While the entropy density sG_5 as a function of ϕ_h shows essentially the same behavior for the three different values of b (see the left panel of figure 5.11), the temperature as a function of ϕ_h (see figure 5.10) reflects the three possible types of the phase transition just described. The different cases result in the different types of the behavior of s/T^3 for $T \rightarrow T_c$ as exhibited in figure 5.12. The second-order phase transition is the limiting case between the first-order and the crossover transitions.

#	γ	b	$-M^2L^2$	Δ	ϕ_h^c	T_cL	T_c -type	Phase transition
3a	$\sqrt{1/2}$	1.8	2.4	≈ 3.265	≈ 3.94	≈ 0.155	inflection	crossover
3b	$\sqrt{1/2}$	1.942	2.116	≈ 3.373	≈ 4.27	≈ 0.157	inflection	2nd order
3c	$\sqrt{1/2}$	2.1	1.8	≈ 3.483	≈ 3.53	≈ 0.160	minimum	1st order

Table 5.2.: Different values of b for $\gamma = \sqrt{1/2}$ result in different types of the phase transition. The case 3b repeats case 3 of table 5.1.

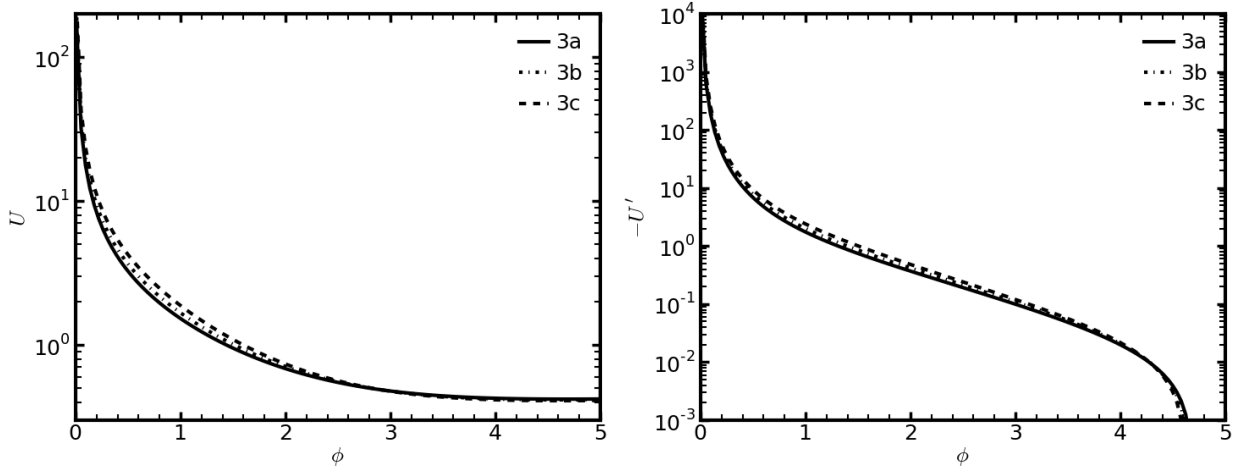


Figure 5.9.: The quantities $U = V/(3V') = -A'|_{\phi_h}$ and $U' = 1/3(1 - VV''/V'^2)$ according to equation (4.45) for the parameter values of table 5.2. Left panel: $U(\phi)$. Right panel: $U'(\phi)$. Note that the curves intercept at $\phi \approx 3$ for U and at $\phi \approx 4.4$ for U' .

The deconfinement temperature T_c

To compare with the lattice data, the deconfinement temperature T_c has to be defined. It is not a priori fixed by the model and is thus an additional assumption. It can however be constrained and defined in a "natural" way. Consider the specific heat C defined by

$$C \equiv T \frac{ds}{dT} = T \frac{ds}{d\phi_h} \frac{d\phi_h}{dT}. \quad (5.9)$$

If $T(\phi_h)$ and $s(\phi_h)$ are both decreasing (as for the curves 3 and 4 in figures 5.5 and 5.7), one has $ds/d\phi_h < 0$, $dT/d\phi_h < 0$ and consequently $C > 0$. If $T(\phi_h)$ reaches a minimum and then increases (as for the curves 1 and 2 in figures 5.5 and 5.7), its derivative changes the sign, $dT/d\phi_h > 0$, and consequently $C < 0$. Thus (as mentioned in the discussion above), the system becomes thermodynamically unstable for $\phi_h > \phi_{min}$, signaling a phase

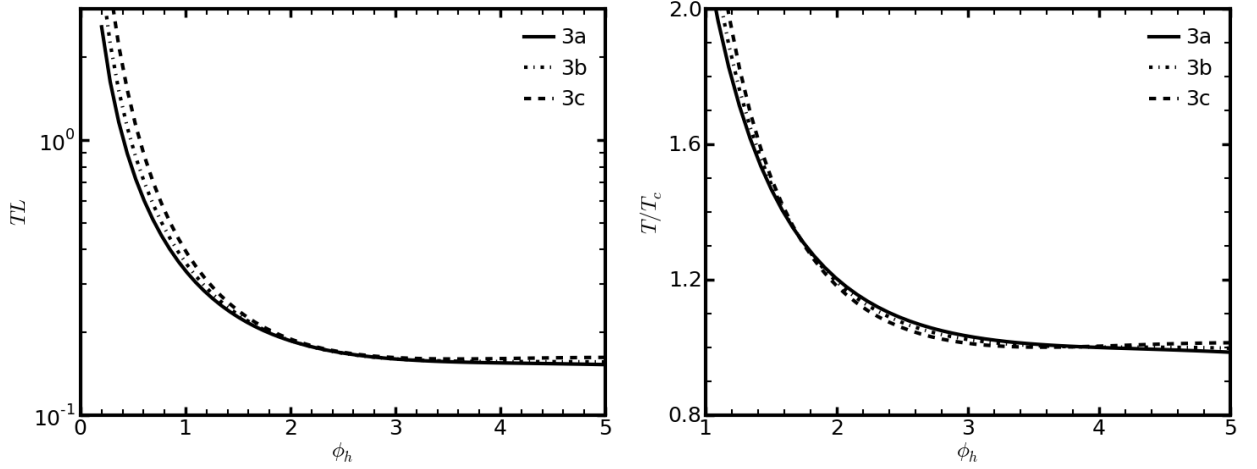


Figure 5.10.: Temperature as a function of ϕ_h for the parameter values of table 5.2. Left panel: temperature TL . Right panel: scaled temperature T/T_c .

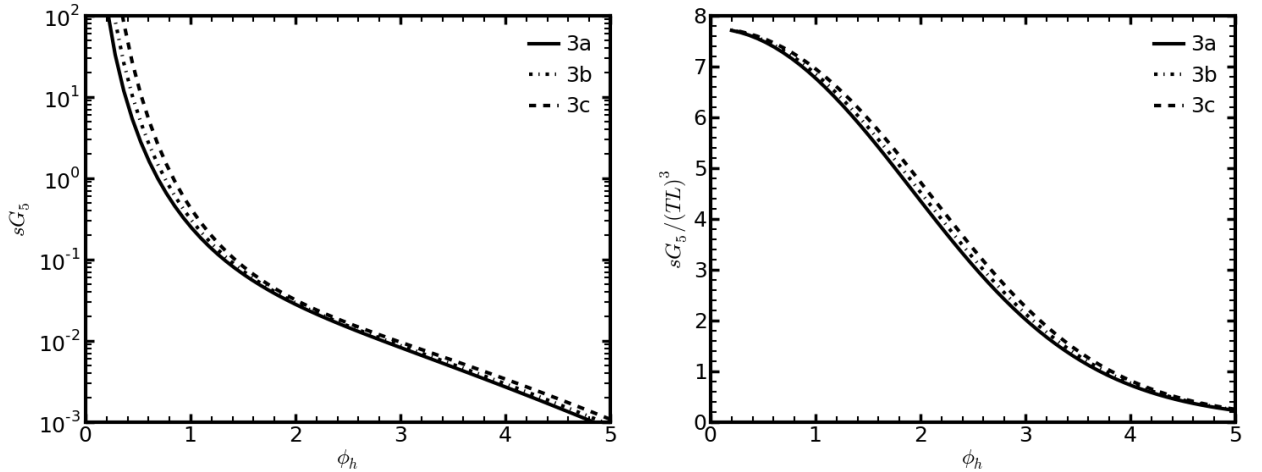


Figure 5.11.: Entropy density as a function of ϕ_h for the parameter values of table 5.2. Left panel: entropy density sG_5 . Right panel: scaled entropy density $sG_5/(TL)^3$.

transition. It is thus "natural" to define

$$T_c = T_{min}, \quad (5.10)$$

i.e. to identify the deconfinement temperature T_c with the first minimum of $T(\phi_h)$. It is however also possible to choose any other value $T_c = T(\phi_h^c)$ with $\phi_h^c < \phi_{min}$.

In the cases, where $T(\phi_h)$ does not have a minimum (as for the curves 3 and 4 exhibited

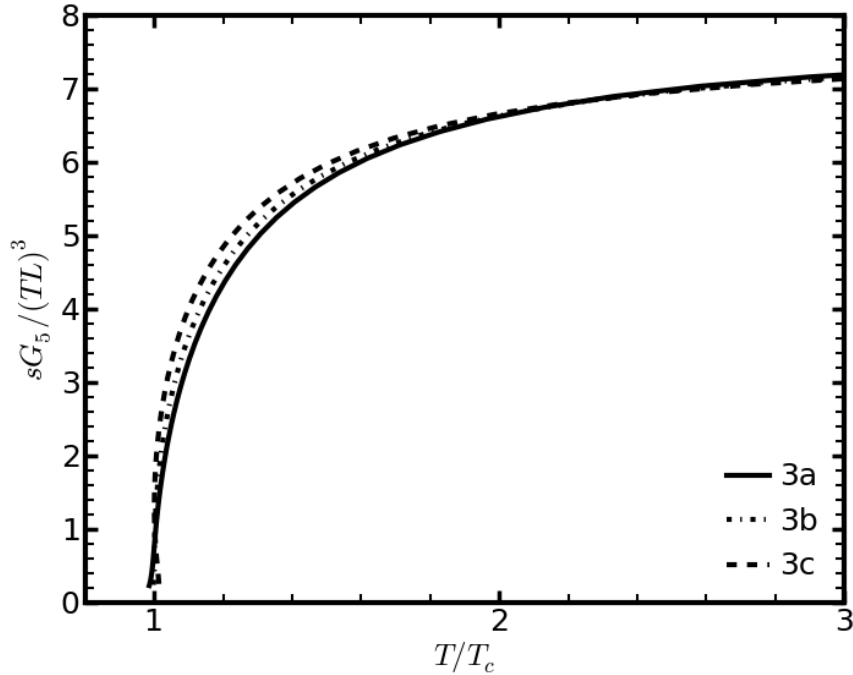


Figure 5.12.: Scaled entropy density as a function of T/T_c for the parameter values of table 5.2.

in figure 5.5) a "natural" definition of T_c , proposed in [41], would be

$$\left. \frac{d^2}{dT^2} \frac{s}{T^3} \right|_{T_c} = 0, \quad (5.11)$$

i.e. T_c is defined as the inflection point of $s/T^3(T)$. But one can in principle also consistently choose T_c at any other value of ϕ_h , $T_c = T(\phi_h^c)$.

In table 5.1, T_c and the corresponding ϕ_h^c were obtained using the respective "natural" definitions (5.10) or (5.11). Equations (5.10) and (5.11) can be combined into the condition that T_c is the location of the maximum of the T -derivative of the scaled entropy density,

$$\frac{d}{dT} \frac{s}{T^3}(T),$$

which recovers equation (5.11).

5.3. Reconstruction of the $SU(3)$ Yang-Mills equation of state

We use now the lattice data of [36] in a bottom-up approach to the equation of state of the $SU(3)$ Yang-Mills plasma. First, we extract from [36] the entropy density as a function of the temperature using

$$sT = I + 4p, \quad (5.12)$$

where we have abbreviated the interaction measure $I = e - 3p$. Then, we use a B-spline interpolation of $s(T)$ to compute the squared speed of sound given by

$$c_s^2(T) = \frac{s}{T} \left(\frac{ds}{dT} \right)^{-1}. \quad (5.13)$$

It should be emphasized that the employed B-spline does not necessarily go through all tabulated values - instead, a smooth interpolation is attempted. The advantage of using $c_s^2(T)$ instead of $s(T)$ is due to the fact that G_5 cancels in equation (5.13). One thus has one less parameter to fit.

We perform the fit in two steps:

1. fit γ and b to $c_s^2(T/T_c)$,
2. fit G_5/L^3 to $s/T^3(T/T_c)$.

The integration constant $p_0/T_c^4 \equiv p(T_c)/T_c^4$, needed for the calculation of the pressure $p(T)$ (B.6), is taken from [36]. Since the B-spline interpolation of both the lattice data and the calculated data points for $s(T)$ becomes unstable for $T \rightarrow T_c^+$ due to the sharp rise of c_s^2 , referring to the weak first-order phase transition of the $SU(3)$ Yang-Mills theory, we fit temperatures in the interval $1.02 \leq T/T_c$ in the first step. We present the results for two ranges of temperatures:

1. Close to T_c : $1 \leq T/T_c \leq 10$. This is the strongly coupled region relevant for heavy ion collisions.
2. Up to the asymptotic region: $1 \leq T/T_c \leq 1000$. With the new lattice data [36] at our disposal, it is interesting to perform a fit in a large range of temperatures.

Having determined $s(T)$ and $p(T)$, the interaction measure $I(T)$ is obtained straightforwardly via equation (5.12). The initial values of the parameters can be obtained using input from the Yang-Mills theory. This is explained in appendix C, cf. equations (C.4), (C.7), (C.12) and the related discussion.

First temperature interval

The fit is performed as follows: γ and b are given as parameters. First the $T(\phi_h)$ dependence is roughly scanned by computing the temperature T at 10 points between ϕ_h^{min} and ϕ_h^{max} . Hereby, ϕ_h^{min} is given by the asymptotic formula (4.55) with $LT_{UV} = 6$. (As seen in table 5.1, $T_c L < 1$ holds for all parameter values considered. We choose $LT_{UV} = 6$ to make sure that $T/T_c \gtrsim 4$ for $\phi_h = \phi_h^{min}$.) To make sure that ϕ_h^c is reached, we take a rather large value $\phi_h^{max} = 6.5$. Having computed $T(\phi_h)$, one can estimate T_c and its type (minimum or inflection point). Next, the temperature T is again computed at 10 points in the interval between $0.7\phi_h^c$ and $1.05\phi_h^c$ to determine T_c with a relative accuracy of $\approx 10^{-3}$ and the corresponding value ϕ_h^c . New bounds are set for ϕ_h : $\phi_h^{min} = 0.5$,⁵ $\phi_h^{max} = \phi_h^c$. Now, $T(\phi_h)$ and $s(\phi_h)$ are computed at 20 points, and the squared speed of sound $c_s^2(T/T_c)$ is obtained via a B-spline interpolation of the $s(T)$ curve and equation (5.13). Finally, the sum of squares

$$\chi^2 = \frac{1}{n} \sum_{i=0}^n (c_s^2(T_i/T_c) - c_{s,L}^2(T_i/T_c))^2 \quad (5.14)$$

is computed, where the points T_i/T_c are taken from [36] in the range $t_{min} \leq T_i/T_c \leq t_{max}$ and $c_{s,L}^2(T_i/T_c)$ is the squared speed of sound computed at T_i , obtained from the B-spline interpolation of $s(T)$, equation (5.12), of the lattice data [36]. Hereby, t_{min} and t_{max} are respectively the lower and upper bounds of the three T/T_c -intervals listed below. Minimizing χ^2 the optimal parameter values γ and b are obtained. The parameter G_5/L^3 is fixed by a separate χ^2 -fit of the scaled entropy density $s/T^3(T/T_c)$ to lattice data [36] on the points $t_{min} \leq T_i/T_c \leq t_{max}$, keeping γ and b fixed.⁶

We fit three temperature ranges:

1. $1 \leq T/T_c \leq 2$. Here, the emphasis lies in particular on an accurate reproduction of the peak of the scaled interaction measure I/T^4 .
2. $2.5 \leq T/T_c \leq 10$. In this case, the focus lies on the reproduction of the fall-off of the scaled interaction measure I/T^4 .
3. $1 \leq T/T_c \leq 10$. Here, a reproduction of the whole temperature interval relevant for the LHC is performed.

⁵The value $\phi_h^{min} = 0.5$ turned out to be a good estimate for $T/T_c \approx 10$ for the parameter range found in table 5.3.

⁶More generically, the problem can be posed as a solution of the non-linear least squares $\chi^2(\gamma, b; G_5, T_c L)$ equations. Standard methods include e.g. the Levenberg-Marquardt algorithm. Since $T_c L$ is adjusted as described above, we solve instead the $\chi^2(\gamma, b)$ minimization with G_5 adjusted separately.

Our results, obtained with the method just described and employing the solution technique described in section 4.3, are summarized in tables 5.3 and 5.4. It should be noted that the numerics are rather sensitive to the values of the parameters, therefore, in table 5.3 the values are given with necessary digits. The exact vales of M^2L^2 and Δ can be obtained with equation (5.8).

Fit	Range	γ	b	G_5/L^3	$-M^2L^2$	Δ
1	$1 \leq T/T_c \leq 2$	0.709	2.156	1.215	≈ 1.720	≈ 3.510
2	$2.5 \leq T/T_c \leq 10$	0.641	2.081	1.138	≈ 0.769	≈ 3.798
3	$1 \leq T/T_c \leq 10$	0.702	2.188	1.188	≈ 1.538	≈ 3.569

Table 5.3.: Parameter values of the $s(T)$ fit in the range $1 \leq T/T_c \leq 10$.

Fit	T_cL	T_c -type	$10^6 \times \chi_{e_s}^2$	$10^3 \times \chi_s^2$
1	0.164	minimum	4.6	1.5
2	0.100	inflection	7.7×10^{-3}	0.020
3	0.158	minimum	4.5	8.5

Table 5.4.: Deconfinement temperatures and sums of squares of the $s(T)$ fit in the range $1 \leq T/T_c \leq 10$.

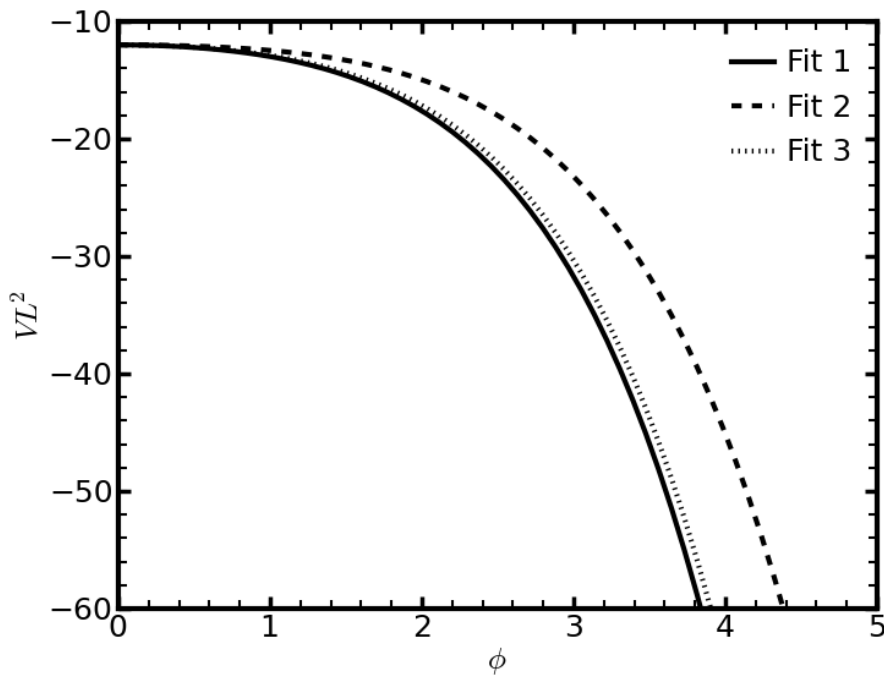


Figure 5.13.: The potential $V(\phi)$ for the parameter values of table 5.3.

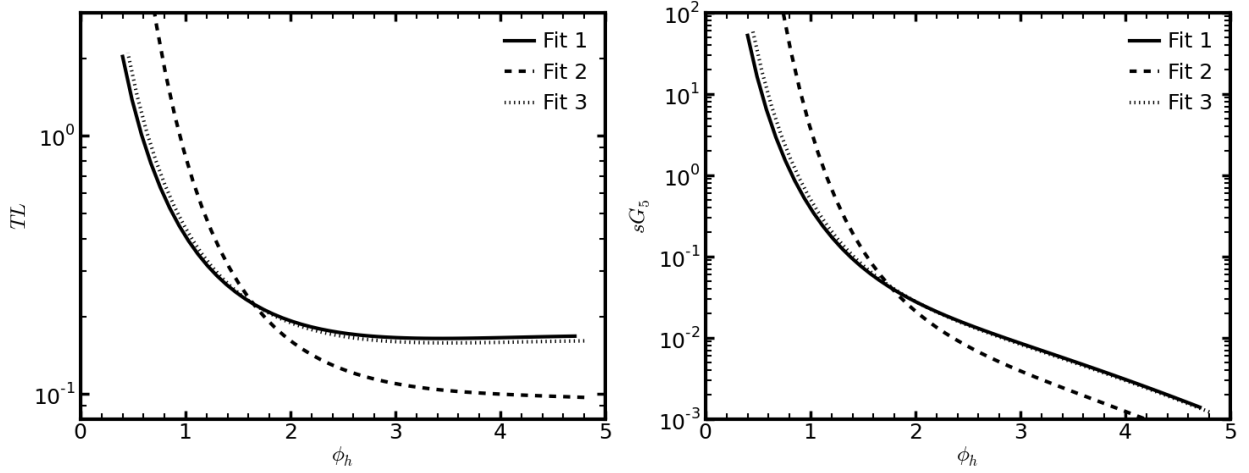


Figure 5.14.: Temperature and entropy density as functions of ϕ_h for the parameters values of table 5.4. Left panel: temperature TL . Right panel: entropy density sG_5 .

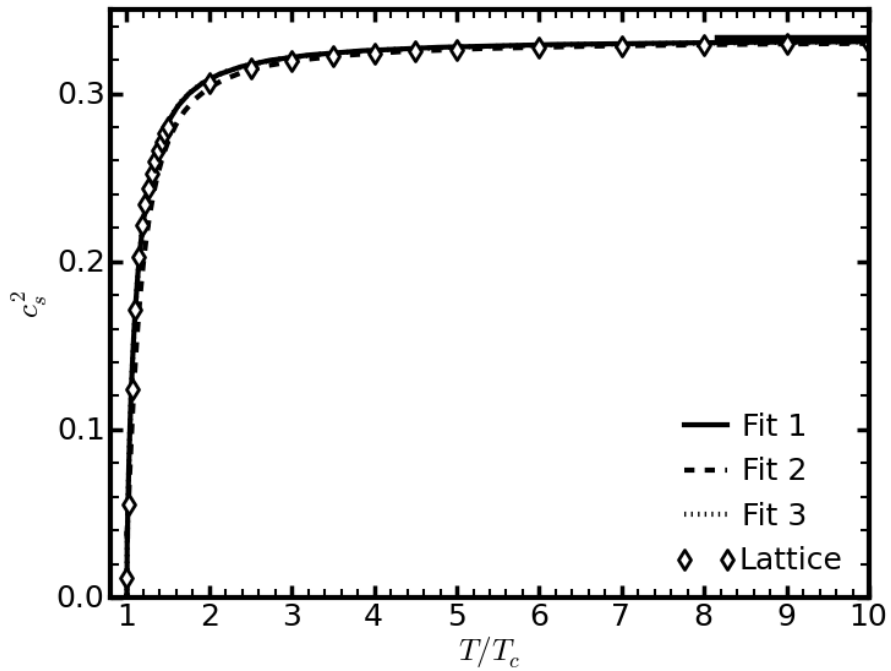


Figure 5.15.: Squared speed of sound c_s^2 . Diamonds: values extracted from the lattice data of [36], curves: fit of the model. The horizontal line on the right denotes the ideal gas value $c_s^2 = 1/3$.

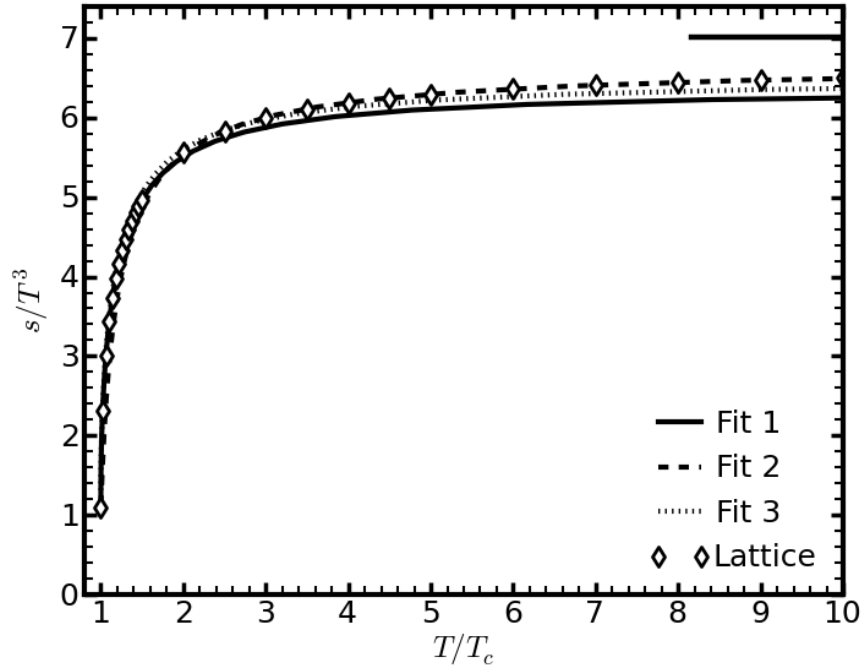


Figure 5.16.: Scaled entropy density s/T^3 . Diamonds: values of the lattice data of [36], curves: fit of the model. The horizontal line on the right denotes the Stefan-Boltzmann limit (B.9).

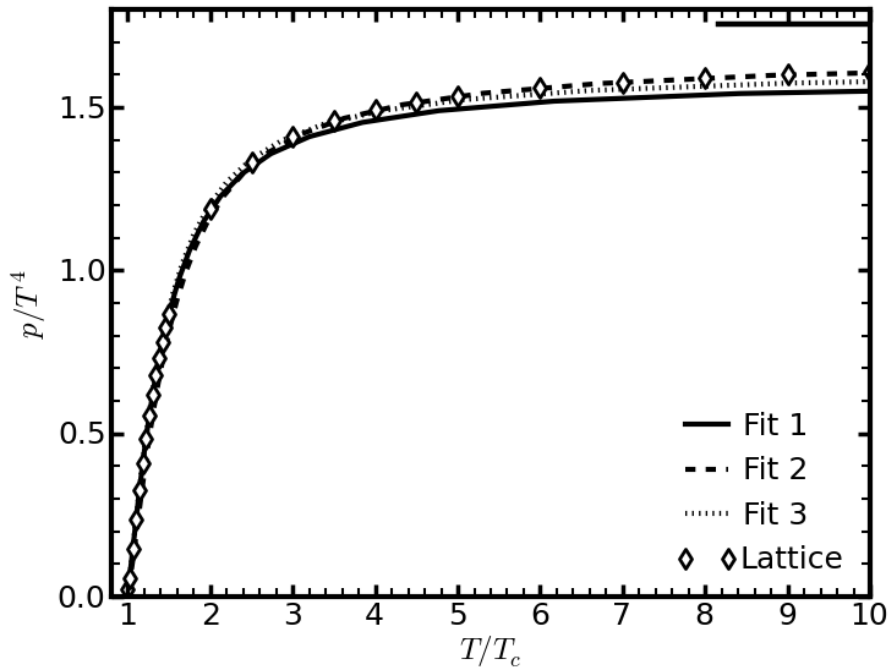


Figure 5.17.: Scaled pressure p/T^4 . Diamonds: values of the lattice data of [36], curves: fit of the model. The horizontal line on the right denotes the Stefan-Boltzmann limit (B.10).

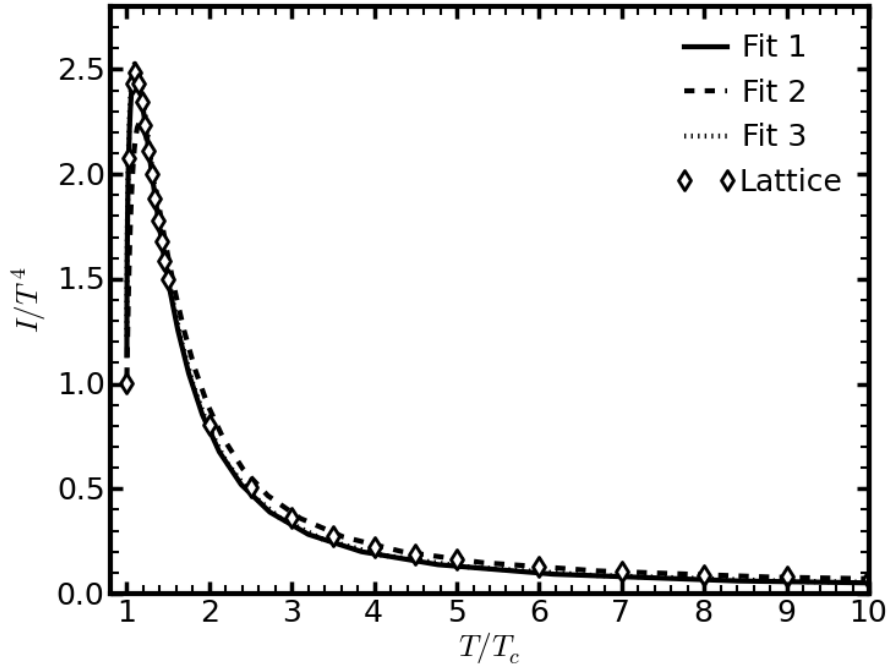


Figure 5.18.: Scaled interaction measure I/T^4 . Diamonds: values of the lattice data [36], curves: fit of the model.

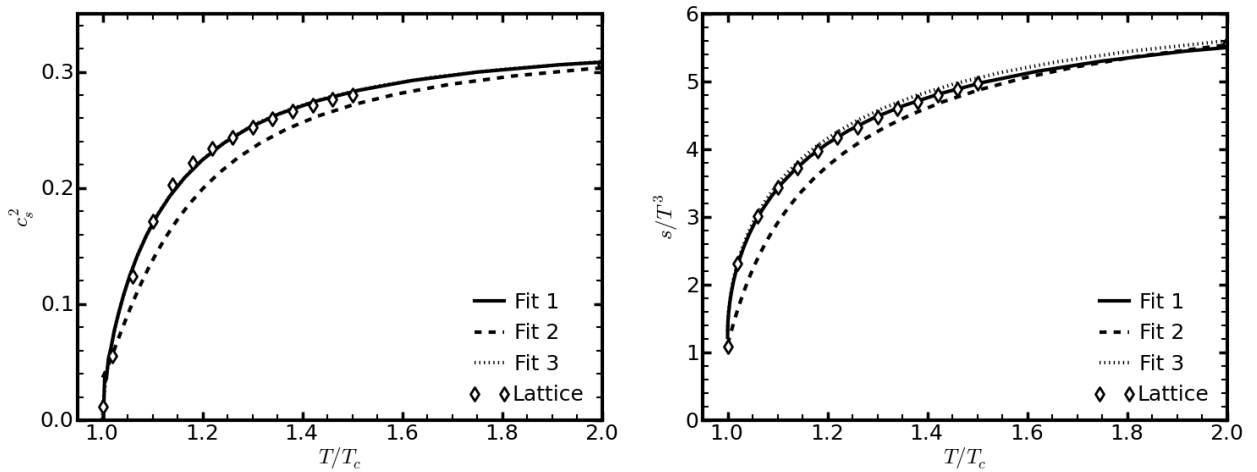


Figure 5.19.: Zoom into the range $1 \leq T/T_c \leq 2$. Left panel: squared speed of sound c_s^2 . Right panel: scaled entropy density s/T^3 . Diamonds: values of the lattice data [36], curves: fit of the model.

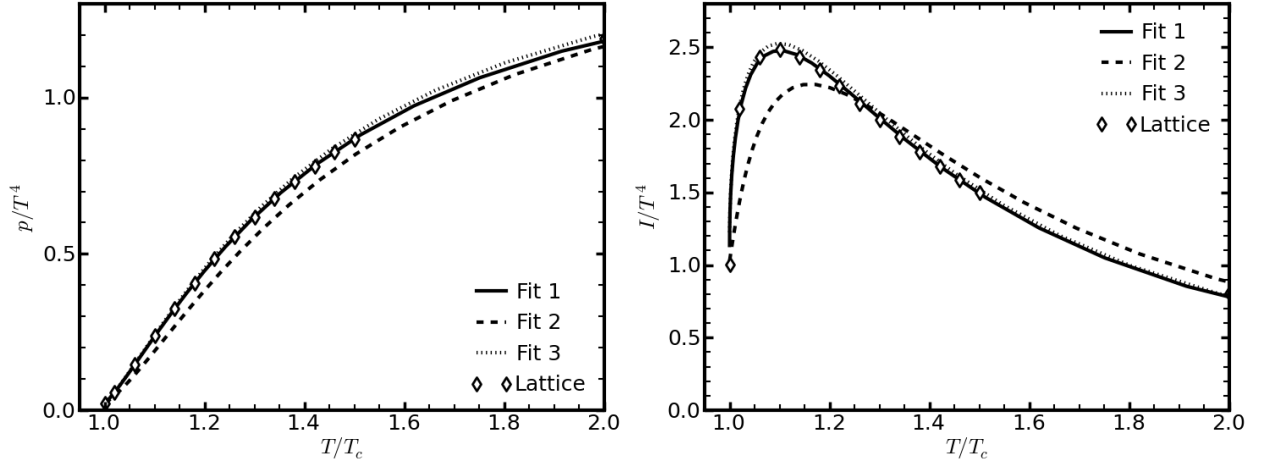


Figure 5.20.: Zoom into the range $1 \leq T/T_c \leq 2$. Left panel: scaled pressure p/T^4 . Right panel: scaled interaction measure I/T^4 . Diamonds: values of the lattice data [36], curves: fit of the model.

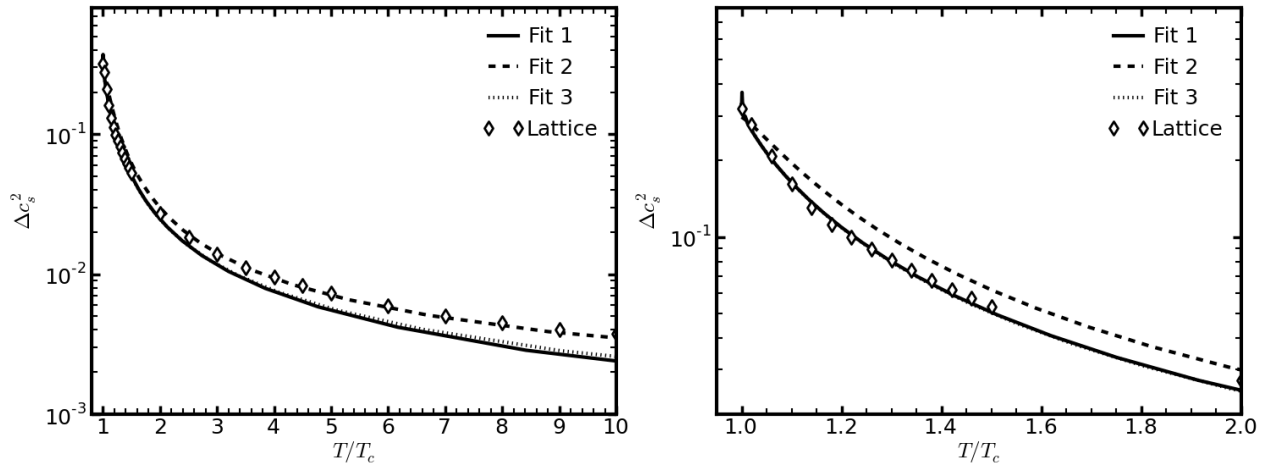


Figure 5.21.: The conformality measure $\Delta c_s^2 \equiv 1/3 - c_s^2$. Left panel: full temperature interval $1 \leq T/T_c \leq 10$. Right panel: zoom into the range $1 \leq T/T_c \leq 2$. Diamonds: values extracted from the lattice data [36], curves: fit of the model.

Second temperature interval

In the asymptotic region $T/T_c \gtrsim 10$, the temperature (4.53) and entropy density (4.54) are close to their asymptotic values given by equations (4.56) and (4.55). The metric coefficients $A(\phi)$ and $B(\phi)$ are accordingly

$$A(\phi) \approx \frac{\ln \phi}{\Delta - 4} + \ln(\Lambda L), \quad (5.15)$$

$$B(\phi) \approx -\ln(\phi(4 - \Delta)). \quad (5.16)$$

Thus, $A' \propto -1/\phi$ computed from equation (4.44), will be large for small values of ϕ , which can lead to numerical instabilities and/or inaccuracies. It makes sense to rewrite equations (4.54) and (4.53) into a more suitable form following [2].

For the entropy density consider equation (4.54) together with equation (4.56). Rewrite equation (4.54) as

$$4sG_5 = \exp\left(3A(\phi_h)\right) = \exp\left(3 \int_{\phi_0}^{\phi_h} d\tilde{\phi} A'(\tilde{\phi}) + \frac{1}{\tilde{\phi}(\Delta - 4)} - \frac{1}{\tilde{\phi}(\Delta - 4)}\right) \quad (5.17)$$

$$= \phi_h^{3/(\Delta-4)} (\Lambda L)^3 \exp\left(-3 \frac{\ln \phi_0}{\Delta - 4}\right) \exp\left(3 \int_{\phi_0}^{\phi_h} d\tilde{\phi} \left(A'(\tilde{\phi}) - \frac{1}{\tilde{\phi}(\Delta - 4)}\right)\right). \quad (5.18)$$

Take the limit $\phi_0 \rightarrow 0$ to obtain

$$4sG_5 = \phi_h^{3/(\Delta-4)} (\Lambda L)^3 \exp\left(3 \int_0^{\phi_h} d\tilde{\phi} \left(A'(\tilde{\phi}) - \frac{1}{\tilde{\phi}(\Delta - 4)}\right)\right). \quad (5.19)$$

The asymptotic behavior is now isolated and the divergent behavior of $A'(\phi)$ is canceled by the $1/(\phi(\Delta - 4))$ term. For $\phi_h \rightarrow 0$ the integral in (5.19) approaches zero and $s \rightarrow s_{UV}$, where s_{UV} is given by equation (4.56).

We now bring the expression for the temperature (4.53) into a similar form. We first derive two relations that will be used in the manipulation of equation (4.53). Note from equation (4.46) that

$$f'|_{\phi_h} = -\frac{L^2 V}{3A'} e^{2B}|_{\phi_h}. \quad (5.20)$$

Note further that equation (4.52) can be written as

$$B(\phi_h) = B(\phi_0) + \int_{\phi_0}^{\phi_h} d\tilde{\phi} \left(\left(\ln A'(\tilde{\phi}) \right)' + \frac{1}{6A'(\tilde{\phi})} \right) \quad (5.21)$$

$$= B(\phi_0) + \ln A'(\phi_h) - \ln A'(\phi_0) + \int_{\phi_0}^{\phi_h} d\tilde{\phi} \left(\frac{1}{6A'(\tilde{\phi})} \right). \quad (5.22)$$

One thus has

$$\frac{e^{B(\phi_h)}}{A'(\phi_h)} = \frac{e^{B(\phi_0)}}{A'(\phi_0)} \exp\left(\int_{\phi_0}^{\phi_h} d\tilde{\phi} \frac{1}{6A'(\tilde{\phi})}\right) = -\exp\left(\int_{\phi_0}^{\phi_h} d\tilde{\phi} \frac{1}{6A'(\tilde{\phi})}\right), \quad (5.23)$$

where in the second equality we used $e^{B(\phi_0)}/A'(\phi_0) = -1$, following from the asymptotic expressions (5.15) and (5.16). The temperature can now be rewritten as

$$TL = -\frac{f'}{4\pi} e^{A-B}\Big|_{\phi_h} = \frac{L^2 V}{12\pi A'} e^{A+B}\Big|_{\phi_h} = -\frac{L^2 V}{12\pi} \exp\left(A + \int_{\phi_0}^{\phi_h} d\tilde{\phi} \frac{1}{6A'(\tilde{\phi})}\right)\Big|_{\phi_h} \quad (5.24)$$

$$= -\frac{(\Lambda L) L^2 V(\phi_h) \phi_h^{1/(\Delta-4)}}{12\pi} \exp\left(\int_0^{\phi_h} d\tilde{\phi} \left(A'(\tilde{\phi}) - \frac{1}{\tilde{\phi}(\Delta-4)} + \frac{1}{6A'(\tilde{\phi})}\right)\right). \quad (5.25)$$

We use equation (5.20) (second equality) and equation (5.23) (third equality). In the fourth equality of equation (5.25) we have rewritten $e^{A(\phi_h)}$ as in the expression for the entropy density (5.19) and took the limit $\phi_0 \rightarrow 0$. As in (5.19), the asymptotic behavior is isolated, and the integral approaches zero as $\phi_h \rightarrow 0$ and $T \rightarrow T_{UV}$ (4.55), since then $V(\phi_h) \rightarrow -12/L^2$.

Equations (5.19) and (5.25) are the ones used in [2]. We employ these here too to compute the temperature and the entropy density in the range $1 \leq T/T_c \leq 1000$.

Since the calculation of the squared speed of sound from the interpolation of the entropy density tabulated in [36], as described above, becomes unstable for $T/T_c \gtrsim 10$, we start with step 2, i.e. fit the parameters γ , b and G_5/L^3 to $s(T)$.

For small values of ϕ , i.e. for high temperatures, the potential (5.7) is approximated by

$$\lim_{\phi \rightarrow 0} V(\phi) = -\frac{12}{L^2} + \frac{M^2}{2} \phi^2. \quad (5.26)$$

Thus, we expect that a fit in the range $10 \lesssim T/T_c \leq 1000$ uniquely determines the value of $M^2 L^2$. However, to determine the deconfinement temperature T_c the whole potential is probed. To concentrate entirely on the small- ϕ region of V one would have to set the scale differently. This can be done by taking two arbitrary temperature values T_1 and T_2 and requiring that $s(T_1/T_c)$ and $s(T_2/T_c)$, calculated within our model, are equal to the corresponding lattice values; the two equations fix T_c and G_5 . Here, we use the full potential (5.7) to determine T_c and to calculate $M^2 L^2$ via equation (5.8). We fit three

temperature ranges:

1. $2.5 \leq T/T_c \leq 100$. Here, we study the “intermediate” region of the equation of state.
2. $10 \leq T/T_c \leq 1000$. Here, the asymptotic region, where the entropy density logarithmically approaches the Stefan-Boltzmann limit (B.9) is fitted.
3. $1 \leq T/T_c \leq 1000$. A global fit is performed.

Our results are summarized in tables 5.5 and 5.6.

Fit	Range	γ	b	G_5/L^3	$-M^2L^2$	Δ
4	$2.5 \leq T/T_c \leq 100$	0.642	2.072	1.138	≈ 0.800	≈ 3.789
5	$10 \leq T/T_c \leq 1000$	0.594	1.897	1.125	≈ 0.440	≈ 3.887
6	$1 \leq T/T_c \leq 1000$	0.680	2.179	1.160	≈ 1.191	≈ 3.676

Table 5.5.: The parameter values of the fit of the equation of state in the range $1 \leq T/T_c \leq 1000$.

Fit	LT_c	T_c -type	$10^3 \times \chi_s^2$
4	0.098	inflection	3.4×10^{-2}
5	0.076	inflection	8.3×10^{-2}
6	0.136	minimum	7.5

Table 5.6.: Deconfinement temperatures and sums of squares of the fit of the equation of state in the range $1 \leq T/T_c \leq 1000$.

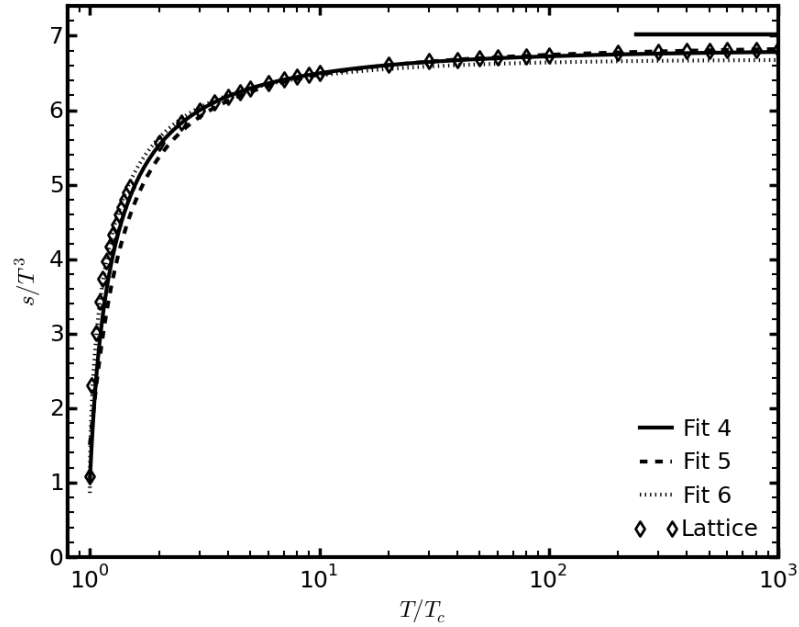


Figure 5.22.: Scaled entropy density s/T^3 for the parameter values of table 5.5. Diamonds: values of the lattice data [36], curves: fit of the model. The horizontal line on the right denotes the Stefan-Boltzmann limit (B.9).

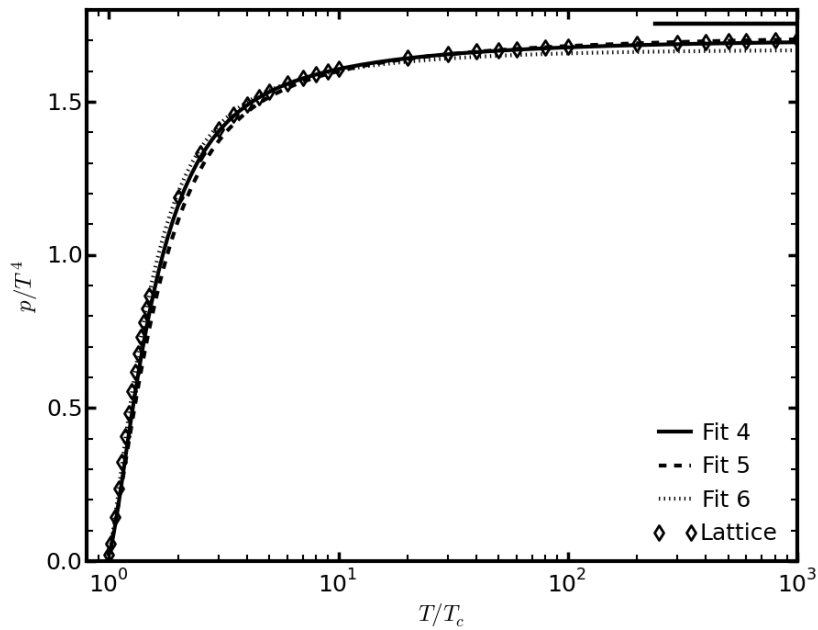


Figure 5.23.: Scaled pressure p/T^4 for the parameter values of table 5.5. Diamonds: values of the lattice data [36], curves: fit of the model. The horizontal line on the right denotes the Stefan-Boltzmann limit (B.10).

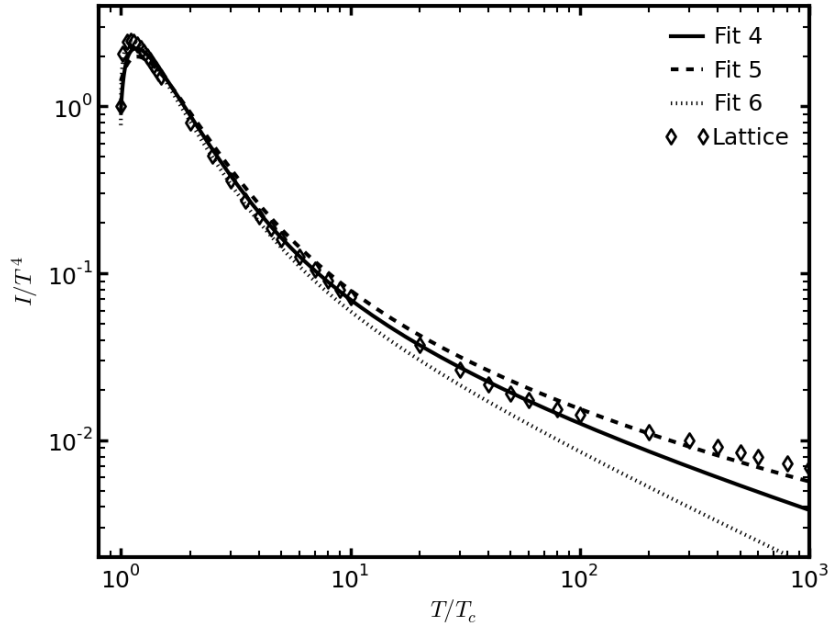


Figure 5.24.: Scaled interaction measure I/T^4 for the parameter values of table 5.5. Diamonds: values of the lattice data [36], curves: fit of the model.

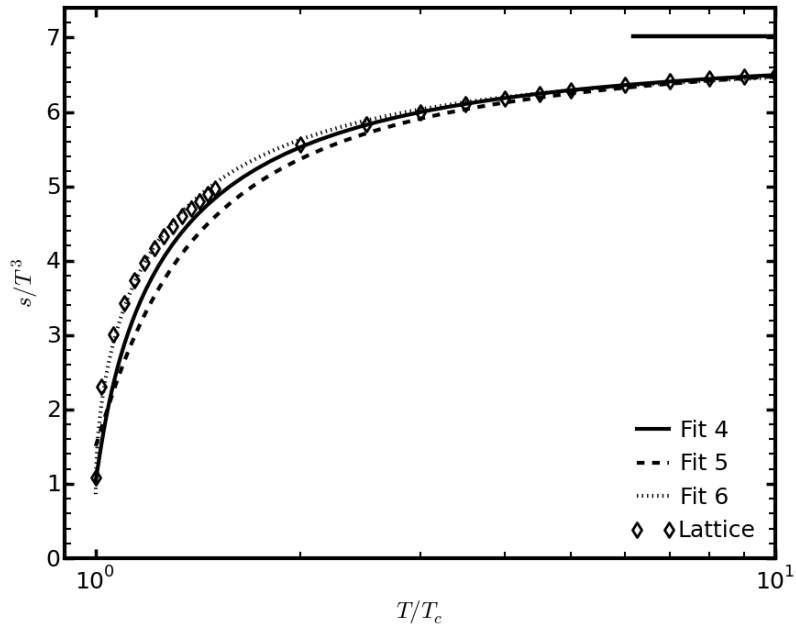


Figure 5.25.: Scaled entropy density s/T^3 for the parameter values of table 5.5. Zoom into the region $1 \leq T/T_c \leq 10$. Diamonds: values of the lattice data [36], curves: fit of the model. The horizontal line on the right denotes the Stefan-Boltzmann limit (B.9).

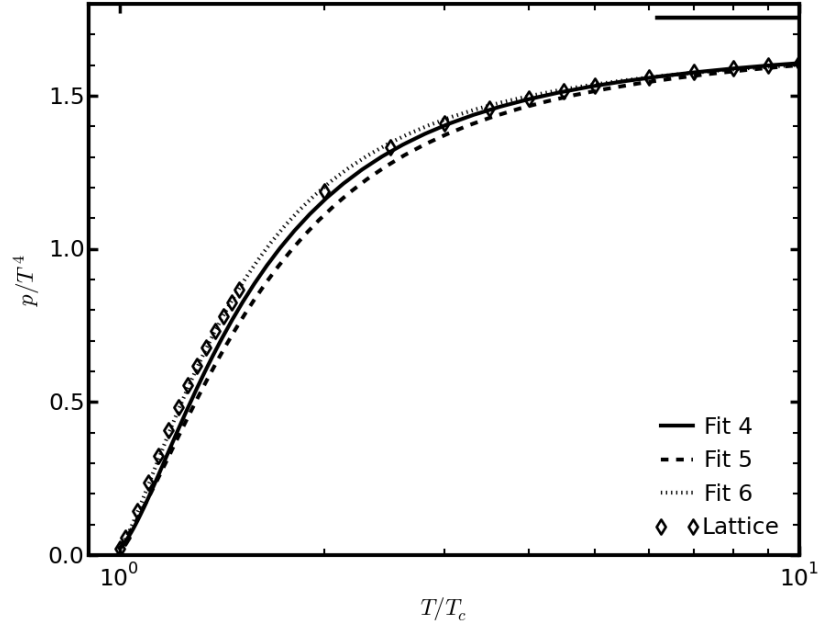


Figure 5.26.: Scaled pressure p/T^4 for the parameter values of table 5.5. Zoom into the region $1 \leq T/T_c \leq 10$. Diamonds: values of the lattice data [36], curves: fit of the model. The horizontal line on the right denotes the Stefan-Boltzmann limit (B.10).

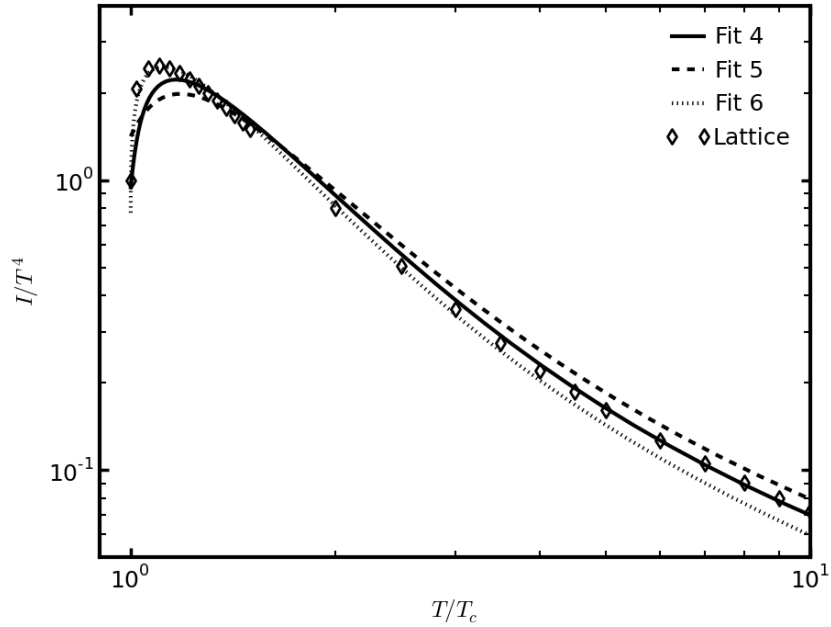


Figure 5.27.: Scaled interaction measure I/T^4 for the parameter values of table 5.5. Zoom into the region $1 \leq T/T_c \leq 10$. Diamonds: values of the lattice data [36], curves: fit of the model.

5.4. Conclusions

Within the model described in section 4.3 we have obtained the optimum values for the parameters γ and b of the potential (5.7) and G_5/L^3 in six temperature ranges. The values are summarized in tables 5.3 and 5.5.

1. $1 \leq T/T_c \leq 2$,
2. $2.5 \leq T/T_c \leq 10$,
3. $1 \leq T/T_c \leq 10$,
4. $2.5 \leq T/T_c \leq 100$,
5. $10 \leq T/T_c \leq 1000$,
6. $1 \leq T/T_c \leq 1000$.

First temperature interval

In the first case, the squared speed of sound c_s^2 , as well as s/T^3 , p/T^4 and I/T^4 are reproduced very well in the range $1 \leq T/T_c \leq 2$ (see figures 5.19 and 5.20), while for $2 \leq T/T_c \leq 10$ the lattice data is underestimated by s/T^3 and p/T^4 (figures 5.16 and 5.17) with an increasing deviation, the maximum deviation of $\approx 7\%$ occurring at $T/T_c = 10$. This is also seen in the left panel of figure 5.21, where the conformality measure Δc_s^2 obtained with the fit is about $2/3$ of that of the lattice data at $T/T_c = 10$.

The second fit, on the other hand, reproduces the data very well in the range $2.5 \leq T/T_c \leq 10$ (see figures 5.16, 5.17 and 5.18), while in the region $1 \leq T/T_c \leq 2$ the fit underestimates the lattice data, the maximum deviation of $\approx 15\%$ occurring at $T/T_c \approx 1.2$ for c_s^2 and s/T^3 (see 5.19). The scaled pressure p/T^4 is systematically underestimated (by $\approx 5\%$) in a broad region. The peak of the scaled interaction measure I/T^4 is shifted to $T/T_c \approx 1.15$, its magnitude is 2.2 instead of 2.5, and it is also slightly broader. The curves of the two fits intercept at $T/T_c \approx 2$ for s/T^3 and p/T^4 and at $T/T_c \approx 1.25$ for I/T^4 . For the temperatures below the interception, the first fit is very accurate and the second fit underestimates the lattice data, while above the interception the situation is converse. The third fit yields essentially the same thermodynamic quantities as the first fit, but showing a smaller deviation for higher temperatures as compared to the first fit.

Second temperature interval

As seen from the figures 5.22, 5.22 and 5.24, all three fits are able to rather well capture the qualitative behavior of the $SU(3)$ Yang-Mills plasma in the whole temperature range $1 \leq T/T_c \leq 1000$. We now focus on the nuances.

The fit of the "intermediate region", reproduces the lattice data very well in the region $2.5 \leq T/T_c \leq 100$ as seen in figures 5.22, 5.22 and 5.24, deviating for $T/T_c \lesssim 2$ and $T/T_c \gtrsim 100$. For $T/T_c < 2.5$, s/T^3 and p/T^4 are underestimated with a deviation of $\approx 10\%$, for $T/T_c \gtrsim 100$ the fit systematically deviates from the lattice data and is about $1/2$ of the scaled interaction measure I/T^4 at $T/T_c = 1000$. Since the parameters of the second and of the fourth fits are very similar, one concludes that the behavior of the equation of state in the "intermediate region" $2.5 \leq T/T_c \leq 100$ is already captured by the fit in the smaller interval $2.5 \leq T/T_c \leq 10$. The fifth fit, concentrating mainly on the asymptotic region, shows for $T/T_c \gtrsim 100$ a minor improvement upon the "intermediate" fit, as best seen in figure 5.24. For lower temperatures however, the fifth fit under(over)estimates s/T^3 , p/T^4 (I/T^4), showing a behavior similar to the fourth fit, but with a bigger deviation.

In contrast to the fourth and fifth fits, the global fit reproduces s/T^3 and p/T^4 especially well in the region $1 \leq T/T_c \leq 10$ (figures 5.16 and 5.17) and also the peak of the scaled interaction measure I/T^4 (see figure 5.27); however, for temperatures $T/T_c \gtrsim 10$, s/T^3 and p/T^4 are underestimated, with a deviation which systematically increases for increasing temperatures. This deviation is most evident in figure 5.24. The mutual behavior of the fourth and sixth fits is similar to the behavior of the first and second fits.

We find a systematic evolution of the parameters from low to high temperatures, which is summarized in table 5.7. The parameters γ , b and G_5/L^3 decrease. The scaling dimension Δ increases and the negative AdS mass $-M^2L^2$ of the scalar field decreases. The deconfinement temperature LT_c decreases.

Fit range	γ	b	G_5/L^3	$-M^2L^2$	Δ	LT_c
$1 \leq T/T_c \leq 2$	0.709	2.156	1.215	≈ 1.720	≈ 3.510	≈ 0.164
$2.5 \leq T/T_c \leq 10$	0.641	2.081	1.138	≈ 0.769	≈ 3.798	≈ 0.100
$10 \leq T/T_c \leq 1000$	0.594	1.897	1.125	≈ 0.440	≈ 3.887	≈ 0.076

Table 5.7.: The evolution of the parameters values of the fits from low to high temperatures.

While the above discussion of the first temperature interval might suggest that the intervals $1 \leq T/T_c \leq 2$ and $2.5 \leq T/T_c \leq 10$ are mutually incompatible (since the third

fit yields essentially the same equation of state as the first one, being slightly better for $T/T_c \approx 10$), one sees from figures 5.25 and 5.27 that the global fit actually does yield the best fit in the interval $1 \leq T/T_c \leq 10$, exhibiting a deviation from the lattice data clearly discernible only in figure 5.27, where the scaled interaction measure is underestimated by $\approx 15\%$ at $T/T_c = 10$, and being slightly less accurate than the first fit for $T/T_c \approx 1$.⁷ We thus regard the first, second and sixth fits as our final results: the first fit reproduces very well the direct vicinity of the phase transition, the second fit reproduces very well the fall-off of the scaled interaction measure and extends to $T/T_c \approx 100$, and the global fit reproduces best the region $1 \leq T/T_c \leq 10$ relevant for heavy-ion collisions. Compare figures 5.28, 5.29 and 5.30. We now proceed to calculate the shear and bulk viscosities for the these three parameter sets.

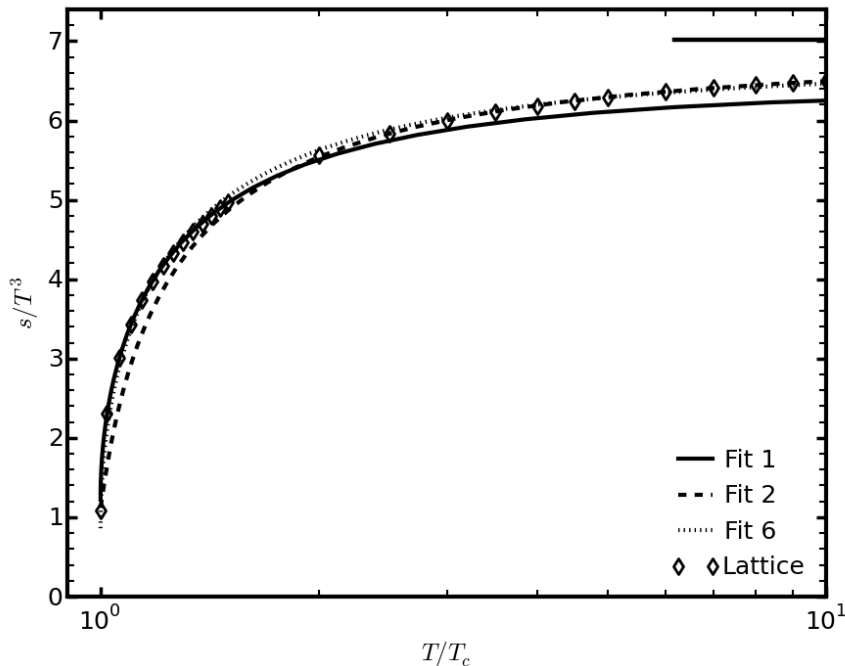


Figure 5.28.: Scaled entropy density s/T^3 . Comparison of the 1st, 2nd and 6th fits in the interval $1 \leq T/T_c \leq 10$. Diamonds: values of the lattice data [36], curves: fits. The horizontal line on the right denotes the Stefan-Boltzmann limit (B.9). One sees the improvement by the global fit.

⁷If one wants to reproduce also the scaled interaction measure I/T^4 with an accuracy of $\leq 5\%$, the statement made above of course still holds: the intervals $1 \leq T/T_c \leq 2$ and $2.5 \leq T/T_c \leq 10$ are incompatible when using the potential 5.7. This is best seen in figure 5.30.

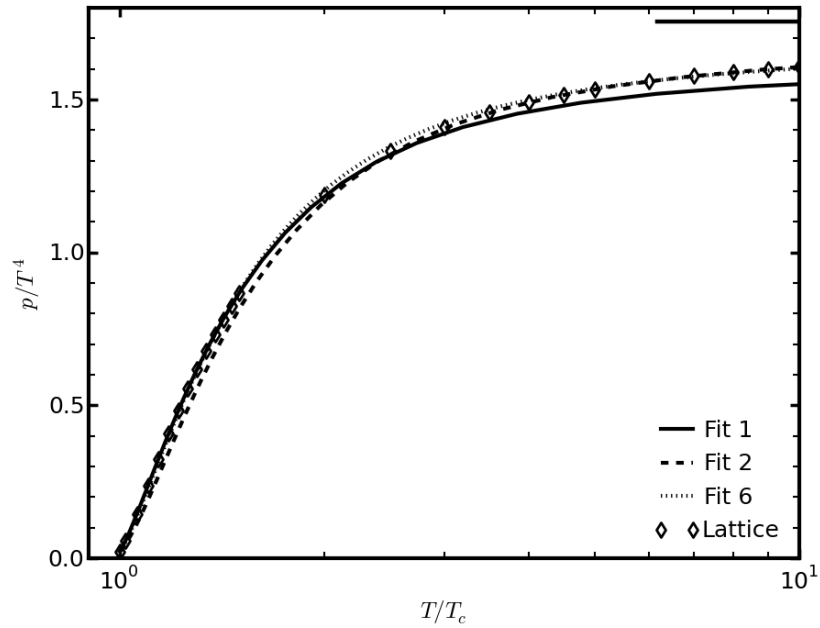


Figure 5.29.: Scaled pressure p/T^4 . Comparison of the 1st, 2nd and 6th fits in the interval $1 \leq T/T_c \leq 10$. Diamonds: values of the lattice data [36], curves: fits. The horizontal line on the right denotes the Stefan-Boltzmann limit (B.10). One sees the improvement by the global fit.

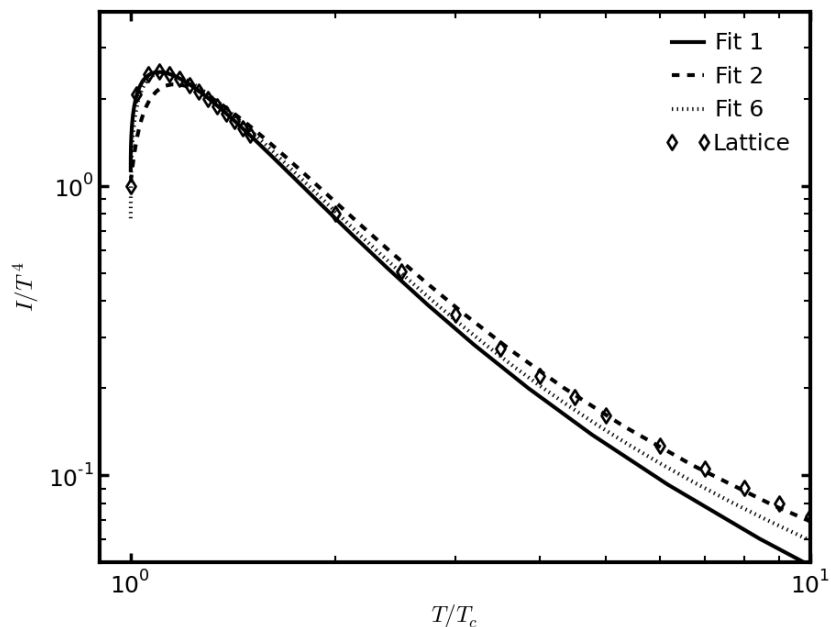


Figure 5.30.: Scaled interaction measure I/T^4 . Comparison of the 1st, 2nd and 6th fits in the interval $1 \leq T/T_c \leq 10$. Diamonds: values of the lattice data [36], curves: fits. One sees that the global fit yields a good interpolation between the 1st and 2nd fits in the interval considered.

6. The shear and bulk viscosities

6.1. Kubo formulae

The bulk and shear viscosities ζ and η describe the relaxation of a fluid towards thermal equilibrium after a small deviation away from it. To compute $\zeta(T)$ and $\eta(T)$ we use the Kubo formulae, known from linear response theory. Define retarded correlators of the energy momentum tensor $T_{\mu\nu}$ by (the special shear mode corresponding to T_{12} and the bulk mode to T_k^k)

$$G_R^\eta(\omega) = -i \int dt d^3x e^{i\omega t} \theta(t) \langle [T_{12}(t, \vec{x}), T_{12}(0, 0)] \rangle, \quad (6.1)$$

$$G_R^\zeta(\omega) = -i \frac{1}{4} \int dt d^3x e^{i\omega t} \theta(t) \langle [T_i^i(t, \vec{x}), T_k^k(0, 0)] \rangle. \quad (6.2)$$

(In this section, Greek indices run from 0 to 3 and Latin indices from 1 to 3). The shear and bulk viscosities are given by the Kubo formulae

$$\eta = - \lim_{\omega \rightarrow 0} \frac{1}{\omega} \text{Im} G_R^\eta(\omega), \quad (6.3)$$

$$\zeta = - \frac{1}{9} \lim_{\omega \rightarrow 0} \frac{1}{\omega} \text{Im} G_R^\zeta(\omega). \quad (6.4)$$

Equations (6.3) and (6.4) are derived as follows.¹ One considers a small perturbation $h_{\mu\nu}$ to a theory defined by an action S_0 , i.e.

$$S = S_0 + \frac{1}{2} \int d^4x T^{\mu\nu} h_{\mu\nu}, \quad (6.5)$$

where $T^{\mu\nu}$ is the energy momentum tensor. Within perturbation theory, the expectation value $\langle T^{\mu\nu}(x) \rangle$ to leading order is given by

$$\langle T^{\mu\nu}(x) \rangle = \langle T^{\mu\nu}(x) \rangle_0 - \frac{1}{2} \int d^4y G_R^{\mu\nu, \alpha\beta}(x-y) h_{\alpha\beta}(y), \quad (6.6)$$

¹See appendix A of [41] and appendix A of [17] for details.

where

$$iG_R^{\mu\nu,\alpha\beta}(x-y) \equiv \theta(x^0 - y^0) \langle [T^{\mu\nu}(x), T^{\alpha\beta}(y)] \rangle, \quad (6.7)$$

is the response function and $\langle T^{\mu\nu}(x) \rangle_0$ is the unperturbed expectation value. Fourier transforming equation (6.6) one obtains for $\delta \langle T_{\mu\nu}(x) \rangle \equiv \langle T_{\mu\nu}(x) \rangle - \langle T_{\mu\nu}(x) \rangle_0$

$$\delta \langle T_{ij}(\omega, \vec{0}) \rangle = -\frac{1}{2} G_R^{kl}{}_{ij}(\omega, \vec{0}) h_{kl}(\omega, \vec{0}), \quad (6.8)$$

where, assuming $h_{\mu 0} = h_{0\nu} = 0$, we consider only the spatial components ij . In addition, we have taken the long wavelength limit $\vec{k} \rightarrow \vec{0}$.

Consider on the other hand the decomposition of the energy momentum tensor of a viscous fluid without conserved charges

$$T^{\mu\nu} = (e + p)u^\mu u^\nu + pg^{\mu\nu} - P^{\mu\alpha} P^{\nu\beta} \left[\eta(u_{\beta;\alpha} + u_{\alpha;\beta} - \frac{2}{3}g_{\alpha\beta}u^\lambda{}_{;\lambda}) + \zeta g_{\alpha\beta}u^\lambda{}_{;\lambda} \right], \quad (6.9)$$

where a semicolon denotes covariant differentiation, u^μ is the fluid four-velocity, and $P^{\mu\nu} \equiv g^{\mu\nu} + u^\mu u^\nu$ is a u^μ -orthogonal projector. Consider a small spatial perturbation h_{ij} around the Minkowski metric $g_{ij} = \eta_{ij} \rightarrow \eta_{ij} + h_{ij}$. The spatial components of the perturbation δT_{ij} of $T^{\mu\nu}$, the latter given by equation (6.9), are

$$\delta T_{ij} = ph_{ij} - \frac{1}{2} K h_k{}^k \delta_{ij} + \delta_{ij} \eta (-\partial_t h_{ij} + \frac{1}{3} \delta_{ij} \delta^{kl} \partial_t h_{kl}) - \frac{1}{2} \zeta \delta_{ij} \delta^{kl} \partial_t h_{kl}, \quad (6.10)$$

where $K = -V \partial p / \partial V$ is the bulk modulus. The Fourier transform of equation (6.10) lets us obtain

$$\delta T_{ij} = h_{kl}(\omega) \left(p \delta_i{}^k \delta_j{}^l - \frac{1}{2} K \delta_{ij} \delta^{kl} \right) + \frac{i\omega}{2} h_{kl}(\omega) \left[\eta (\delta_i{}^k \delta_j{}^l + \delta_i{}^l \delta_j{}^k - \frac{2}{3} \delta_{ij} \delta^{kl}) + \zeta \delta_{ij} \delta^{kl} \right]. \quad (6.11)$$

Compare equations (6.8) and (6.11). Set $i = k = 1$ and $j = l = 2$ to obtain equation (6.3); perform a trace over ij and kl to obtain equation (6.4). Note that the concrete form of the perturbation $h_{ij}(\omega)$ is arbitrary. The interpretation of equations (6.3) and (6.4) is that the transport coefficients η and ζ can be obtained from the response of the fluid to a small perturbation.² Note that for a conformally invariant fluid $T^\mu{}_\mu = e - 3p = 0$ and subsequently $\zeta \equiv 0$. Thus, besides the interaction measure I and the conformality measure Δc_s^2 (see appendix B.2), the bulk viscosity ζ is another measure for the deviation of a fluid from ideal behavior. The general interpretation is as follows: the shear (bulk) viscosity is a measure of the medium resistance against volume (shape) conserving deformations.

²In fact, given any conserved current operator J^μ , the long-wavelength, low frequency limit of the associated response function G_R defines a transport coefficient.

6.2. The holographic correlator

We make use of the AdS/CFT prescription for computing correlators, reviewed in section 3.4.3. In [41] it was shown that

$$\text{Im}G_R^{\{\eta,\zeta\}}(\omega) = -\frac{\mathcal{F}^{\{\eta,\zeta\}}(\omega)}{16\pi G_5}, \quad (6.12)$$

where $\mathcal{F}(\omega)$ is a functional of the linearly perturbed metric $g_{\mu\nu}^{\{\eta,\zeta\}}$ and its derivatives on the gravity side. Equation (6.12) can be motivated by noting that the gauge theory energy momentum tensor $T^{\mu\nu}$ is dual to the metric $g_{\mu\nu}$ of the deformed AdS_5 space. Thus, by the AdS/CFT correspondence, as described in section 3.4.3, the correlators (6.1) and (6.2) can be obtained from the dual gravity theory by computing the renormalized action $S_{GRAV}^{[ren]}[g_{\mu\nu}^{\{\eta,\zeta\}}]$, evaluating it on the solutions of the equations of motion of $g_{\mu\nu}^{\{\eta,\zeta\}}$, and taking functional derivatives with respect to the boundary values. The heuristic interpretation of equation (6.12) is that the gauge theory transport coefficients η and ζ are proportional to the probability of a graviton to "fall" from the boundary into the black hole [43]. We now review the construction and evaluation of $\mathcal{F}^{\{\eta,\zeta\}}$, closely following [41].

6.2.1. Perturbation of the metric

The metric of section 4.3 is used, encoded in the following infinitesimal line element squared and henceforth referred to as $g_{\mu\nu}^{(0)}$

$$ds^2 = e^{2A}(-f dt^2 + d\vec{x}^2) + L^2 e^{2B} \frac{d\phi^2}{f}. \quad (6.13)$$

The metric (6.13) is now perturbed $g_{\mu\nu}^{(0)} \rightarrow g_{\mu\nu}^{\{\eta,\zeta\}}$. As discussed in section 6.1 the concrete form of the perturbation is arbitrary. The form chosen below leads to relatively simple expressions for the determinants g^η and g^ζ .

For the shear perturbation, the metric is perturbed as $g_{\mu\nu}^\eta = g_{\mu\nu}^{(0)} + \delta g_{\mu\nu}^\eta$, i.e.

$$g_{\mu\nu}^\eta = \begin{pmatrix} -f e^{2A} & 0 & 0 & 0 & 0 \\ 0 & e^{2A} & e^{2A} \lambda H_{12} & 0 & 0 \\ 0 & e^{2A} \lambda H_{12} & e^{2A} & 0 & 0 \\ 0 & 0 & 0 & e^{2A} & 0 \\ 0 & 0 & 0 & 0 & L^2 e^{2B}/f \end{pmatrix}. \quad (6.14)$$

For the bulk perturbation, the metric is perturbed as $g_{\mu\nu}^{\zeta} = g_{\mu\nu}^{(0)} \delta g_{\mu\nu}^{\zeta}$, i.e.

$$g_{\mu\nu}^{\zeta} = \begin{pmatrix} g_{00} & 0 & 0 & 0 & 0 \\ 0 & g_{11} & 0 & 0 & 0 \\ 0 & 0 & g_{11} & 0 & 0 \\ 0 & 0 & 0 & g_{11} & 0 \\ 0 & 0 & 0 & 0 & g_{44} \end{pmatrix} \quad (6.15)$$

with

$$g_{00} = -f e^{2A} \left(1 + \frac{\lambda}{2} H_{00}\right)^2, \quad (6.16)$$

$$g_{11} = e^{2A} \left(1 + \frac{\lambda}{2} H_{11}\right)^2, \quad (6.17)$$

$$g_{44} = \frac{L^2 e^{2B}}{f} \left(1 + \frac{\lambda}{2} H_{44}\right)^2. \quad (6.18)$$

Here, $H_{\mu\nu}$ are the perturbations to the respective components of the metric $g_{\mu\nu}^{(0)}$ and $\lambda \ll 1$ is a formal extension parameter. The shear and bulk perturbations decouple and are treated separately. From now on, we set $L \equiv 1$, following [41].

6.2.2. Linearized Einstein equations

To obtain the equations of motion of $H_{\mu\nu}$ the Einstein equations for the perturbed metrics (6.14) and (6.15) are set up. One obtains equations proportional to powers of λ ; terms proportional to λ^1 yield the linearized equations. The quantities A , B and f are the same functions as in section 4.3 and obey the unperturbed Einstein equations (4.34-4.37). These unperturbed equations are used to simplify the equations for $H_{\mu\nu}$.

For the shear viscosity, the $(x_1 x_2)$ Einstein equation proportional to λ yields

$$H''_{12} + \left(4A' + B' + \frac{f'}{f}\right) H'_{12} + \omega^2 \frac{e^{2B-2A}}{f^2} H_{12} = 0. \quad (6.19)$$

For the bulk viscosity, the (tt) , (x_1x_1) and (ϕ, ϕ) Einstein equations proportional to λ yield respectively

$$H'_{00} = \frac{1}{12A'^2 f^2} \left[2f^2 \left(1 - 6A'^2 - 3A' \frac{f'}{f} \right) H'_{11} - \left(f f' (1 - 24A'^2) - 6A' f'^2 - 12\omega^2 A' e^{2B-2A} \right) H_{11} \right], \quad (6.20)$$

$$H''_{11} = \left(-\frac{1}{3A'} - 4A' + 3B' - \frac{f'}{f} \right) H'_{11} - \left(\frac{f'}{f} \frac{A''}{A'} + \omega^2 \frac{e^{2B-2A}}{f^2} \right) H_{11}, \quad (6.21)$$

$$H_{44} = \frac{1}{A'} \left[H'_{11} - \frac{f'}{2f} H_{11} \right]. \quad (6.22)$$

Observe that equation (6.21) decouples, and that H_{00} and H_{44} can be expressed in terms of H_{11} . Thus, it is sufficient to solve (6.21). This is an advantage of using the metric (6.13).

6.2.3. Construction of the correlator

The action for the respective perturbed metric $g_{\mu\nu}^\eta$ and $g_{\mu\nu}^\zeta$ is given by the Einstein-Hilbert part of (4.1):

$$S_p = \frac{1}{16\pi G_5} \int d^5x \sqrt{-g} R[g^{\{\eta, \zeta\}}]. \quad (6.23)$$

Renormalization and complexification

To obtain a well-defined action and finite correlators the former has to be renormalized [24], that is one has to determine counterterms which cancel the divergences in the limit $\phi \rightarrow 0$:

$$S_{p,ren} = S_p + S_{ct}, \quad (6.24)$$

where S_{ct} is of the schematic form

$$S_{ct} = \frac{1}{16\pi G_5} \int d^5x \left(\partial_t \mathcal{L}^t + \partial_\phi \mathcal{L}^\phi \right). \quad (6.25)$$

The boundary terms are the gravity analogue of counterterms in quantum field theory regularization.

The procedure is now to evaluate (6.23) using $g_{\mu\nu}^\eta$ and $g_{\mu\nu}^\zeta$ and to separate S_p into

$$S_{p,ren} = \frac{1}{16\pi G_5} \int d^5x \mathcal{L}, \quad (6.26)$$

$$S_{ct} = \frac{1}{16\pi G_5} \int d^5x \left(\partial_t \mathcal{L}^t + \partial_\phi \mathcal{L}^\phi \right), \quad (6.27)$$

and keep only \mathcal{L} , which is equivalent to the subtraction of the counterterms S_{ct} . Having determined \mathcal{L} it is then complexified, $\mathcal{L} \rightarrow \mathcal{L}_C$, by passing from $H_{\mu\nu}$ to a complex field $\hat{h}_{\mu\nu}$. Hereby, \mathcal{L} depends on $H_{\mu\nu}(t, \phi)$ and its derivatives, and \mathcal{L}_C depends on $\hat{h}_{\mu\nu}(t, \phi)$ and its derivatives. The complexified lagrangian \mathcal{L}_C is constructed to yield the equations of motion (6.19) and (6.20-6.22) for the shear and bulk perturbations, respectively, for a harmonic time dependence $\hat{h}_{\mu\nu}(t, \phi) = e^{-i\omega t} h_{\mu\nu}(\phi)$. The equations of motion of $h_{\mu\nu}$ are then used to re-express \mathcal{L}_C as a total derivative

$$\mathcal{L}_C = \partial_\phi J + h_{\mu\nu}^* \left(\frac{\partial \mathcal{L}_C}{\partial h_{\mu\nu}^*} - \frac{d}{d\phi} \frac{\partial \mathcal{L}_C}{\partial h_{\mu\nu}^{*'}} \right) = \partial_\phi J. \quad (6.28)$$

As shown in [41], J is the sought for Green's function

$$\lim_{\phi \rightarrow 0} J(\omega) = G_R(\omega). \quad (6.29)$$

Note that, to compute η and ζ , one only needs the imaginary part and defines

$$\mathcal{F} = -\text{Im } J. \quad (6.30)$$

Combine (6.30) and (6.29) to obtain (6.12). Since only $\text{Im } J$ has to be calculated, we will see that a simplification will occur, since a rigorous renormalization procedure can be circumvented.

Shear perturbation

Evaluating (6.23) with (6.14) yields

$$\mathcal{L} = \frac{1}{2f} e^{2A+B} \dot{H}_{12}^2 - \frac{f}{2} e^{4A-B} H_{12}'^2, \quad (6.31)$$

$$\mathcal{L}^t = -\frac{2}{f} e^{2A+B} H_{12} \dot{H}_{12}, \quad (6.32)$$

$$\mathcal{L}^\phi = 2f e^{4A-B} H_{12} H_{12}' + f A' e^{4A-B} H_{12}'^2. \quad (6.33)$$

Here, \mathcal{L}^t and \mathcal{L}^ϕ were constructed by demanding that, to obtain second-order equations of motions, \mathcal{L} should depend only on H_{12} and its first derivatives. This however does not fix \mathcal{L}^ϕ . To see this, add any multiple of H_{12}^2 to \mathcal{L}^ϕ and the requirement is still satisfied. An unambiguous determination of \mathcal{L}^t and \mathcal{L}^ϕ would require a rigorous holographic renormalization procedure. This can however be circumvented by adding a term $1/2 \partial_\phi(GH_{12}^2)$ to \mathcal{L} , where G is an arbitrary differentiable real function of ϕ . The lagrangian (6.31) now becomes

$$\mathcal{L} = \frac{1}{2f} e^{2A+B} \dot{H}_{12}^2 - \frac{f}{2} e^{4A-B} H_{12}'^2 + \frac{1}{2} G' H_{12}^2 + G H_{12} H_{12}'. \quad (6.34)$$

In principle, G is determined by holographic renormalization [24], but we will shortly see that it enters only the real part of the correlator and thus does not have to be known explicitly.

Now construct \mathcal{L}_C , so that the equation of motion for h_{12} coincides with (6.19) and obtain (with $\hat{h}_{12}(t, \phi) = e^{-i\omega t} h_{12}(\phi)$)

$$\mathcal{L}_C = \frac{\omega^2}{f} e^{2A+B} |h_{12}|^2 - f e^{4A-B} |h_{12}'|^2 + G' |h_{12}|^2 + G(h_{12} h_{12}'^* + h_{12}^* h_{12}'). \quad (6.35)$$

Rewrite (6.35) as in (6.28) to obtain

$$J = -f e^{4A-B} h_{12}^* h_{12}' + G |h_{12}|^2 \quad (6.36)$$

and use (6.30) to arrive at the final result

$$\mathcal{F}^n = -\frac{if e^{4A-B}}{2} (h_{12}^* h_{12}' - h_{12}'^* h_{12}). \quad (6.37)$$

Bulk perturbation

We define

$$\vec{H} = \begin{pmatrix} H_{00} \\ H_{11} \\ H_{44} \end{pmatrix} \quad (6.38)$$

and evaluate (6.23) with (6.15). We proceed as in (6.34) and add a total derivative $1/2 \partial_\phi(\vec{H}^T \mathbf{G} \vec{H})$ to \mathcal{L} , which now takes the form

$$\mathcal{L} = \frac{1}{2} \vec{H}^T \mathbf{M} \vec{H} + \vec{H}'^T \mathbf{M}^\phi \vec{H} + \frac{1}{2} \dot{\vec{H}}^T \mathbf{M}^{tt} \dot{\vec{H}} + \frac{1}{2} \vec{H}'^T \mathbf{M}^{\phi\phi} \vec{H}' + \frac{1}{2} \partial_\phi(\vec{H}^T \mathbf{G} \vec{H}), \quad (6.39)$$

where

$$\mathbf{M} = -\frac{3}{2}e^{4A-B}[-f(1-24A'^2) + 6A'f'] \begin{pmatrix} 0 & 1/2 & 0 \\ 1/2 & 1 & 0 \\ 0 & 0 & 1/6 \end{pmatrix}, \quad (6.40)$$

$$\mathbf{M}^\phi = -\frac{3}{4}e^{4A-B} \begin{pmatrix} 0 & 6A'f' & -2A'f \\ 6A'f + f' & 2(6A' + f') & -6A'f - f' \\ 0 & 0 & 0 \end{pmatrix}, \quad (6.41)$$

$$\mathbf{M}^{\phi\phi} = -3e^{4A-B}f \begin{pmatrix} 0 & 1/2 & 0 \\ 1/2 & 1 & 0 \\ 0 & 0 & 0 \end{pmatrix}, \quad (6.42)$$

$$\mathbf{M}^{tt} = \frac{3e^{2A+B}}{f} \begin{pmatrix} 0 & 0 & 0 \\ 0 & 1 & 1/2 \\ 0 & 1/2 & 0 \end{pmatrix}, \quad (6.43)$$

and \mathbf{G} is a symmetric differentiable matrix depending on ϕ .

Construct \mathcal{L}_C by demanding that it leads to the equations of motion (6.20-6.22) for

$$\vec{h} = \begin{pmatrix} h_{00} \\ h_{11} \\ h_{44} \end{pmatrix} \quad (6.44)$$

with $\vec{h}(t, \phi) = e^{-i\omega t}\vec{h}(\phi)$. One obtains

$$\mathcal{L}_C = \vec{h}^{*T}\mathbf{m}\vec{h}' + \vec{h}^{*T}\mathbf{k}\vec{h} + \vec{h}^{*T}\mathbf{b}\vec{h} + \vec{h}^{*T}\mathbf{b}^{*T}\vec{h}', \quad (6.45)$$

with

$$\mathbf{m} = \mathbf{M}^{\phi\phi}, \quad (6.46)$$

$$\mathbf{k} = L^2\omega^2\mathbf{M}^{tt} + \mathbf{M} + \mathbf{G}', \quad (6.47)$$

$$\mathbf{b} = \mathbf{M}^\phi + \mathbf{G}. \quad (6.48)$$

Rewrite (6.45) as (6.28) to obtain

$$J = \vec{h}^{*T}(\mathbf{m}\vec{h}' + \mathbf{b}\vec{h}) \quad (6.49)$$

and use (6.30) to arrive at

$$\mathcal{F}^\zeta = \frac{i}{2} [\vec{h}^{*T} (\mathbf{m}\vec{h}' + \mathbf{b}\vec{h}) - (\vec{h}^{*T} + \vec{h}^{*T} \mathbf{b}^T) \vec{h}]. \quad (6.50)$$

Using the equations of motion (6.20-6.22), we express h_{00} and h_{44} through h_{11} and h'_{11} to finally obtain

$$\mathcal{F}^\zeta = -\frac{if e^{4A-B}}{8A'^2} (h_{11}^* h'_{11} - h_{11}^{*'} h_{11}). \quad (6.51)$$

6.2.4. Solution of the linearized equations

We recall equations (6.19) and (6.21) for h_{12} and h_{11} :

$$h''_{12} + \left(4A' + B' + \frac{f'}{f}\right) h'_{12} + \omega^2 \frac{e^{2B-2A}}{f^2} h_{12} = 0, \quad (6.52)$$

$$h''_{11} + \left(\frac{1}{3A'} + 4A' - 3B' + \frac{f'}{f}\right) h'_{11} + \left(\frac{f'}{f} \frac{A''}{A'} + \omega^2 \frac{e^{2B-2A}}{f^2}\right) h_{11} = 0. \quad (6.53)$$

Since the fluxes (6.37) and (6.51) are independent of the radial coordinate, one can solve the equations (6.52) and (6.53) at any value of ϕ . This is most easily done at $\phi \approx \phi_h$.

Consider the equations (6.52) and (6.53) close to the horizon. The quadratically divergent terms $\propto 1/f^2$ dominate and (6.52) and (6.53) become

$$h''_{ij} + \left(\frac{\omega}{4\pi T}\right)^2 \left(\frac{f'(\phi_h)}{f}\right)^2 h_{ij} = 0, \quad (6.54)$$

where we approximated $e^{2(B-A)} \approx e^{2(B(\phi_h)-A(\phi_h))}$ and used the first equality of (4.53). Taylor expanding f around the horizon, $f \approx 0 + f'(\phi_h)(\phi - \phi_h) + \dots$, one obtains

$$h''_{ij} + \left(\frac{\omega}{4\pi T}\right)^2 \frac{1}{(\phi_h - \phi)^2} h_{ij} = 0. \quad (6.55)$$

Equation (6.55) is a wave equation with the general solution

$$h_{ij} = c_{ij}^+ (\phi_h - \phi)^{i\omega/4\pi T} + c_{ij}^- (\phi_h - \phi)^{-i\omega/4\pi T}, \quad (6.56)$$

where c_{ij}^+ and c_{ij}^- are integration constants; the term $\propto c_{ij}^+$ is an outgoing wave, and the term $\propto c_{ij}^-$ is an ingoing wave.

Since the transport coefficients (6.3) and (6.4) are given by the $\omega \rightarrow 0$ limits of the corresponding correlators (6.1) and (6.2), one can further expand around $\omega = 0$, which

yields

$$h_{ij} = c_{ij}^+ \left[1 + \frac{i\omega}{4\pi T} \ln(\phi_h - \phi) \right] + c_{ij}^- \left[1 - \frac{i\omega}{4\pi T} \ln(\phi_h - \phi) \right]. \quad (6.57)$$

As seen from (6.57), the amplitudes c_{ij}^+ and c_{ij}^- can be obtained by solving (6.52) and (6.53) with $\omega \equiv 0$, that is by solving the simpler equations

$$\tilde{h}_{12}'' + \left(4A' + B' + \frac{f'}{f} \right) \tilde{h}_{12}' = 0, \quad (6.58)$$

$$\tilde{h}_{11}'' + \left(\frac{1}{3A'} + 4A' - 3B' + \frac{f'}{f} \right) \tilde{h}_{11}' + \frac{f'}{f} \frac{A''}{A'} \tilde{h}_{11} = 0. \quad (6.59)$$

Boundary conditions

We impose the following boundary conditions:

$$|h_{ij}(0)|^2 = 1, \quad (6.60)$$

$$c_{ij}^+ = 0. \quad (6.61)$$

Condition (6.60) means choosing a boundary value $|\Phi_0|^2 = 1$, as described in section 3.4.3. It is arbitrary, since the sources Φ_0 are set to zero in the calculation of the correlator (3.37).³ Condition (6.61), dictated by causality, means keeping an *ingoing* wave at the horizon. With (6.61) the general solution (6.56) becomes

$$h_{ij} = c_{ij}^- (\phi_h - \phi)^{-i\omega/4\pi T}, \quad (6.62)$$

where we only have to determine c_{ij}^- . As explained at the end of the last section this will be done by solving the $\omega \equiv 0$ equations (6.58) and (6.59).

For the $\omega \equiv 0$ equations (6.58) and (6.59), the boundary conditions (6.60) and (6.61) transform into

$$\tilde{h}_{ij}(0) = 1, \quad (6.63)$$

$$\tilde{h}_{ij}(\phi_h) < \infty. \quad (6.64)$$

Thus, we look for solutions that are normalized to 1 at the boundary and that are regular at the horizon.

³It is common to normalize a wave to unit amplitude at infinity (in our case at $\phi = 0$), see e.g. [44]. Moreover, the functional derivative simplifies in this case.

Shear viscosity

Equation (6.58) yields

$$\tilde{h}_{12}(\phi) = \tilde{a}_{12} + \tilde{b}_{12} \int_0^\phi d\tilde{\phi} \frac{e^{-4A+B}}{f}, \quad (6.65)$$

where \tilde{a}_{12} and \tilde{b}_{12} are integration constants. The term $\propto \tilde{b}_{12}$ diverges logarithmically at the horizon due to $f(\phi_h) = 0$. Thus to satisfy (6.64) we have to set $\tilde{b}_{12} = 0$. The condition (6.63) further fixes $\tilde{a}_{12} = 1$ and we arrive at the trivial solution

$$\tilde{h}_{12}(\phi) = 1. \quad (6.66)$$

It follows that $c_{12}^- = 1$. We have thus completely determined $h_{12}(\phi)$ at $\phi \approx \phi_h$:

$$h_{12}(\phi) = (\phi_h - \phi)^{-i\omega/4\pi T}. \quad (6.67)$$

Insert (6.67) into (6.37), perform the derivatives and use the approximations leading to (6.55) to obtain

$$\mathcal{F}^\eta = \omega e^{3A(\phi_h)}. \quad (6.68)$$

Combine (6.3), (6.12) and (6.68) to obtain the final result:

$$\eta = \frac{e^{3A(\phi_h)}}{16\pi G_5}. \quad (6.69)$$

Recalling equation (4.54) reproduces the celebrated shear viscosity to entropy density ratio, also known as the Kovtun-Son-Starinets (KSS) bound [34]

$$\frac{\eta}{s} = \frac{1}{4\pi}. \quad (6.70)$$

Equation (6.70) however turned out not to be a strict bound, see [26, 27].

Bulk viscosity

Since an analytical solution to equation (6.59) is not known, c_{11}^- will be determined by solving (6.59) numerically. Consider equation (6.59) close to the horizon using $f'/f \approx 1/(\phi - \phi_h)$ and neglecting terms that are regular at $\phi = \phi_h$:

$$\tilde{h}_{11}'' + \frac{1}{\phi - \phi_h} \tilde{h}_{11}' + \frac{1}{\phi - \phi_h} \frac{A''}{A'} \tilde{h}_{11} = 0. \quad (6.71)$$

Notice that $A''/A' < 0$ since A' is monotonous and $A' \approx 1/(\phi(\Delta - 4))$ for $\phi \rightarrow 0$; define $x \equiv \phi_h - \phi$ and $a \equiv -A''(\phi_h)/A'(\phi_h) > 0$. Equation (6.71) becomes (a prime denoting now d/dx)

$$\tilde{h}_{11}'' + \frac{1}{x}\tilde{h}_{11}' + \frac{a}{x}\tilde{h}_{11} = 0. \quad (6.72)$$

The general solution of (6.72) is

$$\tilde{h}_{11} = \tilde{a}_{11}J_0(2\sqrt{ax}) + \tilde{b}_{11}Y_0(2\sqrt{ax}), \quad (6.73)$$

where J_0 and Y_0 are Bessel functions of respectively the first and second kind, and \tilde{a}_{11} and \tilde{b}_{11} are integration constants. Expand the general solution around $x = 0$:

$$\tilde{h}_{11} = \hat{a}_{11} + \hat{b}_{11} \ln x. \quad (6.74)$$

We see that, in order to satisfy (6.64), we have to require

$$\tilde{h}_{11}'(\phi_h) = 0. \quad (6.75)$$

Thus, for the numerical solution of equation (6.59) we use the boundary conditions (6.63) and (6.75). Since equation (6.59) is homogeneous, it is easiest to start the integration at $\phi = \phi_h$ with

$$\tilde{h}_{11}(\phi_h) = 1, \quad (6.76)$$

$$\tilde{h}_{11}'(\phi_h) = 0, \quad (6.77)$$

and determine $c_{11}^- = 1/\tilde{h}_{11}(0)$ from the numerical solution.

In analogy to (6.68), one inserts (6.62) into (6.51) to obtain

$$\mathcal{F}^\zeta = \omega |c_{11}^-|^2 \frac{e^{3A(\phi_h)}}{4A'(\phi_h)^2}. \quad (6.78)$$

Combine (6.4), (6.12) and (6.78) to arrive at the final expression for ζ

$$\zeta = |c_{11}^-|^2 \frac{s}{36\pi A'(\phi_h)^2}. \quad (6.79)$$

6.3. Bulk viscosity in the approach by Gubser et al.

To check our code,⁴ we first make sure that figure 3 of [41] is reproduced. In table 6.1 we collect the parameters. In figure 6.1 we show the results of our numerical calculation.

#	γ	b	$-M^2L^2$	Δ	ϕ_h^c	T_cL	T_c -type	Phase transition
A	0.606	2.057	≈ 0.293	≈ 3.925	≈ 4.36	≈ 0.704	inflection	crossover
B	0.606	1.503	≈ 1.401	≈ 3.612	≈ 3.69	≈ 0.060	inflection	crossover

Table 6.1.: Parameter values used in [41] for the calculation of the bulk viscosity.

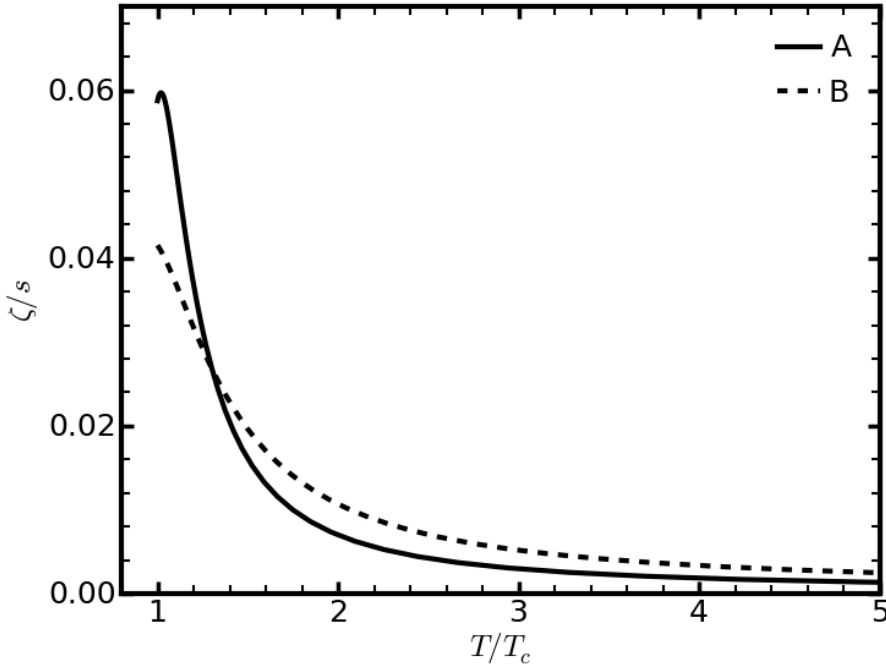


Figure 6.1.: The bulk viscosity to entropy density ratio ζ/s as a function of the scaled temperature computed in the interval $1 \leq T/T_c \leq 5$ for the parameter values of table 6.1. Compare figure 3 of [41].

The bulk viscosity is computed for the optimal parameter values, which are collected in table 5.3. The results for the scaled bulk viscosity ζ/T^3 and for the the bulk viscosity to entropy density ratio ζ/s are shown in figures 6.2 and 6.3. Both quantities exhibit a sharp rise for $T \rightarrow T_c^+$.

⁴A program to calculate the entropy density s , the temperature T and the bulk viscosity ζ was written using the computer algebra system `sage`.

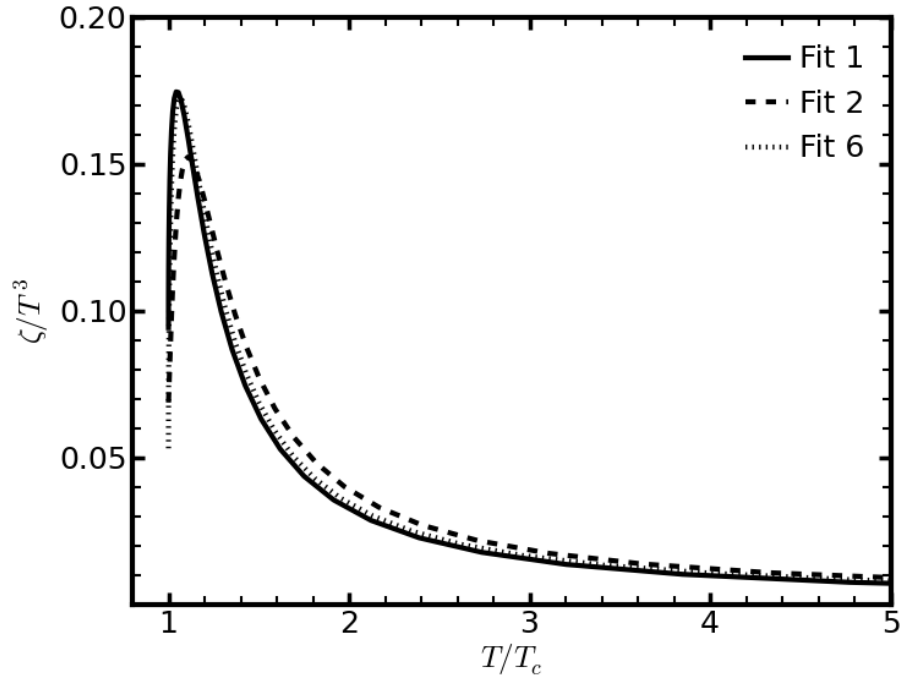


Figure 6.2.: The scaled bulk viscosity ζ/T^3 as a function of the scaled temperature for the parameter values of the first, second and sixth fits.

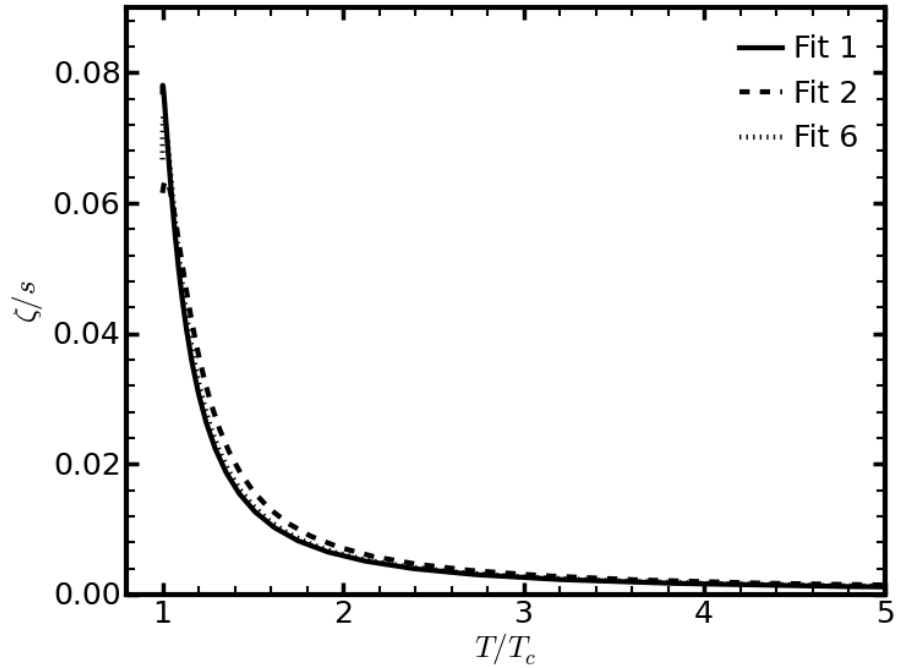


Figure 6.3.: The bulk viscosity to entropy density ratio ζ/s as a function of the scaled temperature for the parameter values of the first, second and sixth fits.

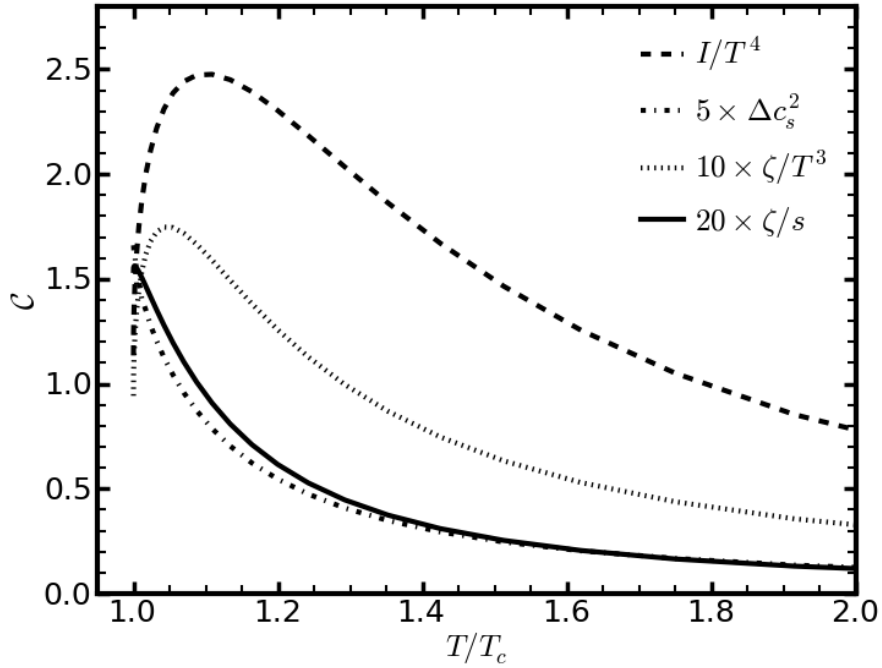


Figure 6.4.: Deviation of the $SU(3)$ Yang-Mills plasma from conformality for $T \rightarrow T_c$ for the parameter set of the first fit of table 5.3.

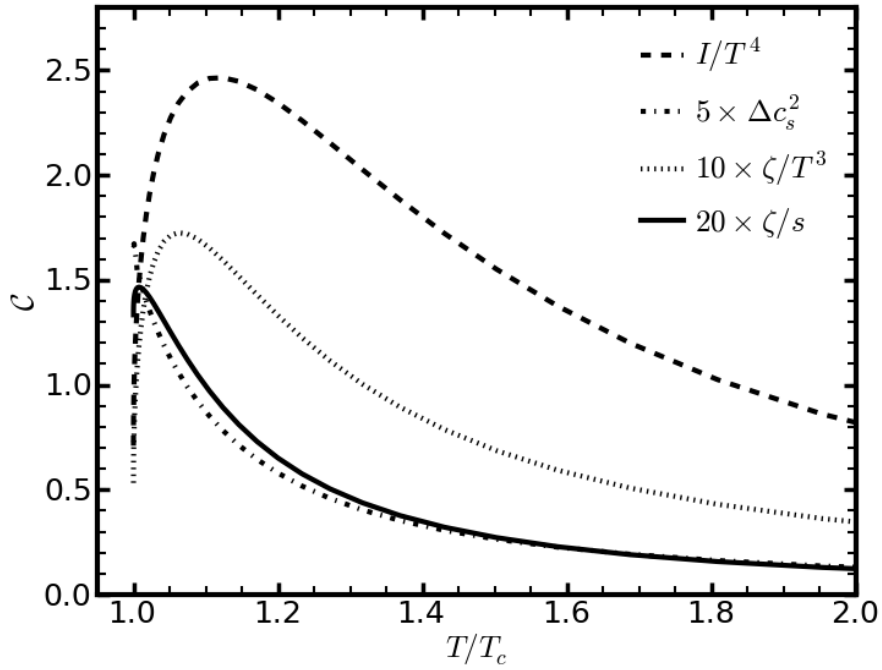


Figure 6.5.: Deviation of the $SU(3)$ Yang-Mills plasma from conformality for $T \rightarrow T_c$ for the parameter set of the sixth fit of table 5.5.

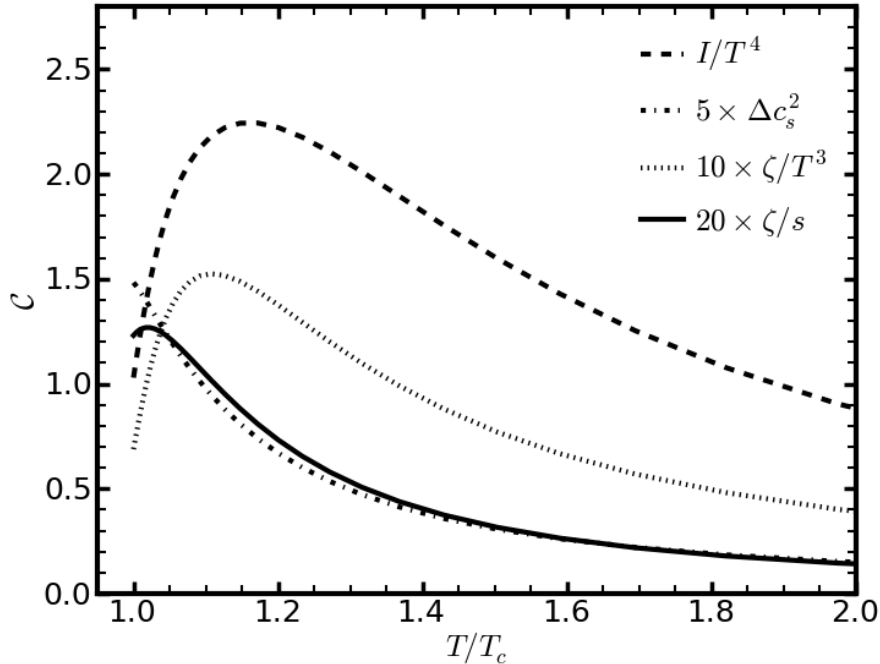


Figure 6.6.: Deviation of the $SU(3)$ Yang-Mills plasma from conformality for $T \rightarrow T_c$ for the parameter set of the second fit of table 5.3.

In figure 6.4 we show the final results concerning the deviation of the $SU(3)$ Yang-Mills plasma from the conformal behavior for $T \rightarrow T_c$ within the holographic model. One observes that, for $T \rightarrow T_c$, any quantity measuring the non-conformality of the gluon plasma exhibits a rather sharp rise. The locations of the maxima and their relative magnitudes are however different, see tables 6.2, 6.3 and 6.4.

\mathcal{C}	$T/T_c(\max[\mathcal{C}])$	$\max[\mathcal{C}]/\mathcal{C}(T/T_c = 2)$	$\max[\mathcal{C}]/\mathcal{C}(T/T_c = 4)$
I/T^4	≈ 1.109	≈ 3.2	≈ 13.3
Δc_s^2	1.0	≈ 13.4	≈ 44.4
ζ/s	≈ 1.001	≈ 13.3	≈ 48.3
ζ/T^3	≈ 1.042	≈ 5.4	≈ 17.9

Table 6.2.: Locations and relative magnitudes of the maxima of the quantities \mathcal{C} for the parameter set of the first fit.

\mathcal{C}	$T/T_c(\max[\mathcal{C}])$	$\max[\mathcal{C}]/\mathcal{C}(T/T_c = 2)$	$\max[\mathcal{C}]/\mathcal{C}(T/T_c = 4)$
I/T^4	≈ 1.124	≈ 3.0	≈ 12.1
Δc_s^2	1.0	≈ 12.8	≈ 40.5
ζ/s	≈ 1.008	≈ 12.0	≈ 42.4
ζ/T^3	≈ 1.062	≈ 5.0	≈ 16.1

Table 6.3.: Locations and relative magnitudes of the maxima of the quantities \mathcal{C} for the parameter set of the sixth fit.

\mathcal{C}	$T/T_c(\max[\mathcal{C}])$	$\max[\mathcal{C}]/\mathcal{C}(T/T_c = 2)$	$\max[\mathcal{C}]/\mathcal{C}(T/T_c = 4)$
I/T^4	≈ 1.172	≈ 2.5	≈ 9.8
Δc_s^2	1.0	≈ 9.9	≈ 31.8
ζ/s	≈ 1.018	≈ 9.0	≈ 32.2
ζ/T^3	≈ 1.108	≈ 4.0	≈ 12.7

Table 6.4.: Locations and relative magnitudes of the maxima of the quantities \mathcal{C} for the parameter set of the second fit.

6.4. Conclusions

Following the holographic approach to the determination of the transport coefficients established by Gubser et al. [41], we have calculated the shear and bulk viscosities of the $SU(3)$ Yang-Mills plasma within the holographic model for the parameter sets of the first, second and sixth fits obtained in section 5.3 and collected in tables 5.3 and 5.5. As discussed in the end of section 5.4, the first parameter set reproduces the equation of state in the vicinity of the phase transition $1 \leq T/T_c \leq 2$, the second set reproduces the region $2.5 \leq T/T_c \leq 10$ and the sixth set yields the best description in the whole region $1 \leq T/T_c \leq 10$.

The shear viscosity to entropy density ratio is constant and saturates the KSS bound, $\eta/s = 1/(4\pi)$. As discussed in section 3.5.3, the constant η/s ratio is, if at all, a realistic scenario only for $T \approx T_c$ and should actually vary with temperature. This feature can be incorporated into the model by considering higher order curvature corrections to the action (4.1); first steps in this direction were taken in [26,27]. The bulk viscosity to entropy density ratio ζ/s , as well as the scaled bulk viscosity ζ/T^3 , show a steep rise for $T \rightarrow T_c^+$.

Consider figures 6.4, 6.5 and 6.6. It is evident that the $SU(3)$ Yang-Mills plasma, being approximately conformal for high temperatures $T/T_c \gtrsim 100$, strongly deviates from conformality for $T \rightarrow T_c^+$. The different quantities $\mathcal{C} = \{I/T^4, \Delta c_s^2, \zeta/s, \zeta/T^3\}$, charac-

terizing this deviation, peak at slightly different temperature values and exhibit slightly different relative magnitudes, as summarized in tables 6.2, 6.3, 6.4. Note that for the first parameter set, which accurately reproduces the $SU(3)$ Yang-Mills plasma equation of state in the interval $1 \leq T/T_c \leq 2$, the peaks are sharper and closer to T_c as compared to the second parameter set, while the sixth parameter set lies in between (compare figures 6.4, 6.5, 6.6 and tables 6.2, 6.3, 6.4). This behavior points to a systematic dependence of ζ/T^3 and ζ/s on the scaled interaction measure I/T^4 : A sharper and larger maximum of I/T^4 leads to sharper and larger maxima of ζ/T^3 and ζ/s ; further, the location of the maximum of I/T^4 determines the locations of the maxima of ζ/T^3 and ζ/s .

Provided that the holographic model describes the $SU(3)$ Yang-Mills plasma "well enough" (i.e., that qualitatively, figure 6.4 still holds for the gluon plasma) and that a similar behavior arises for the full QCD, a measurement of the respective maxima can be used to accurately pinpoint the temperature of the deconfinement transition.

7. Conclusions

Following essentially the work of Gubser et al. [2, 41] and Huang et al. [1] we have studied the thermodynamics of the Yang-Mills plasma within the context of the AdS/CFT correspondence. The model used by us, section 4.3, is the minimal setting which can reproduce the equation of state of the Yang-Mills plasma. As discussed in section 4.1, one needs additional input, this can be either the AdS deformation A , or the scalar field potential V . In the latter case one has the analogy suggested by equation (2.10): the conformal invariance of the Yang-Mills theory, broken by quantum fluctuations due to the non-vanishing β function is translated into a deformation of the conformally invariant black hole AdS space due to the scalar field profile resulting from a non-trivial potential $V(\phi)$.

Since the focus of our work was the quantitative reproduction of the $SU(3)$ Yang-Mills theory equation of state above the deconfinement transition and the subsequent calculation of the bulk viscosity, we did not extend our model to temperatures below T_c . Thus, we did not study the gravity analogue of the confinement-deconfinement phase transition (see e.g. [33]) and did not calculate observables associated with the confined phase of the theory, like e.g. glueball mass spectra and spectral functions. Further, we stayed with the "heuristic" definition of T_c , as discussed in section 5.2. While the Improved Holographic QCD model of Kiritsis et al. [33] can be regarded as more thorough, the virtue of our model lies in its simplicity. Given an arbitrary potential with the required behavior for $\phi \rightarrow 0$, the equation of state $s(T)$ can directly be obtained by numerically solving the differential equation (4.44) and performing the integrals (5.19) and (5.25). With a suitable determination of the ϕ_h -range, as described in section 5.3, a fit to the lattice data can be achieved. The metric coefficients are obtained from the equations (4.51), (4.52) and (4.43) and the bulk viscosity can be calculated by numerically solving equation (6.59). Note that, once the equation of state $s(T)$ is fixed, the viscosities are obtained without introducing any additional parameters; this is an advantage compared to the quasiparticle model, where relaxation times have to be introduced, see [38].

Our results, section 5.3, suggest that the $SU(3)$ Yang-Mills equation of state can be reproduced to a high accuracy with the compact form of the potential (5.7) by suitable parameter

adjustments, however only for isolated temperature ranges. In the low-temperature regime we fitted the ranges $1 \leq T/T_c \leq 2$ and $2.5 \leq T/T_c \leq 10$ and $1 \leq T/T_c \leq 10$; using the corresponding parameters sets given in table 5.3 one can achieve a very good agreement with the $SU(3)$ Yang-Mills theory equation of state in the first two temperature intervals, while, for an accurate reproduction of the complete low-temperature range $1 \leq T/T_c \leq 10$, a modification of the potential (5.7) is needed. We also performed fits concentrating on and extending into the high temperature regime, i.e. for the ranges $2.5 \leq T/T_c \leq 100$, $10 \leq T/T_c \leq 1000$ and $1 \leq T/T_c \leq 1000$; the parameters are summarized in table 5.5. We find that the behavior in the "intermediate" region $2.5 \leq T/T_c \leq 100$ is already well captured by the fit in the interval $2.5 \leq T/T_c \leq 10$. The asymptotic region $10 \leq T/T_c \leq 1000$ can be well reproduced by another set of parameters. We conclude that, when using the potential (5.7), the equation of state can be roughly divided into two regions when considering s/T^3 and p/T^4 : the low-temperature region $1 \leq T/T_c \lesssim 10$ and the high-temperature region $10 \lesssim T/T_c \leq 1000$; the global (sixth) and the asymptotic (fifth) fits reproduce the equation of state very well in the respective intervals (compare figures 5.28, 5.29 and 5.22, 5.23). When considering the scaled interaction measure I/T^4 , we suggest a division into three regions: the direct vicinity of the phase transition $1 \leq T/T_c \leq 2.5$, the intermediate region $2.5 \leq T/T_c \lesssim 100$ and the asymptotic region $100 \lesssim T/T_c \leq 1000$. In these three regions the optimum parameters are given by the first, second/fourth and fifth fit respectively (compare figures 5.30 and 5.24). The global fit yields the best fit of I/T^4 when considering the larger low-temperature range $1 \leq T/T_c \leq 10$.

Accepting larger relative deviations of the scaled interaction measure I/T^4 from the lattice data, one can reproduce the even the larger interval $1 \leq T/T_c \leq 100$. Hereby, when the peak of I/T^4 is to be accurately reproduced, the parameters of the global fit should be taken, while, if one desires a high accuracy when describing in particular the region $2.5 \leq T/T_c \leq 100$, the parameters of the second/fourth fit are the optimum ones.

The bulk viscosity, computed for the first, second and sixth fits, shows both as ζ/T^3 and as ζ/s a steep rise for $T \rightarrow T_c^+$. The location of the maximum of ζ/T^3 lies slightly above the deconfinement temperature T_c , while the maximum of ζ/s almost coincides with T_c . We find that the shape of the peak of the scaled interaction measure I/T^4 is reflected by the scaled bulk viscosity ζ/T^3 and by the bulk viscosity to entropy density ratio ζ/s : A sharper and higher maximum of I/T^4 leads to sharper and higher maxima of ζ/T^3 and ζ/s ; the locations of the respective maxima are shifted analogously. Compare figures 6.4, 6.5, 6.6 and tables 6.2, 6.3, 6.4.

The significance of this thesis lies within the now provided possibility to put calculations, related to the deconfinement transition and/or chiral symmetry breaking (e.g. calculations of in-medium glueball or meson spectral functions and glueball or meson mass spectra), which are presently often done on the background of pure black hole AdS space (see [45–47]) with $s/T^3 = \text{const}$ (B.5), into a more realistic setting. A qualitatively different behavior may occur: note that, in our case, on the conformal background with $s/T^3 = \text{const}$, one would have $\zeta \equiv 0$.¹ Given the lattice data, the potential can be adjusted such that the metric coefficients reproduce the equation of state $s(T)$ of the pure Yang-Mills theory or of QCD to a fairly high accuracy in the desired temperature range. Although we did not extend our analysis to temperatures $T/T_c < 1$, we expect that the parameters of the potential used by Gubser et al., equation (5.7), can be further adjusted to reproduce the equation of state also in the range $0.8 \lesssim T/T_c \lesssim 1.4$. It is of course desirable and perhaps illuminating to find a potential which would reproduce the pure Yang-Mills theory or QCD equation of state in the whole range $0.8 \leq T/T_c \leq 1000$ with a high accuracy. This question marks the direction of future work.

Among the necessary improvements of the holographic model there are:

- Setting up a model which allows for a temperature dependent η/s , most favorably such that one can achieve a match to the perturbative results.
- Including quark degrees of freedom which are important also for $\mu = 0$.
- While he have focused on the equation of state and on the transport coefficients, for ongoing experiments of relativistic heavy-ion collisions at RHIC and LHC, other observables (e.g. jet quenching and drag coefficients, in-medium spectral functions of hadrons etc.) are of interest which are also accessible within the AdS/QCD correspondence.

¹The calculation of spectral functions, etc. is similar to the calculation of ζ : one considers a field "living" on a fixed background spacetime given by the metric coefficients, and obtains e.g. the correlator of the dual operator. In the case of ζ , we have seen that the field in question is the linear perturbation of the metric itself. For e.g. mesons one would consider scalar, pseudo-scalar, vector, etc. fields. The calculation of the correlators will however be analogous to the one reviewed in section 6.2.

A. Einstein equations and Anti-deSitter space

A.1. Einstein equations

The field equations of general theory of relativity, usually referred to as Einstein equations, can be derived from the following action (here written down in $d = 5$ dimensions):

$$S = S_{EH} + S_M + S_{GH} = \frac{1}{16\pi G_5} \int d^5x \sqrt{-g} (R + \mathcal{L}_M) + S_{GH}. \quad (\text{A.1})$$

$S_{EH} \propto \int d^5x \sqrt{-g} R$ is the Einstein-Hilbert action, $S_M \propto \int d^5x \sqrt{-g} \mathcal{L}_M$ is the action of the matter on a pseudo-Riemannian manifold defined by the (to be calculated) metric tensor $g_{\mu\nu}$ and S_{GH} is the Gibbons-Hawking term needed to obtain a well-defined action when considering manifolds with a boundary; the Gibbons-Hawking term insures that the geometry of the boundary is kept fixed while performing the variation with respect to the metric $g_{\mu\nu}$. The square root of the metric fundamental determinant $\sqrt{-g}$, where $g \equiv \det |g_{\mu\nu}|$, ensures general covariance, i.e. invariance of (A.1) under coordinate transformations.

Variation of the Einstein-Hilbert action S_{EH} with respect to $g_{\mu\nu}$ yields the Einstein tensor

$$E_{\mu\nu} = R_{\mu\nu} - \frac{1}{2} R g_{\mu\nu}, \quad (\text{A.2})$$

where $R_{\mu\nu}$ is the Ricci tensor.

Variation of the matter action S_M with respect to $g_{\mu\nu}$ defines the symmetric energy-momentum tensor $T_{\mu\nu}$ (with a comma denoting the partial derivative, i.e. $X_{,\alpha} \equiv \partial X / \partial x^\alpha$)

$$T_{\mu\nu} = \frac{1}{\sqrt{-g}} \frac{\delta(\sqrt{-g} \mathcal{L}_M)}{\delta g^{\mu\nu}} = \frac{1}{\sqrt{-g}} \left(\frac{\partial(\sqrt{-g} \mathcal{L}_M)}{\partial g^{\mu\nu}} - \left(\frac{\partial(\sqrt{-g} \mathcal{L}_M)}{\partial g^{\mu\nu, \alpha}} \right)_{,\alpha} \right). \quad (\text{A.3})$$

Requiring that the variation of the total action vanishes, $\delta S = 0$, one obtains the Einstein equations

$$R_{\mu\nu} - \frac{1}{2} R g_{\mu\nu} = T_{\mu\nu}. \quad (\text{A.4})$$

Since the Einstein tensor is divergence-free by the contracted Bianchi identities (where $X_{;\alpha}$ is the covariant differentiation of a geometric object X)

$$E^{\mu\nu}{}_{;\nu} \equiv \left(R^{\mu\nu} - \frac{1}{2} R g^{\mu\nu} \right)_{;\nu} = 0 \quad (\text{A.5})$$

one obtains the local energy-momentum conservation

$$T^{\mu\nu}{}_{;\nu} = 0 \quad (\text{A.6})$$

which defines the equations of motion for the matter. Equation (A.5) ensures the integrability of the Einstein equations.

The model for the Yang-Mills thermodynamics is defined by the action (A.1) with

$$\mathcal{L}_M = -\frac{1}{2} \partial_\mu \phi \partial^\mu \phi - V(\phi), \quad (\text{A.7})$$

where ϕ is a scalar field with a standard kinetic term and a potential V .

A.2. Anti-deSitter space

Consider the action (A.1) and introduce the cosmological constant by setting $\mathcal{L}_M = V_0 = \Lambda = \text{const} < 0$. Consider further the following ansatz for the line element squared

$$ds^2 = e^{2A(z)} \left(-dt^2 + d\vec{x}^2 + dz^2 \right). \quad (\text{A.8})$$

There are only two independent nontrivial Einstein equations (A.4):

$$A'^2 - A'' = 0, \quad (\text{A.9})$$

$$\Lambda e^{2A} + 12A'^2 = 0, \quad (\text{A.10})$$

where equations (A.9) and (A.10) follow from the components $((tt) + (zz), (zz))$ of the corresponding Einstein equations.

Integrating (A.9) one obtains

$$A = -\ln \left(\frac{c_1 + z}{c_2} \right), \quad (\text{A.11})$$

where c_1 and c_2 are integration constants. Insert (A.11) into (A.10) to obtain

$$c_2 = L^2 = -\frac{12}{\Lambda}. \quad (\text{A.12})$$

Demanding invariance of (A.8) under scalings, $x^\mu \rightarrow kx^\mu$, further determines $c_1 = 0$. One thus has

$$A = \ln \frac{L}{z}. \quad (\text{A.13})$$

We have defined the AdS scale L and obtain the pure *AdS* metric in Fefferman-Graham coordinates:

$$ds^2 = \frac{L^2}{z^2} \left(-dt^2 + d\vec{x}^2 + dz^2 \right). \quad (\text{A.14})$$

Note that the metric diverges for $z \rightarrow 0$, therefore care should be taken when imposing boundary conditions.

It is possible to introduce a black hole into *AdS* space by adding a function $f(z; z_h)$ to the metric. Requiring that $f(0) = 1$ yields the asymptotically *AdS* space, and $f(z_h; z_h) = 0$ defines the black hole horizon. The metric is now of the form

$$ds^2 = e^{2A(z)} \left(-f(z)dt^2 + d\vec{x}^2 + \frac{dz^2}{f(z)} \right). \quad (\text{A.15})$$

Accordingly, there are three independent Einstein equations:

$$A'^2 - A'' = 0, \quad (\text{A.16})$$

$$3A'f' + f'' = 0, \quad (\text{A.17})$$

$$12fA'^2 - f'' + \Lambda e^{2A} = 0. \quad (\text{A.18})$$

(From the respective components $(tt)/f^2 + (zz)$, $(tt)/f + (x_i x_i)$, (zz)). Solve (A.17) remembering the boundary conditions $f(0) = 1$, $f(z_h; z_h) = 0$ and using $A = \ln \frac{L}{z}$ to obtain

$$f(z; z_h) = 1 - \frac{z^4}{z_h^4}, \quad (\text{A.19})$$

and the black hole AdS metric

$$ds^2 = \frac{L^2}{z^2} \left(- \left(1 - \frac{z^4}{z_h^4} \right) dt^2 + d\vec{x}^2 + \frac{dz^2}{1 - \frac{z^4}{z_h^4}} \right). \quad (\text{A.20})$$

Equation (A.18) is fulfilled and becomes (A.10) in the limit $z \rightarrow 0$.

We have worked step by step, first considering pure *AdS* space, then adding a black hole into it. In the second case the space becomes pure *AdS* only in the limit $z \rightarrow 0$. In this sense it is a natural extension to consider a deformed *AdS* space, where A and f are

no longer given by the simple functions (A.13) and (A.19), but have a more complicated form. Since the AdS/CFT correspondence demands asymptotically an *AdS* space we will recognize (A.12), (A.13) and (A.19) as boundary conditions in the generalized deformed setting, see (4.7-4.10) . Note that one is forced to introduce at least one more function to ensure consistency of the equations - otherwise A and f are always given by (A.13) and (A.19).

B. Thermodynamics

B.1. Black hole thermodynamics

It was postulated by Hawking [48] and conjectured by Bekenstein [49] that a black hole can be endowed with a temperature T_H and an entropy S_{BH} . The Hawking temperature is defined by

$$T_H = \frac{\kappa}{2\pi} \Big|_h = \frac{-g_{tt,R}}{4\pi(-g_{tt}g_{RR})^{\frac{1}{2}}} \Big|_{R=R_h}, \quad (\text{B.1})$$

where κ is the surface gravity at the black hole horizon and the indices RR stand generically for the radial component of the metric, that is the coordinate defining the black hole horizon by $R = R_h$. The Bekenstein-Hawking entropy is

$$s_{BH} = \frac{A_h}{4G_5 V_h}, \quad (\text{B.2})$$

where A_h is the surface of the black hole horizon. The quantity G_5 is here the “Newton constant” and we have already scaled the entropy S_{BH} by the horizon volume V_h to obtain the entropy density $s_{BH} = S_{BH}/V_h$. The factor $1/4$ in (B.2) was conjectured by Bekenstein and Hawking; the first calculation of the Bekenstein-Hawking entropy by counting the number of black hole micro-states was done in a supersymmetric setting by Strominger and Vafa [50], where the factor was confirmed.

Consider the black hole AdS space (A.20). Equations (B.1) and (B.2) yield

$$T = \frac{1}{\pi z_h}, \quad (\text{B.3})$$

$$s = \frac{1}{4G_5} \frac{z_h^3}{L^3}, \quad (\text{B.4})$$

$$\frac{s}{T^3} = \frac{L^3 \pi^3}{4G_5} = \text{const.} \quad (\text{B.5})$$

Since $s/T^3 = \text{const}$, we see by comparing with (B.9) that the thermodynamic relation $s(T)$ of a black hole AdS space corresponds to an ideal gas, which is certainly a bad model for

the Yang-Mills theory thermodynamics. However, as described at the end of section A.2, by deforming the black hole AdS space one can achieve $s/T^3 \neq \text{const}$ and, even better, one can construct a deformation such that the equation of state $s(T)$ of the SU(3) Yang-Mills theory is quantitatively reproduced. This is the idea behind the holographic Yang-Mills thermodynamics model. The quantitative reproduction of the SU(3) Yang-Mills equation of state is one goal of this thesis.

Observe that in equation (B.2) the entropy is proportional to the *area*, not as one would naively expect to the volume of the black hole horizon. This has led physicists to consider far-reaching consequences, potentially radically changing our understanding of the world. The main idea drawn from (B.2) is that all information of the 3-dimensional world we live in is - or can be - stored on 2-dimensional surfaces, be it the horizons of black holes or the surface of our universe itself. This idea is known as the “holographic principle”, mainly promoted by Susskind [51]. In fact, the AdS/CFT correspondence (see chapter 3) is thought to be the most prominent manifestation of this principle: a quantum field theory on a 4-dimensional manifold describes *one-to-one* a theory of quantum gravity in 5 dimensions and vice versa.

B.2. Standard thermodynamics

In this section we collect standard thermodynamic relations that will be used throughout the thesis assuming that $s(T)$ is known. The pressure $p(T)$ follows then from

$$p(T) = p_0 + \int_{T_0}^T s(T) dT, \quad (\text{B.6})$$

where $p_0 = p(T_0)$ is an integration constant. One option in our context is to start at the deconfinement temperature: $T_0 = T_c$, $p_0 = p(T_c)$.

The energy density $e(T)$ can be obtained via the Gibbs relation (for $\mu = 0$)

$$sT = e + p. \quad (\text{B.7})$$

The squared speed of sound $c_s^2 = \partial p / \partial e$ is given by

$$c_s^2 = \frac{s}{T} \left(\frac{ds}{dT} \right)^{-1}. \quad (\text{B.8})$$

For an ideal gas of free gluons (Stefan-Boltzmann limit) s can be calculated analytically, p and e follow with (B.6) and (B.7):

$$s_{SB} = \frac{4}{45}\pi^2(N^2 - 1)T^3, \quad (\text{B.9})$$

$$p_{SB} = \frac{1}{45}\pi^2(N^2 - 1)T^4, \quad (\text{B.10})$$

$$e_{SB} = \frac{1}{15}\pi^2(N^2 - 1)T^4 = 3p_{SB}, \quad (\text{B.11})$$

where a $SU(N)$ gauge group was assumed. In the large- N context of the AdS/CFT correspondence one often replaces $(N^2 - 1) \rightarrow N^2$.

The interaction measure I (also called trace anomaly) given by

$$I = e - 3p \quad (\text{B.12})$$

is a useful quantity, as it measures the deviation of a gas from ideal behavior. For an ideal gas of massless particles $e = 3p$ and consequently $I \equiv 0$. Another measure for the deviation of a gas from Stefan-Boltzmann behavior is the conformality measure Δc_s^2 defined as

$$\Delta c_s^2 = \frac{1}{3} - c_s^2. \quad (\text{B.13})$$

For an ideal gas of massless particles $c_s^2 = 1/3$ and $\Delta c_s^2 \equiv 0$. Instead of an ideal gas one may also refer to a conformal gas which obeys by definition the relations $I = 0$, $\Delta c_s^2 = 0$ in three spatial dimensions.

Note that p_0 in (B.6) is an a priori unknown integration constant entering the expressions for p , e and I . In our model, the value of p_0 will be taken from the lattice data.

C. Approximate determination of the parameters

To obtain suitable initial conditions for the fitting procedure in section 5.3, it is useful to calculate the values of the parameters γ , b and G_5/L^3 using input from the Yang-Mills theory.

The parameter γ

For large values of ϕ_h , $\phi_h \gtrsim 4$, the potential (5.7) becomes

$$V \approx -\frac{12}{L^2} e^{\gamma\phi}. \quad (\text{C.1})$$

The potential in equation (C.1) is the Chamblin-Reall potential, for which the analytic solution of the equations (4.34-4.37) is known [2]. The entropy density and the temperature behave as

$$LT_{CR} = \frac{1}{4\pi} \frac{8 - 3\gamma^2}{2 - 3\gamma^2} \exp\left(\left[\frac{\gamma}{2} - \frac{1}{3\gamma}\right]\phi_h\right). \quad (\text{C.2})$$

$$G_5 s_{CR} = \frac{1}{16\pi} \exp\left(-\frac{\phi_h}{\gamma}\right), \quad (\text{C.3})$$

In contrast, the squared speed of sound

$$c_s^2 = \frac{d \ln T}{d \ln s} = \frac{1}{3} - \frac{\gamma^2}{2} \quad (\text{C.4})$$

is independent of the temperature. Assuming, that the Chamblin-Reall behavior arises already for $T \approx T_c$, one can fix γ to the Yang-Mills theory (or QCD) value of the squared speed of sound at T_c . In [2] and [43] the value $\gamma = 0.606$ was obtained using equation (C.4) with $c_s^2 \approx 0.15$, which is the expected value of the squared speed of sound in QCD at $T \approx T_c$ within the hadron resonance gas model.

The parameter b

Consider equation (2.10), which is repeated here for convenience

$$T_\mu^\mu = \frac{\beta(\alpha)}{8\pi\alpha^2} \text{Tr}(F_{\mu\nu}F^{\mu\nu}). \quad (\text{C.5})$$

For any operator \mathcal{O} , the full scaling dimension Δ is defined by

$$\mu \frac{d\mathcal{O}}{d\mu} = -\Delta\mathcal{O}, \quad (\text{C.6})$$

where $\Delta = \Delta_0 + \gamma$, i.e. the full scaling dimension is the sum of the classical dimension and the anomalous dimension. Note that, since the trace of the Yang-Mills energy momentum tensor T_μ^μ is renormalization group (RG) invariant, its scaling dimension is identical to the classical one, i.e. $\Delta = \Delta_0 = 4$. Differentiate equation (C.5) with respect to $\mu d/d\mu$ to obtain for the scaling dimension Δ of $\text{Tr}(F_{\mu\nu}F^{\mu\nu})$:

$$\Delta = 4 + \frac{d\beta(\alpha)}{d\alpha} - \frac{2\beta(\alpha)}{\alpha}, \quad (\text{C.7})$$

where, to obtain the second term on the right hand side, we used

$$\frac{\mu}{\beta(\alpha)} \frac{d\beta(\alpha)}{d\mu} = \frac{d\mu}{d\alpha} \frac{d\beta(\alpha)}{d\mu} = \frac{d\beta(\alpha)}{d\alpha}. \quad (\text{C.8})$$

With the knowledge of the perturbative Yang-Mills β function and with the so obtained $\alpha(\mu)$ -dependence one can match the scaling dimension Δ of $\text{Tr}(F_{\mu\nu}F^{\mu\nu})$, which appears in the potential (5.7) via equation (5.8) to the perturbative result at some energy scale μ using equation (C.7).

The parameter G_5

The 5D ‘‘Newton constant’’ is related to the rank N of the boundary theory $SU(N)$ gauge group by the AdS/CFT correspondence via

$$G_5 = \frac{1}{16\pi M_p^3 N^2}, \quad (\text{C.9})$$

where M_p is the Planck mass. Equate the expressions for s/T^3 of the black hole AdS space (B.5) and the Stefan-Boltzmann limit (B.9) to obtain using (C.9)

$$\frac{L^3 \pi^3}{4G_5} = 4\pi^4 L^3 M_p^3 N^2 = \frac{4}{45} \pi^2 (N^2 - 1). \quad (\text{C.10})$$

One thus has

$$(LM_p)^3 = \frac{1}{45\pi^2} \frac{N^2 - 1}{N^2}. \quad (\text{C.11})$$

Inserting (C.11) into (C.9) one obtains

$$\frac{L^3}{G_5} = \frac{16}{45\pi} (N^2 - 1). \quad (\text{C.12})$$

Set $N = 3$ to obtain

$$\frac{G_5}{L^3} \approx 1.1044. \quad (\text{C.13})$$

D. Reviews of the AdS/CFT correspondence

We list a number of reviews on the AdS/CFT correspondence.

- [13]: an extensive review touching many string theoretic aspects, as well as different versions of the correspondence.
- [15]: a review with an emphasis on supersymmetric aspects.
- [52]: a review starting from general relativity, well suited for a reader unfamiliar with string theory and supersymmetry.
- [25]: a review focusing on different aspects of the correspondence, including sample calculations.
- [17]: an extensive review, focusing on the application of the correspondence to QCD and Heavy-Ion Collisions, requires no prior knowledge of string theory or supersymmetry.
- [30]: a top-down oriented review on the description of mesons within the AdS/CFT correspondence.

Bibliography

- [1] D. Li, S. He, M. Huang, and Q.-S. Yan, JHEP **1109**, 041 (2011), 1103.5389.
- [2] S. S. Gubser and A. Nellore, Phys. Rev. **D78**, 086007 (2008), 0804.0434.
- [3] T. van Ritbergen, J. Vermaseren, and S. Larin, Phys. Lett. **B400**, 379 (1997), hep-ph/9701390.
- [4] W. E. Caswell, Phys. Rev. Lett. **33**, 244 (1974).
- [5] B. Friman (ed.) *et al.* *The CBM physics book: Compressed baryonic matter in laboratory experiments* Vol. 814 (, 2011).
- [6] J. Kapusta and C. Gale, *Finite-temperature field theory: Principles and applications* (Cambridge University Press, 2006).
- [7] B. Lucini, M. Teper, and U. Wenger, JHEP **0401**, 061 (2004), hep-lat/0307017.
- [8] A. D. Linde, Phys. Lett. **B96**, 289 (1980).
- [9] J. M. Maldacena, Adv. Theor. Math. Phys. **2**, 231 (1998), hep-th/9711200.
- [10] J. Polchinski, *String theory. Vol. 1: An introduction to the bosonic string* (Cambridge University Press, 1998).
- [11] J. Polchinski, *String theory. Vol. 2: Superstring theory and beyond* (Cambridge University Press, 1998).
- [12] K. Becker, M. Becker, and J. Schwarz, *String theory and M-theory: A modern introduction* (Cambridge University Press, 2007).
- [13] O. Aharony, S. S. Gubser, J. M. Maldacena, H. Ooguri, and Y. Oz, Phys. Rept. **323**, 183 (2000), hep-th/9905111.
- [14] J. Polchinski, Phys. Rev. Lett. **75**, 4724 (1995), hep-th/9510017.
- [15] E. D'Hoker and D. Z. Freedman, (2002), hep-th/0201253.

- [16] R. Penrose, *The road to reality: a complete guide to the laws of the universe* (Knopf, 2005).
- [17] J. Casalderrey-Solana, H. Liu, D. Mateos, K. Rajagopal, and U. A. Wiedemann, (2011), 1101.0618.
- [18] <http://functions.wolfram.com/bessel-typefunctions/bessely/>.
- [19] P. Breitenlohner and D. Z. Freedman, *Ann. Phys.* **144**, 249 (1982).
- [20] P. Breitenlohner and D. Z. Freedman, *Phys. Lett.* **B115**, 197 (1982).
- [21] I. R. Klebanov and E. Witten, *Nucl. Phys.* **B556**, 89 (1999), hep-th/9905104.
- [22] E. Witten, *Adv. Theor. Math. Phys.* **2**, 253 (1998), hep-th/9802150.
- [23] S. Gubser, I. R. Klebanov, and A. M. Polyakov, *Phys. Lett.* **B428**, 105 (1998), hep-th/9802109.
- [24] K. Skenderis, *Class. Quant. Grav.* **19**, 5849 (2002), hep-th/0209067.
- [25] J. L. Petersen, *Int. J. Mod. Phys.* **A14**, 3597 (1999), hep-th/9902131.
- [26] A. Buchel, R. C. Myers, and A. Sinha, *JHEP* **0903**, 084 (2009), 0812.2521.
- [27] A. Buchel, M. P. Heller, and R. C. Myers, *Phys. Lett.* **B680**, 521 (2009), 0908.2802.
- [28] T. Sakai and S. Sugimoto, *Prog. Theor. Phys.* **113**, 843 (2005), hep-th/0412141.
- [29] A. Karch, E. Katz, D. T. Son, and M. A. Stephanov, *Phys. Rev.* **D74**, 015005 (2006), hep-ph/0602229.
- [30] J. Erdmenger, N. Evans, I. Kirsch, and E. Threlfall, *Eur. Phys. J.* **A35**, 81 (2008), 0711.4467.
- [31] S. Carlip, *Rept. Prog. Phys.* **64**, 885 (2001), gr-qc/0108040.
- [32] M. Panero, *Phys. Rev. Lett.* **103**, 232001 (2009), 0907.3719.
- [33] U. Gursoy, E. Kiritsis, L. Mazzanti, and F. Nitti, *JHEP* **0905**, 033 (2009), 0812.0792.
- [34] P. Kovtun, D. Son, and A. Starinets, *Phys. Rev. Lett.* **94**, 111601 (2005), hep-th/0405231.
- [35] J. I. Kapusta, (2008), 0809.3746.

- [36] S. Borsanyi, G. Endrodi, Z. Fodor, S. Katz, and K. Szabo, JHEP **1207**, 056 (2012), 1204.6184.
- [37] B. Batell and T. Gherghetta, Phys. Rev. **D78**, 026002 (2008), 0801.4383.
- [38] M. Bluhm, B. Kampfer, and K. Redlich, Phys. Rev. **C84**, 025201 (2011), 1011.5634.
- [39] G. Boyd *et al.*, Nucl. Phys. **B469**, 419 (1996), hep-lat/9602007.
- [40] CP-PACS Collaboration, M. Okamoto *et al.*, Phys. Rev. **D60**, 094510 (1999), hep-lat/9905005.
- [41] S. S. Gubser, S. S. Pufu, and F. D. Rocha, JHEP **0808**, 085 (2008), 0806.0407.
- [42] S. Hawking and D. N. Page, Commun. Math. Phys. **87**, 577 (1983).
- [43] S. S. Gubser, A. Nellore, S. S. Pufu, and F. D. Rocha, Phys. Rev. Lett. **101**, 131601 (2008), 0804.1950.
- [44] W. Unruh, Phys. Rev. **D14**, 3251 (1976).
- [45] A. S. Miranda, C. Ballon Bayona, H. Boschi-Filho, and N. R. Braga, JHEP **0911**, 119 (2009), 0909.1790.
- [46] L.-X. Cui, S. Takeuchi, and Y.-L. Wu, JHEP **1204**, 144 (2012), 1112.5923.
- [47] P. Colangelo, F. Giannuzzi, and S. Nicotri, JHEP **1205**, 076 (2012), 1201.1564.
- [48] S. Hawking, Commun. Math. Phys. **43**, 199 (1975).
- [49] J. D. Bekenstein, Phys. Rev. **D7**, 2333 (1973).
- [50] A. Strominger and C. Vafa, Phys. Lett. **B379**, 99 (1996), hep-th/9601029.
- [51] D. Bigatti and L. Susskind, (1999), hep-th/0002044.
- [52] H. Nastase, (2007), 0712.0689.

Acknowledgements

The author is deeply grateful to his supervisor, Prof. Dr. Burkhard Kämpfer, for numerous helpful discussions and for the kind patience. Inspiring discussions with Falk Wunderlich and Uwe Hernandez Acosta are also gratefully acknowledged.

Many thanks to my friends and family for their support and encouragement.

Erklärung

Hiermit versichere ich, dass ich die vorliegende Arbeit ohne unzulässige Hilfe Dritter und ohne Benutzung anderer als der angegebenen Hilfsmittel angefertigt habe. Die aus fremden Quellen direkt oder indirekt übernommenen Gedanken sind als solche kenntlich gemacht. Die Arbeit wurde bisher weder im Inland noch im Ausland in gleicher oder ähnlicher Form einer anderen Prüfungsbehörde vorgelegt.

Roman Yaresko
Dresden, 08.01.2013